The Effects of Sand Extraction On the Lower Paraná Delta

CEGM3000: Multidisciplinary Project

MP385

Delft University of Technology

TU Delft

FAST

TU Delft | University Fund

The Effects of Sand Extraction On the Lower Paraná Delta

by

MP385

Student Name	Student Number
Victor Ameye	5522056
Niek Appels	5403537
Jasper Biemans	5598974
Mike Intveld	5268672
Laurens van der Knaap	5604443
Stefan Kocken	5586992

Date:	Friday 7th November, 2025
Client:	Instituto Nacional del Agua (INA)
Supervisors:	Eng. Martín Sabarots Gerbec (INA), Dr. Mariano Re (INA)
	Eng. Leandro Kazimierski (INA), Dr. Anne Baar (TU Delft)
Examiners:	Dr. Anne Baar (TU Delft), Dr. Ir. Wout Broere (TU Delft)
Project Duration:	September 2025 - November 2025
Faculty:	Faculty of Civil Engineering and Geosciences, Delft

Cover picture: Own image

TU Delft

Preface

The Multidisciplinary Project is an initiative of ten weeks within the MSc Civil Engineering program at Delft University of Technology. In this project, a group of six students with different specializations join forces to work on a shared assignment. These projects are linked with an external party for whom students create a design or conduct a study on a certain topic. In this case, the work contributes to the knowledge on sand mining in the Lower Paraná Delta, in collaboration with the National Institute of Water (INA) in Buenos Aires, Argentina.

We are grateful for collaborating with the Lamminga Fund Institute, the Delta Futures Lab - Zawabas and FAST University Fund, from whom we had the honour of receiving scholarship grants. In name of the group, we express our gratitude to the INA supervisors who have guided us throughout this project: Eng. Martin Sarabots Gerbec, Dr. Eng. Mariano Re, and Eng. Leandro Kazimierski. We would also like to thank Nicolas Ortiz for his help during the fieldwork and Marina Sarti for everything she has done for us, both on and off the project. Finally, we want to thank our supervisors from TU Delft for their guidance: Dr. Anne Baar and Dr. Ir. Wout Broere, and all interviewed stakeholders who made this work possible.

MP385
Buenos Aires, November 2025

Summary

Sand is one of the most extracted natural resources worldwide, and demand continues to rise along with population and infrastructure development. In Argentina, the Lower Paraná Delta has become a key source of sand for both construction and hydraulic fracturing (fracking) activities. While sand mining can generate short-term economic benefits, its environmental and socioeconomic impacts on the delta remain poorly understood. Therefore, this study aims to answer the following research question: ”What are the morphological and socioeconomic effects of sand extraction in the Lower Paraná Delta and how can these be managed to secure a sustainable future?”. Both river and land-based sand mining and their respective effects on the delta were researched.

The research applied a multidisciplinary approach combining hydraulic, geotechnical, and structural engineering perspectives. Quantitative analyses were based on field measurements, sediment sampling, and hydrodynamic modelling with Delft3D. Additionally, stakeholder interviews and data from the Automatic Identification System (AIS) of vessels were used to assess extraction volumes and local perceptions. This combination allowed for a comparative evaluation of river and dry sand mining.

Results show that river sand extraction remains relatively stable across large parts of the study area, while local government intervention has effectively halted dredging activities in the Paraná Ibicuy, in the northern section of the delta. Current extraction volumes are estimated at approximately 588,000 tons per year. In contrast, dry sand mining has increased sharply, reaching about 2.3 million tons in 2025 in Ibicuy, primarily driven by the growing demand for fracking sand from the Vaca Muerta formation. The established sediment balance of the Paraná Guazú River indicates a negative change in sediment storage of roughly 15,400 tons per day, suggesting a general trend of sediment depletion.

Erosion rates in the study area range between 3 and 7 meters per year, which, although significant, are considerably lower than values reported by some stakeholders. Analyses indicate that natural processes, including river meandering and flood-induced bank instability, are the dominant drivers of bank erosion, while river sand mining does not appear to play a substantial role. Because of their larger scale and intensity, the socioeconomic impacts of dry sand mining are more pronounced, leading to groundwater overuse, road deterioration, and habitat loss. Additionally, low taxation on sand mining activities has enabled these impacts to persist with limited mitigation or compensation. To mitigate erosion, a structural solution in the form of a sheet pile was proposed. Furthermore, Nature-based mitigation strategies have been proposed, the focus lies on floodplains, vegetation and riparian buffer zones.

The accuracy of the study is constrained by the short temporal coverage of field data and the simplified representation of hydrodynamics and sediment transport in the numerical model. To build on these findings, future research should include long-term monitoring, enhanced sediment datasets, and morphodynamic modeling to assess feedbacks between extraction and river response. Integrating Nature-based solutions with targeted structural measures, supported by cost–benefit analyses, would provide a more comprehensive framework for sustainable sand mining management in the Lower Paraná Delta.

Contents

Preface i

Summary ii

1 Introduction 1
- 1.1 Project description . . . 1
- 1.2 Problem statement . . . 2
- 1.3 Objectives . . . 2
- 1.4 Multidisciplinary approach . . . 3
- 1.5 Report outline . . . 4

2 Background study 5
- 2.1 Río Paraná . . . 5
- 2.2 Origin of sediment content in Paraná Guazú . . . 6
- 2.3 Types of sand mining . . . 7
- 2.4 Purposes of extracted sand . . . 8
- 2.5 The effects of sand mining . . . 8
- 2.6 River bank stability . . . 9
- 2.7 Structural solutions for bank erosion . . . 10
- 2.8 Nature-based solutions . . . 11

3 Methodology 13
- 3.1 Analysis of existing data sets . . . 13
- 3.2 Field study . . . 16
- 3.3 Modelling approach . . . 23

4 Stakeholders 25
- 4.1 Stakeholder analysis . . . 25
- 4.2 Interview results . . . 30
- 4.3 Updated stakeholder analysis . . . 32

5 Sand extraction 34
- 5.1 Dredging activities . . . 34
- 5.2 Dry sand mining . . . 36

6 Hydrodynamic and sedimentary analysis 46
- 6.1 Hydrodynamic analysis . . . 46
- 6.2 Field work measurements . . . 53
- 6.3 Sediment balance . . . 61
- 6.4 Hydrodynamic effects on riverbanks . . . 62

7 Delft3D model 71
- 7.1 Model setup . . . 71
- 7.2 Model calibration . . . 74
- 7.3 Model results . . . 76

8 Mitigation Strategies 78
- 8.1 Comparison of structural solutions . . . 78
- 8.2 Sheet pile wall . . . 79
- 8.3 Design of steel sheet pile . . . 83
- 8.4 Nature-based solutions . . . 94
- 8.5 Nature-based solutions for dry sand mining . . . 94
- 8.6 Nature-based solutions for bank erosion . . . 96

9 Discussion **101**
9.1 Sand extraction volumes, purpose and the demand for sand . . . 101
9.2 Hydrodynamic and sedimentary analysis . . . 102
9.3 The effects of sand extraction . . . 104
9.4 Limitations . . . 105

10 Conclusion and recommendations **107**
10.1 Conclusion . . . 107
10.2 Recommendations . . . 109

References **110**

A Safety assessment **116**
A.1 Risk assessment: fieldwork . . . 116

B Unprocessed interview results **118**
B.1 Caretaker at Fisher's club (Club de Pescadores Olivos) . . . 118
B.2 Portmanager (Port of Puerto Ibicuy) . . . 120
B.3 Plant manager (YPF sand mine) . . . 121
B.4 Municipality of Zárate . . . 122
B.5 Mayor of Ibicuy . . . 123
B.6 Landowners . . . 124
B.7 Dredger . . . 125
B.8 Camping owner . . . 127

C Laboratory data **128**
C.1 Bed load samples . . . 128
C.2 Recapitulatory table . . . 128
C.3 Bed load samples pictures . . . 129
C.4 Sieving data tables . . . 131
C.5 Sample processing pictures . . . 132

D Satellite data **133**
D.1 Aqua Monitor data . . . 133
D.2 Google Earth engine data . . . 135

E ADCP results **139**

F Design of steel sheet pile **141**
F.1 Soil profile . . . 141
F.2 Vertical effective stress . . . 142
F.3 Earth pressure and force . . . 142
F.4 Hydrostatic pressure and force . . . 144
F.5 Bending moment . . . 144
F.6 Ultimate Limit and Serviceability Limit State . . . 145

1

Introduction

1.1. Project description

Sand is among the most extracted natural resources in the world. It is an essential component in the production of materials used in daily life including electronics, ceramics, glass, and in key construction materials such as concrete. As global population and infrastructure continue to grow, the demand for sand has increased steadily, leading to extensive mining activities across the globe (WWF, 2019). In Argentina, the Lower Paraná Delta is one of these locations that has become a critical spot for sand mining. Here, dredging companies extract sand from the riverbed and dry sand mining companies from the land. Historically, the sand was used mainly for construction but in recent years, hydraulic fracking has created a new source of demand. While the extraction of sand can be beneficial for the economic development of the area, the impacts of sand mining on the riverbed, biodiversity and the surrounding delta remain insufficiently understood to draw conclusions about the sustainability of this activity.

The study area focuses on a critical location of the Lower Paraná river as well as the surrounding delta. As shown in Figure 1.1, the area of interest stretches roughly from Puerto Ibicuy to Puerto Guazú. It includes a section of the Río Ibicuy, which later bifurcates into the Paraná to form the Paraná Guazú. The total river stretch analysed in this study extends roughly 70 kilometers. Given the dredging activities on the river, the presence of ports within the study area is also annotated in the overview in Figure 1.1, since they serve as key points for the transport of the extracted sand. This study considers sand mining on the river as well as on land, in order to offer a comparative view on the impacts on the delta.

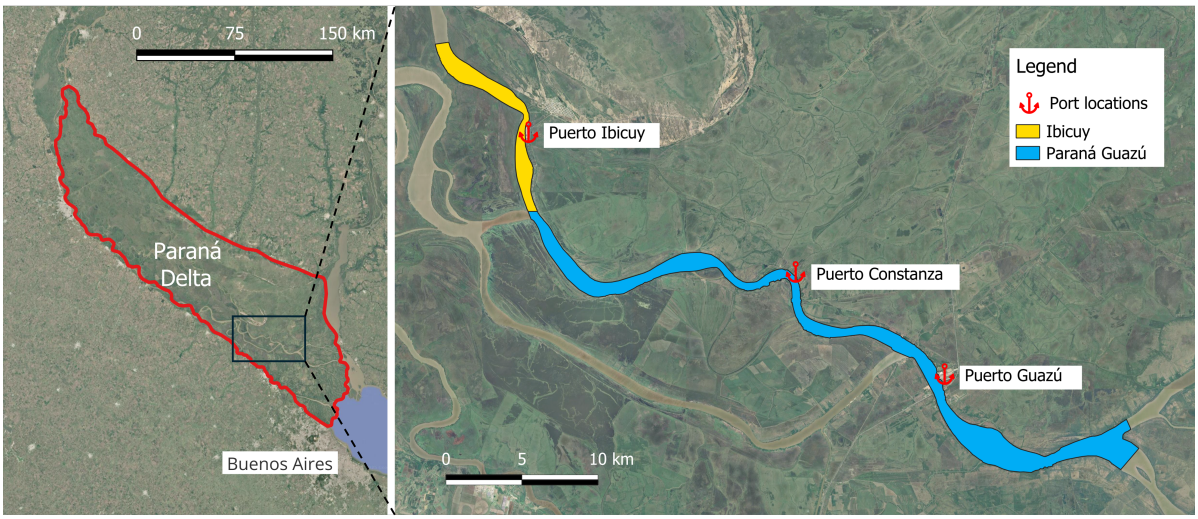

Figure 1.1: Study area (Google Earth, 2025)

This project aims to determine the scale of sand mining in the Lower Paraná Delta, and to assess its diverse impacts on both the river system and surrounding land. By doing so, the study attempts to identify solutions that mitigate negative effects and find a balance that fits the needs of local communities, the existing ecosystem and the ongoing sand demand.

1.2. Problem statement

International case studies highlight the severe impacts of large-scale sand mining, such as in the Mekong Delta. In this region, extensive extraction of sand and aggregates has led to pronounced bed changes over a ten-year period, with an average bed deepening of 1.3 m due to sediment loss. Evidence from the Mekong case study indicates that sand mining is the primary driver of both river-bank erosion and shoreline retreat in the delta (Brunier et al., 2014). Similar concerns about bank erosion and bank stability exist in the Lower Paraná Delta. Furthermore, sand mining can be linked to increased morphological changes that will later impact the delta, especially in terms of sediment supply and coastal erosion.

This example is supported by a study on environmental impacts on the river due to sand mining. It states that if sediment is removed faster than can be replenished by natural transport processes, i.e. the river has a negative sediment balance, the system may experience the following effects due to the imbalance: channel deepening, bank erosion, and changes in flow patterns (Rentier & Cammeraat, 2022). All of these changes can have considerable consequences for navigation, infrastructure stability, aquatic habitats, and flood risk.

Considering the hypothesis that there may be an increasing trend of dredging activities in the Lower Paraná Delta, the hydrodynamic regime of the river and the morphology of the delta may be at risk. Extracting large amounts of sand from the area can thus affect the river's natural sediment balance. Therefore, to fully grasp the extent of these impacts, it is necessary to quantify the amounts extracted, and then compare the extraction rates with the river's natural sediment transport capacity. Without a clear assessment of the situation, the long-term sustainability of the delta and the future of communities and industries dependent on it, remain uncertain.

1.3. Objectives

The comparative studies discussed before show that continued sand mining can cause irreversible damage to the ecological and socioeconomic environment. Therefore, it is suggested to study the evolution of sand extraction in the Lower Paraná Delta and its potential projections and implications. Specifically, an answer to the following research question is sought:

What are the morphological and socioeconomic effects of sand extraction in the Lower Paraná Delta and how can these be managed to secure a sustainable future?

In addition, a number of sub-questions are formulated to guide the reasoning of this report. The project aims to integrate perspectives from multiple disciplines and present the results in a coherent manner.

- How much sand is extracted in the Lower Paraná Delta and what are its main purposes?
- What is the net sediment balance of the specific section in the Paraná Guazú River?
- What are the characteristics of hydrodynamics in the study area?
- What are the erosion processes in the Paraná Guazú river and how are they related to dredging activities?
- How do the effects of river sand mining in the Lower Paraná Delta differ from the effects of dry sand mining?
- What drives the preference for sand from the Lower Paraná Delta?
- Which structural and Nature-based mitigation strategies can be proposed to reduce negative impacts?

1.4. Multidisciplinary approach

The aim of this report is to present a comprehensive assessment of the sustainability of sand mining in the Lower Paraná Guazú Delta. To address the complex study, this report will adopt a multidisciplinary approach, integrating experience from the fields of hydraulic, geotechnical, and structural engineering. Accordingly, the impacts of sand mining are examined from several perspectives. The activities that represent the different disciplines are as follows:

- Hydraulic engineering: Processing available hydrodynamic and sediment data, in order to establish a sediment balance for the Paraná Guazú. Understanding the river flow in the region of interest using a hydrodynamic model through the use of Delft3D software. Furthermore, tidal effects are evaluated, as well as wave interactions and effects on the bank erosion and delta.
- Geotechnical engineering: Investigation of the dry sand mining activities and the geological/ geotechnical characteristics that drive the demand for sand from the region. Finally, identify possible Nature-based mitigation measures for the dry sand mining practices.
- Structural engineering: Consider different structural solutions for bank erosion and come up with a 2D-design for the most feasible one.

The collaboration between disciplines is crucial to achieve a complete understanding of the problem and many analyses require input from multiple fields. For instance, the design of structural measures to mitigate bank erosion depends on the hydrodynamic conditions established by hydraulic engineers and on the soil properties characterized by geotechnical engineers. Similarly, the interpretation of field measurements benefits from continuous discussion among all disciplines to ensure consistency between hydraulic behavior, soil conditions, and structural feasibility. Figure 1.2 visualizes how different aspects were combined to come up with an answer to the research question. The main components of the research question can be found in the middle and are surrounded by their relevant sources.

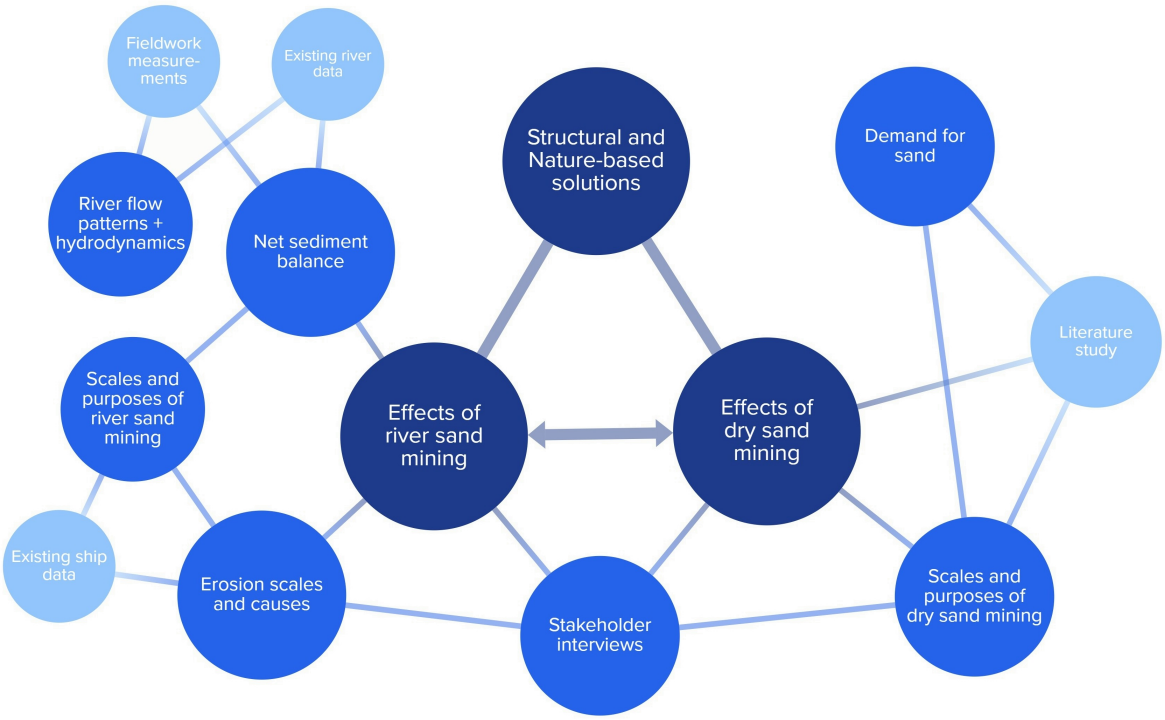

Figure 1.2: Visualization of answering the research question

1.5. Report outline

This section describes the structure of the report. Chapter 2 provides the background study, outlining the context of the problem and supporting later findings with theoretical foundations. Chapter 3 explains the methodology, detailing the data collection process and measurement techniques. Chapter 4 presents a stakeholder analysis, identifying the key parties involved in sand extraction activities and the interview results. Chapter 5 focuses on the sand extraction in the designated area, linking the wet and dry sand mining to the project. Chapter 6 presents an analysis performed on hydrodynamic and sediment data, gathered both from existing data sets and field work measurements. The findings of this chapter are later used in Chapter 7 for a Delft3D model, that serves to reflect the hydrodynamic regime of the study area. Building on these findings, Chapter 8 proposes mitigation strategies to address the identified impacts. Finally, Chapters 9 and 10 conclude the report with a discussion and conclusion, respectively.

2

Background study

This chapter introduces the research that contributes to the contextualization of the Paraná Guazú study. The goal of the background study is to give the reader an understanding of the theory used in later stages of the analysis and to support the problem statement that was given before.

2.1. Río Paraná

Before the in-depth analysis of the Paraná river is carried out, a description of the river system and its key characteristics is necessary. The Argentine river system can be grouped into three watersheds: the Atlantic watershed, which drains into the Argentine Sea, the Pacific watershed, and finally the rivers that do not drain into an ocean but flow inland to permanent or seasonal lakes, swamps, or dry sinks. Of these systems, the Atlantic watershed is the most important one and includes the Río de la Plata Basin, the Patagonian system and several smaller rivers in the province of Buenos Aires (Farber et al., 2024). The Río de la Plata Basin is the most relevant one: it ends in the Río de la Plata estuary and consists of the Paraná, the country's longest river, the Uruguay and their tributaries. The Vía Navegable Troncal (VNT) ends in the Río de la Plata estuary and connects numerous ports to the ocean. Because of this, the VNT is responsible for roughly 80% of the nation's export (Agencia Nacional de Puertos y Navegación, 2025). The Paraná and Paraná Guazú are part of this main waterway. The location of the Paraná river is shown in Figure 2.1.

The Paraná river is formed at the junction of the Grand and Paranaba rivers in central-south Brazil and flows for 4880 km until it reaches the Río de la Plata near Buenos Aires, Argentina (Orfeo & Stevaux, 2002). The river can be split up in three different sections: the upper, middle and lower Paraná. For these sections, the general characteristics related to discharge, channel size, and sediments are discussed.

The Upper Paraná river flows in southwestern direction, from the origin of the Paraná until the confluence with the Paraguay river. Mean annual discharges at Porto São José, located near Porto Primavera at the confluence of the Paraná and Paranapanema in Figure 2.1, are between 6,501 to 13,294 m^3/s. The maximum flow velocity varies between 0.6–0.9 m/s in tributary channels and up to 1.4 m/s in the main channel during floods (Stevaux, 1994). The Upper Paraná river shows a multi-channelled, braided pattern with numerous islands and sand bars, and its floodplain is strongly asymmetrical, being much wider on the right side (widths ranging from 4.2 to 8.5 km) while the left margin erodes the Caiuá Formation (Orfeo & Stevaux, 2002). During normal floods, water enters the floodplain through secondary and abandoned channels, producing slow and non-unidirectional flow, but extreme floods can cause crevasses and temporary channels. The channel is 1200–4500 m wide and 6–17 m deep with a slope of 0.096 m/km (Stevaux, 1994). Finally, the suspended sediment concentration at Porto Rico, just south of Porto São José, equals $14.8 \cdot 10^6$ tons/year and is mainly composed of quartz, mica, and kaolinite. The bed load at this location has a total discharge of $4.04 \cdot 10^6$ tons/year and consists of medium to fine sand (Stevaux, 1994).

Figure 2.1: Rio Paraná (Farber et al., 2024)

After the confluence with the Paraguay river, the Upper Paraná merges into the Middle Paraná river. This part of the river stretches until the start of the delta, just south of Rosario City. Near Corrientes City, South of the confluence, the mean annual discharge is 16,941 m^3/s, with summer floods (February to March) and spring low water levels, reaching maximum values above 50,000 m^3/s. The channel width ranges from 1.9 to 4.7 km, with depths of 15–20 m and a slope of 0.085 m/km (Orfeo & Stevaux, 2002). Below the Paraguay River confluence, suspended sediment concentrations are highly variable due to differences in discharge, confluence angle, and sediment characteristics between both rivers. The suspended solid concentration ranges from 18 to 554 mg/l, with the right margin showing much higher values (up to 1221 mg/l) than the left (maximum 88 mg/l) (Depetris & Griffin, 1968). The suspended load is mainly silt (61–66%) on the right margin and clay (79%) on the left, with minor fine sand. The bed load is composed mostly of medium to fine sand. Finally, the total sediment discharge is estimated at $158.4 \cdot 10^6$ tons/year, with suspended load contributing 75% of that (Orfeo & Stevaux, 2002).

The final and smallest part of the Paraná is the Paraná Delta, that ranges for around 320 kilometers, from Diamante, Entre Ríos, until the Río de la Plata near Buenos Aires. It is divided into three regions: the Upper delta (from Diamante to Villa Constitución, Santa Fe province), the Middle delta (from Villa Constitución to Puerto Ibicuy, Entre Ríos province) and the Lower delta (from Puerto Ibicuy to the mouth of the Río de la Plata estuary). As mentioned in the introduction, this study focuses on the Lower delta specifically. Just upstream of the delta apex, near the city of Paraná, the mean annual discharge is 18,500 m^3/s with peak discharges up to 60,000 m^3/s (Wester et al., 2018). Its width varies between 18 and 60 kilometres. The Paraná Delta is characterized by many islands, which exist due to the large amounts of sediment that the Paraná Delta carries: at its mouth it transports approximately 160 million tons of sediment per year. The particle load distribution is as follows: 25% consists of clay, 60% is silt and around 15% can be characterized as sand (AcademiaLab, n.d.). This sediment is deposited in the joint Paraná and Uruguay estuary, the Río de la Plata.

2.2. Origin of sediment content in Paraná Guazú

In the previous section, the quantities and distributions of sediment transport were described. However, a key step in the construction of the sediment balance of the Rio Paraná Guazú, located in the Lower Paraná Delta, is to identify the origin of its sediment. As shown in Figure 2.1, the Lower and Middle Paraná receive discharge from three main tributaries: the Bermejo, Paraguay, and Upper Paraná river. The total average discharge in the Middle Paraná is 18,389 m^3/s, of which 78% is supplied by the upper Paraná. López Weibel et al. (2022) report that the Bermejo contributes only 2% of this discharge. Nev-

ertheless, the Bermejo is the dominant source of sediment, due to intense erosion in the Andes Eastern Mountain Range within its basin. During the wet season (November to April), multiple tributaries in the basin contribute large sediment flows, accumulating to an annual suspended sediment load of $106 \cdot 10^6$ tons per year at El Colorado gauge station.

It is noteworthy that around 90% of the sediment reaching the Paraná River today originates from the Bermejo River. However, this high share results from the construction of the Itaipú Dam in 1971, located in southern Brazil near the border with Argentina and Paraguay. The dam has reduced the total sediment supply by about 50% compared to pre-dam conditions. Consequently, what once represented 90% of the total sediment input now accounts for only 56%. This shows that human intervention has been disrupting the natural sediment inflow for decades (Hiba, 2024).

From all the sediment transported in the river, only a fraction ends up in the delta (AcademiaLab, n.d.). In the delta, the water's velocity d.ecreases, causing suspended particles in the water to settle. These floating particles contain gravels, sands and clays which over time and distance decrease in particle size due to mutual erosion. This transport of sediment contributes to the sediment balance of the river. Besides that, deltas are also characterized by high vegetation growth. When this vegetation dies, the organic material will change into peat due to the governing pressures. So, in a delta one expects to find relatively soft soils (sands) and very soft soils (clay and peat). Dotted with islands, the delta contains wetlands that are a source of ecosystem services such as flood and drought buffering, water purification, erosion control and coastal protection, climate regulation, as well as the provision of shelter, feeding and breeding sites for various wildlife species. For this reasons, rich biodiversity of the delta territory is characterised by flora and fauna and the microorganisms living in the river. The sediment itself contains particles that are used by the flora and fauna as nutrition and act as a filter system for water quality. The microorganisms in the water also feed on it. Therefore, they are dependent on the transport of sediment in the river (Hiba, 2024).

In recent years, wetlands have received increasing attention for their crucial role in mitigating climate change. As outlined in the previous paragraph, they act as natural buffers against floods and droughts and serve as important carbon sinks. Despite the importance of deltas, the ecosystems remain under great threat from human action. It is estimated that globally, 85 percent of wetlands that existed three centuries ago have been destroyed or drastically transformed (Hiba, 2024).

In summary, while the Paraguay and Upper Paraná river provide most of the fluvial discharge to the downstream delta, the Bermejo River delivers the majority of sediments (López Weibel et al., 2022). These sediments pass through the whole river channel, end up in the deltas while contributing to the biodiversity of the whole Paraná region. Deltas are strategic ecological elements that need to be protected for the sake of the river's biodiversity and pollution indexes. For this reason, the stretch of river beginning in the Bermejo basin and continuing via the Paraguay and Middle Paraná to the Paraná Guazú is of particular importance in this study.

2.3. Types of sand mining

To learn more about the effects of sand mining, the general procedure of mining sand should be explained. Due to the significant demand of sand in human society, various extraction techniques exist. Extraction can be done through so-called dry sand mining, where sand is won from the land, or through river sand mining. For river extraction, the focus of this study lies on in-stream mining. Both river and dry sand mining processes are relevant for the study and therefore explained in the following paragraph.

In-stream mining is the extraction of sand and gravel from the active channel of a river (Padmalal & Maya, 2014). A number of types of in-stream dredging exist. Bar scalping or skimming is the most common extraction practice, consisting of removing the lower two thirds of a bar while leaving the top third to minimize alteration of the riverbed's initial conditions. Dry pit channel mining involves creating a dry pit using mechanical or manual tools to extract sand or gravel; the remaining pits act as head cuts that modify upstream flow during high-water seasons. Wet pit channel mining, typically carried out in perennial rivers, produces similar effects and damages as the dry pit method. Bar excavation takes place downstream of a bar to capture sand and gravel being transported by the current. Finally, in-stream traps involve digging a hole to collect sediment during high flow periods, which can later be retrieved once water levels drop (Padmalal & Maya, 2014).

2.4. Purposes of extracted sand

Creating a clear understanding of the sand extraction processes highly contributes to understanding the bigger picture of potential problems and stakeholder relations. For this reason, the purpose of the sand extraction is discussed here. The extracted sand can be used for different reasons. Historically, silica sand was used as a raw material for the glass industry, as well as the construction industry, for the cement creation, but since the introduction of fracking, sand miners have found a new market for their product. Therefore, the history of fracking is explained below.

In the 1970's, geologists became increasingly aware that large volumes of gas existed in low-permeability sandstones. However, conventional methods did not allow for economic extraction of gas from these so-called tight reservoirs (Law & Spencer, 1992). Hydraulic fracturing, also called fracking, is a method that was first tested in 1947 and then applied on large scale in the 1970's. It is used to extract oil and natural gas from these low-permeability rock formations, shale formations being the primary example (Denchak, 2019). The technique starts by drilling a long vertical well. As soon as the desired rock formation is reached, drilling gradually turns horizontal and steel pipes called casings are inserted into the well. Small holes are perforated in the casing and then fracking fluid is pumped in at a pressure high enough to create new fractures or open existing ones in the surrounding rock. This allows previously unavailable oil or gas to flow to the surface (Denchak, 2019).

The fracking fluid contains as much as 97% of water, and the leftover 3% are called 'proppants'. These proppants are small, solid particles that keep the fractures in the rock formation open after the pressure from injection is removed. Sand, or more specifically silica sand, is the most widely-used proppant in the fracking industry (Denchak, 2019). Sand is thus an essential substance to keep the drilled pores open and to allow for the fossil fuels to flow out.

2.5. The effects of sand mining

This section suggests a framework for possible effects that arise due to river sand mining, based on existing literature. As mentioned before, rivers maintain an equilibrium between erosion, transport, and deposition of sediments. However, in-stream sand mining can disrupt this balance. This happens through direct disruption of the channel geometry or through so-called incision and related undercutting of banks (Padmalal & Maya, 2014). The direct disruption of the river bed depends on the type of sand mining technique applied. In the case of pit excavation, the river bed is locally lowered and a so-called nick point is created. Through bar skimming the river bed is widened (Padmalal & Maya, 2014). For the remainder of this section, the consequent effects of the local river bed lowering (the nick point) are discussed.

Channel incision causes the nick point to migrate both upstream and downstream. In the case of high flows, due to its shape, the nick point is the point where most erosion occurs. Water plunges over the step and erodes the bed at the base. As flows continue, the drop migrates upstream, a process which is often called head-cutting in literature. On the other hand, a process called 'hungry water' causes downstream migration of the pit (Padmalal & Maya, 2014). At the mining pit the water level is deeper, which causes the flow velocity to reduce locally. This leads to a decrease in flow energy and thus to more deposited sediment. When the flow leaves the mining area, water levels are shallower again meaning that flow velocity and energy significantly increase. A lot of sediment has been deposited in the nick point, meaning that the water is not using its full sediment carrying capacity anymore. In other words, the water is 'hungry' for sediment and erosion downstream increases (Padmalal & Maya, 2014).

Through the combined effects of head-cutting and hungry water, the mining pit can extend beyond the initial dimensions caused by direct disruption. This happens in both downstream and upstream directions, as summarized in Figure 2.2. Hackney et al. (2020) have demonstrated that sand mining has the potential to lower bed levels sufficiently to cause river bank instability.

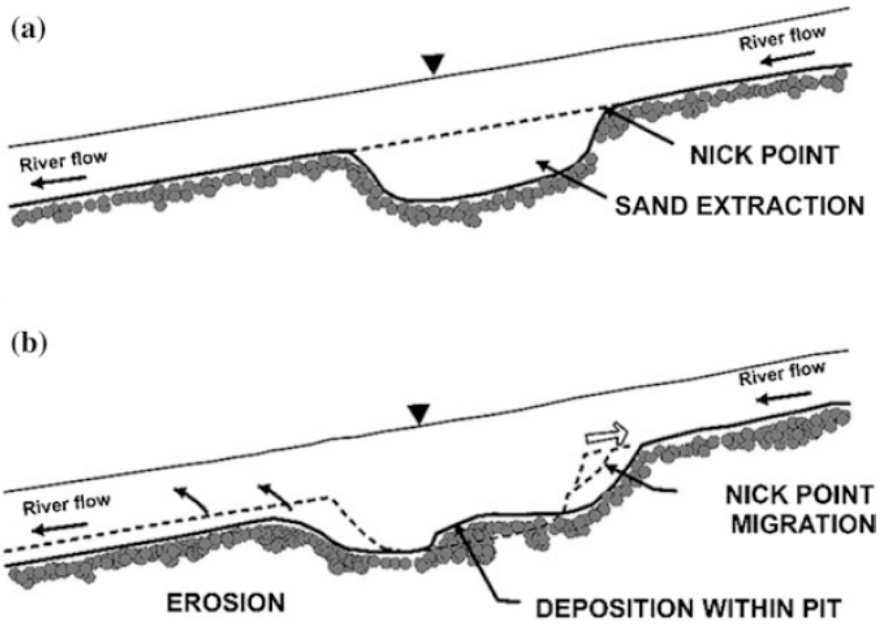

Figure 2.2: (a) direct disruption leads to a locally lowered water bed. (b) channel incision makes the pit migrate upstream through head cutting and downstream through 'hungry' water (Padmalal & Maya, 2014).

Previous studies have shown that bed coarsening can also occur as a result of sand mining. Fine particles are removed, leading to a greater concentration of coarse, gravelly, particles. This effect can also be seen upstream (Padmalal & Maya, 2014). Further, sand mining can lead to changes in both water quality and quantity. The process of dredging fine sand stirs fine organic and inorganic particles, thereby increasing the turbidity of the water. This reduces light penetration, which means less photosynthesis and ultimately less organic growth in the water (Sharip & Zaki, 2014).

As mentioned before, mining pits are often places with significant deposition of particles. Fine, nutrient-rich particles can settle and get trapped in the pits. This then reduces the transport of nutrients from the river to the coastal waters (Padmalal & Maya, 2014). Concerning water quantity, the most relevant effects are related to the groundwater: the lowering of the river bed through direct disruption or channel incision can lead to a lower groundwater table. This can lead to settlements or have negative effects on flora and fauna surrounding the river (Rentier & Cammeraat, 2022).

2.6. River bank stability

Following the study on the effects of sand mining on the river bed, it is relevant to look at the effects on river banks. Dry sand extraction does not influence the bank stability unless the location of extraction is the river bank itself. Therefore, this section only concerns the topic of river sand extraction. The mining of river sand can create instabilities in the river bed as shown in the previous section. This can potentially act on river banks because of the fact that the river channel goes deeper, influencing the discharge and increasing its water influence on the banks (Hackney et al., 2020). In general, there are several ways that water has potential negative impacts on the river bank. Bank failure can be caused by house placement, soil saturation, weight on the river bank, vegetation and tectonic events; but most of them are due to the variation of the water level and waves. The reason behind this is that the river bank is naturally eroded when water exerts a force on it (Government of South Australia, 2024). The river bank is divided into three parts: the toe, the bank and the overbank zone. The toe of the bank is the most susceptible to erosion when in contact with high water levels, seen in the Figure 2.3.

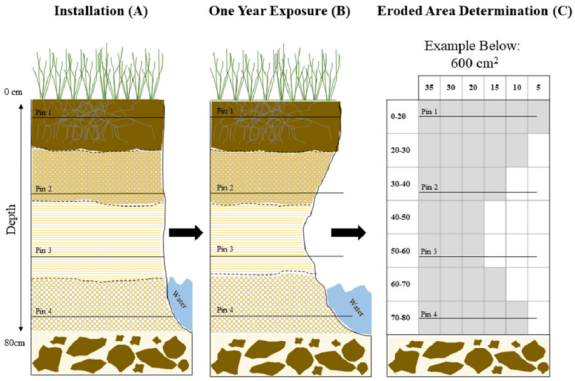

Figure 2.3: Effect of water on bank after one year (Government of South Australia, 2024)

When the combination of high water level with strong current is highest, the bank zone is affected by tidal currents or waves. This is because, as seen in Figure 2.3, water erodes the layer of the bank where the extra water level pushes, creating a dent inside the soil layer. Consequently, after some time the upper overbank area has less and less support underneath, thus becoming unstable and collapsing. Repeating this process takes the river bank further inside the land, increasing the channel width and absorbing the land near the river bank.

Finally, it must be noted that the effects of sand mining can be diverse: previous studies have shown negative impacts on biodiversity, including reduced benthic fauna, disrupted fish spawning habitats, and depletion of natural mosquito predators such as dragonflies (Padmalal & Maya, 2014). The socioeconomic effects of mining can vary, in the short-term it often provides employment, income, and government revenue through royalties and taxation. However, in the long-term the operation can cause a reduction in access to clean water and can cause water scarcity, especially in dry periods. Additionally, loss of land and access to land together with loss of trees and vegetation can jeopardize the local food security. Finally, infrastructure can be damaged by the lowering of the river bed and/or the groundwater table (Padmalal & Maya, 2014).

2.7. Structural solutions for bank erosion

River sand extraction can create damage to banks and therefore it is necessary to include mitigations into the background study. An example is retaining structures that can be used to stabilize the river banks. Multiple possibilities include:

- Sheet pile wall
  Sheet pile walls are a common retaining structure and consist of vertical barriers made of interlocking sections. They are a lightweight option and can be removed, which makes them reusable across multiple projects. Another advantage is the fact that installation is relatively easy and therefore cheap. However, sheet pile walls also have limitations. In hard soils and soils with boulders or cobbles, installation becomes difficult. Further, installation can disturb nearby areas through sounds and vibrations. These vibrations can even cause settlements to occur (Korff, 2023).
- Diaphragm wall
  Diaphragm walls are deep, reinforced concrete retaining structures. They provide excellent structural stability and are capable of resisting significant lateral soil and water pressures. One of their key advantages is water tightness, as they effectively prevent groundwater seepage. They are also suitable for a wide range of soil conditions, and offer durability due to the use of reinforced concrete. On the downside, they are costly to build and require significant time and space due to the specialized equipment, skilled labor, and extensive excavation work that is needed (Korff, 2023).
- Precast concrete wall
  Precast concrete walls are constructed by manufacturing structural elements in a factory environment before transporting them to the construction site. This process allows for superior quality

control. Moreover, precast construction can significantly speed up project timelines, as elements are produced in large quantities and quickly installed on-site. Precast concrete offers a long service life with minimal maintenance. Drawbacks of precast concrete walls include: the elements are heavy and thus require specialized transportation and installation equipment (McNeil Engineering, 2023). Further, the production and transport processes have notable environmental impacts, and repairs or replacements can be complex and costly.

- Auger pile wall or soldier pile wall
  Auger pile walls and soldier pile walls are widely used in construction for retaining slopes. Auger pile walls are formed by drilling and casting concrete in place, while soldier pile walls consist of vertical steel or timber H-piles with horizontal boards or panels placed between them. They are generally cost-effective solutions that generate minimal vibrations, making them suitable for urban areas and sites sensitive to noise or disturbance. Both systems offer flexibility, allowing adjustments to pile placement, size, and depth to suit specific project requirements. However, leakage between adjacent piles is a relevant risk when it comes to these types of walls (Korff, 2023). Maintaining proper overlap between piles is also critical to ensure structural stability and continuity of the wall.

2.8. Nature-based solutions

Nature-based solutions (NbS) align with the goals of climate resilience and sustainable development, and exploring NbS is essential for the Paraná Guazú and its surrounding ecosystems. As highlighted in the preceding sections, the Paraná Guazú could face significant environmental pressures due to sand mining. The ecological and socioeconomic consequences of these disruptions underscore the need for sustainable mitigation strategies that go beyond traditional engineering approaches. As a start, one may read the general definition of Nature-based solutions:

"A set of actions to protect, conserve, restore, sustainably use and manage natural or modified terrestrial, freshwater, coastal and marine ecosystems, which address social, economic and environmental challenges effectively and adaptively, while simultaneously providing human well-being, ecosystem services, resilience and biodiversity benefits" (Eiselin, 2022)

Nature-based solutions is an initiative launched by International Union for Nature Conservancy (IUCN) at the start of the 21st century (Cassin, 2021). Its aim is to fulfill the seven goals set by the IUCN found in Figure 2.4 (Dunlop et al., 2024).

Figure 2.4: Seven goals for achieving a good NbS (Dunlop et al., 2024)

Implementations of NbS often face resistance from stakeholders, particularly when these solutions are compared to traditional engineered approaches. This resistance stems from several key factors:

- Lack of knowledge: local communities and stakeholders may be sceptical of NbS due to their less straightforward approach compared to conventional infrastructure such as concrete walls or revetments. The abstract or long-term benefits of NbS such as ecosystem restoration, flood regulation, or biodiversity enhancement can be harder to accept as a plan.
- Natural uncertainties: NbS often rely on natural processes, which can introduce risks in terms of feasibility and maintenance. Stakeholders may question whether these solutions can deliver the same level of protection or economic return as traditional non-sustainable engineering solutions.
- Economic profitability: a decent return on investment is essential for securing funding and support from investors. Without clear evidence of effectiveness and other financial benefits, stakeholders such as investors, mayors, and community leaders may hesitate to choose this path.

If solutions are presented, they must be clear, easy to implement and without a lot of financial constraints. After all, without funding of the project there is no execution.

3

Methodology

This chapter details the methodological approach employed to address the research questions. It outlines the systematic collection of data from diverse sources, including publicly available time series and original field measurements obtained during this study. The gathered data served as the foundation for developing analytical models, which were subsequently used to investigate the sub-questions and ultimately provide answers to the main research question.

3.1. Analysis of existing data sets

The following sections present the datasets used to analyse the situation and derive conclusions in the following chapters. Each dataset is described in detail, clarifying its relevance and role in the analysis. A summary is provided in Table 3.1.The first source of data was the *Instituto Nacional del Agua* (INA). Since collaboration between TU Delft and INA is a central aim of this study, an “our data is your data” policy was applied, under which data were openly exchanged. Through this approach, INA provided a large number of datasets, which are presented in Table 3.1. In addition, background knowledge about water discharge, erosion and negative impacts was shared in the form of publications and reports produced by INA staff and contacts. Furthermore, INA supplied geospatial datasets, including bathymetric surveys and a Digital Elevation Model (DEM) of the study area.

INA also provided a number of public sources for further hydrodynamic analysis and GIS applications. These included flow data from multiple gauging stations and publicly available bathymetric datasets. Examples are the Sistema Nacional de Información Hídrica (SNIH), point-based water level measurements from the governmental department Alerta, and water level records from the Prefectura Naval Argentina (PNA). An overview of these datasets is provided in Table 3.1. Finally, additional data were obtained through other stakeholder contacts. For example, the Dutch Embassy provided a case study on Nature-based solutions (NbS) for the Paraguay River. More information on the approach with stakeholders can be found in Section 3.2.1.

Table 3.1: Summary of data sources

Name	Description of data type	Source
Comparative studies	Background literature on geomorphology of similar areas	INA
INA Dataviewer	Historical observations and simulations of water level and discharge time series	INA
DEM of lower Paraná	GeoTIFF file containing a Digital Elevation Model of the study area	INA
Bathymetry (GIS)	Results from field campaigns in and around study area (2011, 2015, 2018)	INA
Sand extraction permits	Agreements on locations and volumes of dredged sand	INA
MarineTraffic	Live AIS vessel data	Marine Traffic, 2025
Prefectura Naval Argentina	Water level measurements	Prefectura Naval Argentina, 2025
SNIH	Water level, discharge, fine and course sediment concentration	SNIH, 2025
AquaMonitor	Deltares tool that represents water gains and losses based on historical satellite imagery	Deltares, 2025a
Bathymetry (pdf)	Detailed bathymetries along Paraná river in pdf-format	Agencia Nacional de Puertos y Navegación, 2025
Google Earth	Satellite imagery of the globe. Can be used for a chosen time period of 1984-now	Google Earth, 2025

3.1.1. SNIH measurement stations

The measurement stations from the SNIH that were used for the data collection are discussed in this section. In order to have accurate estimations of the sediment content in the Lower Paraná, it is interesting to consider its origin. As discussed in Section 2.2, most of the sediments in the Middle Paraná originate from the Bermejo river in northern Argentina. A representative measurement station for this river is found near El Colorado, Formosa province. Here, the SNIH reports long series of measurements of water elevation, discharge and sediment concentrations. Moving downstream, the Bermejo confluences with the Paraguay river. Merely 80 kilometres further downstream, the confluence of the Paraguay and Paraná river is located, near the city of Corrientes. Here, a drastic change in fluvial discharge occurs. Therefore, a station that represents the flow in the Middle Paraná was sought. Approximately 500 kilometres downstream of the confluence, the Túnel subfluvial station near Santa Fe provides data. See Figure 2.1 for the location of El Colorado and Paraná (near Santa Fe).

As explained in Chapter 2, the two main tributaries of the Paraná that later flow into the Río de la Plata are the Paraná de las Palmas and the Paraná Guazú. To examine the distribution of discharge and sediment concentrations over these tributaries, two stations were selected and are shown in Figure 3.1. First, the Zárate station was considered on the Paraná de las Palmas. On the Paraná Guazú, the Brazo Largo station was selected for data analysis. Table 3.2 presents the data for all stations considered. Note that every dataset contains measurements of water level, discharge, fine sediment concentration and course sediment concentration. Most of the data was measured monthly, however some information was recorded on shorter time intervals.

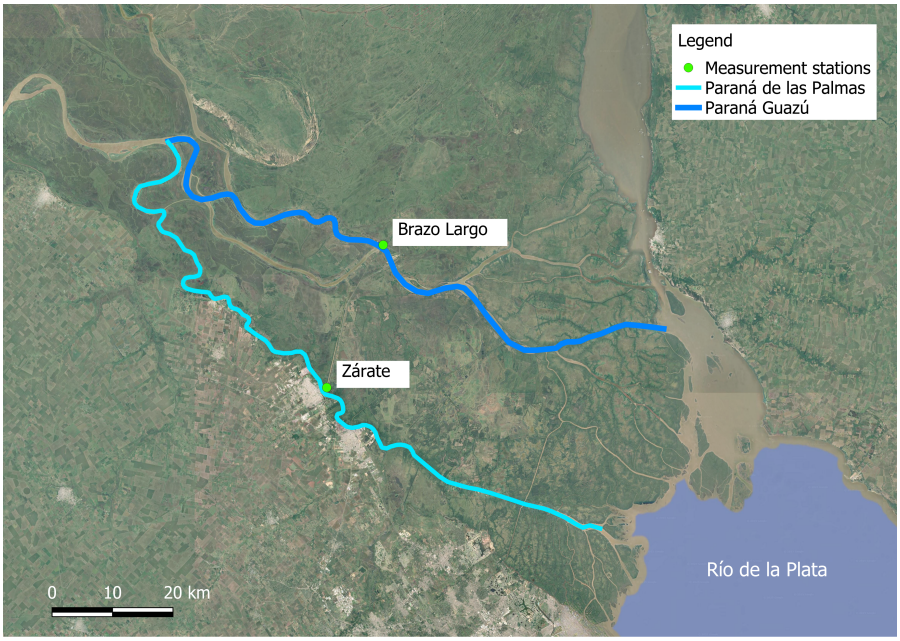

Figure 3.1: Measurement stations of interest on Paraná de las Palmas and Paraná Guazú (Google Earth, 2025)

Table 3.2: Selection of SNIH measurement stations

Station	SNIH ID	River	Data availability
El Colorado	2602	Bermejo	1968–2025
Túnel Subfluvial	3050	Middle Paraná	1983–2025
Zárate	4001	Paraná de las Palmas	1993–2025
Brazo Largo	4002	Paraná Guazú	1993–2025

3.1.2. Sand mining quantities

The number of vessels involved in river dredging activities on the Paraná Guazú was determined using AIS (Automatic Identification System) data. Vessel movements between dredging sites and ports were monitored through MarineTraffic. Although historical records were not available, the daily activity observed during the study period provided an estimate of sand extraction volumes. Alternatively, a collection of dredging permits in the river was considered. To avoid adverse impacts on the hydraulic regime of the river due to dredging, companies must first obtain permits from the *National Water Institute* (INA). These permits specify the locations and volumes of the proposed dredging activities. The information they provide serves as an estimate of the total material being removed from the river, thereby influencing the sediment balance. Therefore, the permits were analysed for the area of interest. Subsequently, the information gathered from AIS data and extraction permits were combined, resulting in estimates of volumes that are dredged in the study area. In addition, conversations with stakeholders provided insights and made a comparison with the results of the data collection possible.

The information about dry sand mining was gained through different sources. The main sources were a literature review and the semi-structured interviews, which are explained Section 3.2.1. These were used to gather data on dry sand mining quantities, usage purposes, and the factors influencing demand for sand from the region. The literature review provided background and quantitative information, while interviews offered insights from stakeholders directly involved in sand extraction and use in the study area.

3.2. Field study

The goal of the fieldwork was to obtain data from measurements on the boat using different devices, as well as obtaining resourceful information from chosen stakeholders in the area of the fieldwork. This data would then be filtered and analysed to help support conclusions.

3.2.1. Stakeholders

In this study, a qualitative research was carried out to explore perceptions and experiences related to sand extraction in the lower delta area. For this, interviews were conducted to capture insights from participants with diverse perspectives.

A qualitative approach was chosen because it allows for a detailed understanding of participant's views and interpretations. This design is particularly suited to capture the complexity of social and environmental issues and to highlight the ways in which different stakeholders experience the delta region and the activities related to it. Data were collected through semi-structured interviews, a method that combines prepared guiding questions with the flexibility to follow up on unexpected but relevant topics raised by participants. This format ensured that key themes were consistently addressed in interviews while also allowing interviewees to elaborate on issues they considered important. In practice, a topic guide with questions per stakeholder was developed to provide structure, but the interviewer encouraged open-ended responses and probed further where clarification or depth was needed. During the interview, responses were written down in key words. The prepared questions for specific stakeholders as well as their unprocessed responses are given in Appendix B.

In case of language barriers, the questions and responses were translated to English by INA staff members. Most stakeholders were approached by email to get in contact or were reached on-site. After each interview, permission was asked to quote and name the stakeholder in the report. Table 4.1 gives an overview of stakeholders who were contacted, when and by which method.

Table 3.3: Overview of stakeholder approach

Date	Occupation	Method
12-09-2025	Fishers	Email
12-09-2025	Ports	Email
12-09-2025	Filmmakers	Whatsapp
24-09-2025	Landowners	Whatsapp and On-site
25-09-2025	Agencia Nacional de Puertos y Navegación (ANPYN)	Email
25-09-2025	Dredgers	On-site
25-09-2025	Camping owner	Email and On-site
30-09-2025	Prefectura Naval Argentina (PNA)	Email

3.2.2. Measurement variables and equipment

In this section, the types of measurements are explained as well as the locations of measurements taken. The goal of the fieldwork was to obtain data from critical sections in the study area, specifically those sections that were deemed critical for establishing the sediment balance. Two important locations in the study area are the confluence from the Ibicuy and Paraná Guazú, and that of the Paraná Guazú and Talabera. In these sections, sediment samples and flow measurements were recorded. Once this data was gathered, it was analysed and compared to previously obtained data to draw conclusions.

The first measured type of data is the flow velocity profile of the river. This was recorded by a SonTek RiverSurveyor M9 Acoustic Doppler Current Profiler (ADCP). This device consists of two components both placed on a floating board held next to the boat while advancing. The components are a vertical acoustic echo sounder beam placed on the back end of the floating board, and a rectangle shape box containing a microprocessor that computes the data on the front end of the board, as seen in Figure 3.2.

Figure 3.2: SonTek M9 installed in the field

The specialty of the SonTek M9 is that it uses multiple acoustic frequencies to find a high resolution range of depths and flow velocities, while still tracking the geo-referenced position of the vessel using GNSS (Xylem, n.d.). The flow velocity is expressed in the form of a vector and the significance of this data lies in the fact that flow velocity is needed to compute the discharge.

Secondly, the bathymetry, the depth of a channel at the position of the boat on a given timestep, was recorded by using two different methods: the ADCP and the Garmin echosounder. Moving over the whole width of the channel yielded a cross-sectional bathymetry, indicating what depth lies at what coordinate. The echosounder was attached to a pole on the side of the boat, and dipped into the water while the boat was moving. This pole was connected to the Garmin screen showing depth and bathymetry of the channel, as can be seen in Figure 3.3. In addition, this screen allowed for monitoring of possible disruption of the river bed. The profile was taken on the whole trajectory between Puerto Guazú to Ibicuy in both upstream and downstream directions. The profile is shown in Figure 3.8.

(a) Echosounder attached to boat

(b) Garmin material

Figure 3.3: Echosounder and Garmin measurements

From the bathymetry and flow velocity, the discharge can be determined. The flow velocity $\mathbf{v}$ was integrated over the depth and width of the channel (through a cross-section) which in the end yielded the discharge. Equation 3.1 summarizes this procedure.

$$Q = \iint_A \mathbf{v} \cdot d\mathbf{A} \tag{3.1}$$

Where:

- Q is the discharge [m^3/s];
- $\mathbf{v}$ is the flow velocity vector [m/s];
- A is the cross-sectional area perpendicular to the flow [m^2];
- $d\mathbf{A}$ is an infinitesimal area element.

The number of measurements required for a single cross section was defined by the variability of the measurements. That is, a minimum of two measurements was carried out, which was deemed to suffice when the second discharge measurement fell within 10% of the first one. In addition, correct operation of the vessel's velocity was essential for reliable discharge results: it was made sure that the boat speed never exceeded the flow velocity perpendicular to the cross section under consideration.

Further, data was gathered on the suspended sediment concentration of the river. This was done by collecting water with the help of an APEMA BS6A peristaltic pump connected to two plastic tubes. The first tube was short and was used to insert water into the plastic bottles on the boat. The second, longer tube was connected to a weight, which could be lowered into the river until a certain depth. At the desired depth, the fluid was pumped to the surface and collected in the plastic bottles. Then, samples were sealed in order to be sent to the water quality lab in the hydraulic section on the INA site, as seen in Figure 3.4. Here, concentrations of fine sediments were determined for all samples. The evolution of the concentrations along the study area is studied in Chapter 6.

(a) Filling the samples

(b) APEMA BS6A device

Figure 3.4: Suspended sediment measurements

Finally, the bed load was a necessary measurement for a complete analysis. The method used for this parameter was scraping the bottom layer of the channel with a metal shaped container. The goal was to retrieve samples that represent the granulometry of the bed at different depths. During the measurements, a rope was tied to the metal container, which was dropped until it reached the local bed. Then, with help of the current and the movement of the boat, the container was dragged along

with the horizontal movement and sediment was gradually collected. Once this was done, the rope and the container were pulled up and restored in the boat. The last step was to collect sediment and put it in a plastic bag. These samples were later analysed in the lab. The metal container as well as the sediment samples are shown in Figure 3.5.

(a) Bed load samples from the fieldwork

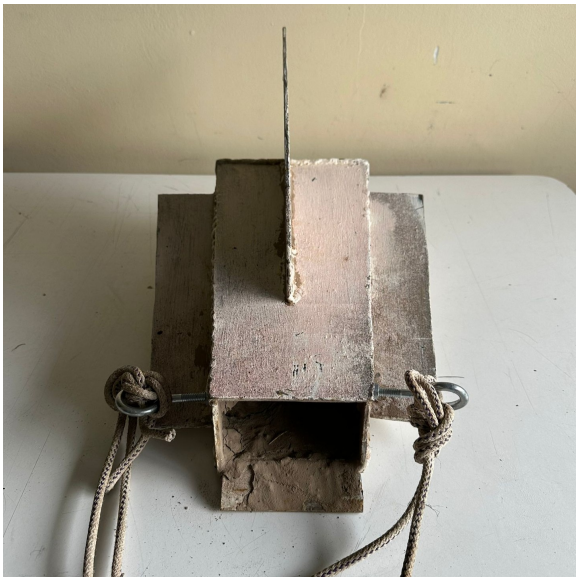

(b) Metal container used

(c) Oven to dry samples

Figure 3.5: Bed load measurements

A total of 7 samples from 4 different locations was collected. The first three locations were the cross sections around the extracting point in the bifurcation of the Paraná Guazú with the Talabera river. For each of these three cross sections, two samples were taken from the soil, one at 10 meters depth and one at 15 meters depth. The final sample was taken at 10 meters depth in the cross section upstream close to Puerto Ibicuy. All samples were sieved with six differently sized sieves, which took 10 minutes per sample. Before sieving, the samples were crushed to prevent particles from clustering. The sieving machine is presented in Figure 3.6 and the whole collection of annotated samples can be found in Appendix C.

Figure 3.6: Sieving machine

3.2.3. Locations of interest

The measurement campaign was spread out over two main locations. The first location contains a number of cross sections and sediment samples recorded at the confluence of the Talabera and the Paraná Guazú. Figure 3.7 shows a summary of the performed measurements. In total, three sections were studied with the following measurements per cross section:

- 2 ADCP profiles, yielding bathymetry, discharge and flow velocity;
- 2 bed load samples at different locations with different depths;
- 5 suspended sediment samples at a single location with varying depths.

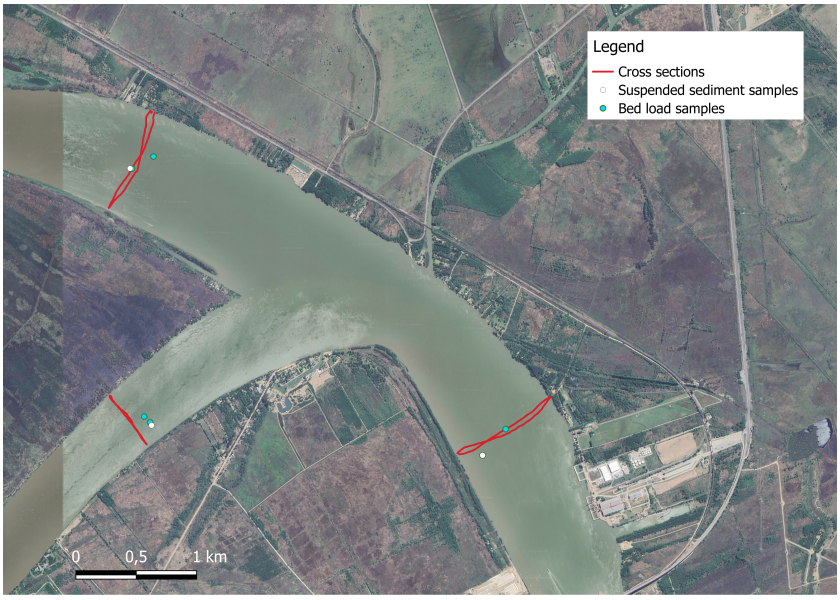

Figure 3.7: Measurement location confluence Talabera-Paraná Guazú (Google Earth, 2025)

The second location contains measurements at Puerto Ibicuy. Here, cross sections were measured in the vicinity of the confluence of the Ibicuy and the Paraná Guazú. In addition, the echosounder was active. Its recorded tracks can be found in Figure 3.8. The following results were found for location 2:

- 6 ADCP profiles: 2 profiles each for the most upstream and most downstream cross section, respectively. 1 profile for those in between;
- 1 bed load sample near Puerto Ibicuy;
- 2 longitudinal profiles along the confluence of Talabera and Paraná Guazú (dredging location), measured upstream and downstream to study dune migration. While navigating, GPS applications were used to make sure the paths were identical (see Figure 3.9).

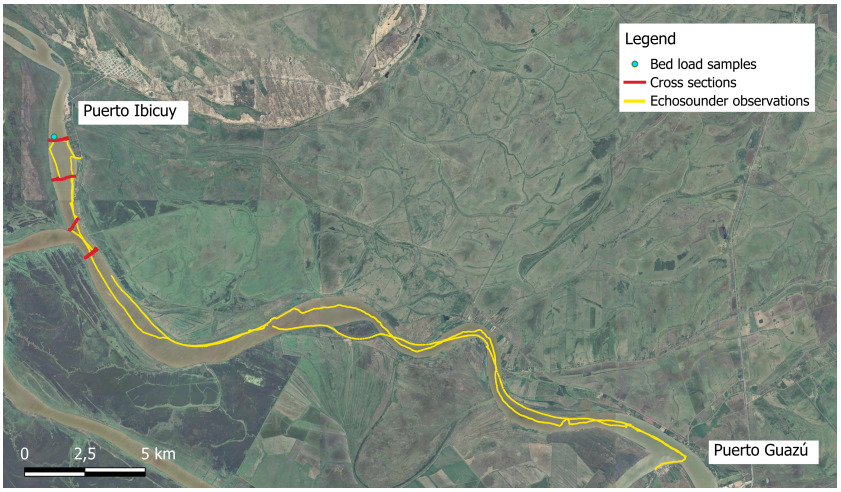

Figure 3.8: Measurement locations Puerto Ibicuy-Puerto Guazú (Google Earth, 2025)

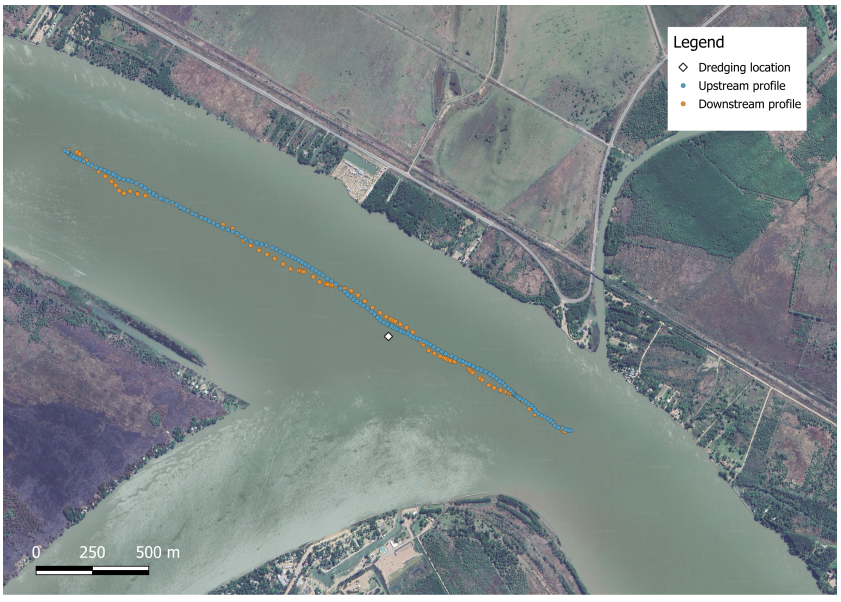

Figure 3.9: Measurement tracks of longitudinal profiles (Google Earth, 2025)

Bank erosion is a theme of significant importance to this study. During the field trip, critical locations of erosion were visited. These analyses were often accompanied with pictures taken by a drone. The chosen critical location for erosion is the river bank at camping 'La Blanqueada', situated in the outer side of the curve near Puerto Constanza as seen in Figure 3.10.

Figure 3.10: Location of camping La Blanqueada (Google Earth, 2025)

This would allow for a comparison with satellite data obtained from software such as Aqua Monitor from Deltares. This software was used to alert critical erosion points along the Paraná Guazú in a broader scale. After the first map data was obtained from the satellite imagery, it was deemed necessary to investigate actual areas and lengths of land that have been subject to water gains and losses. Then, the precise location of coast erosion was in turn analysed using Google Earth. The satellite database of Deltares was used for different time stamps, starting from 1984. The reason behind this is that the Deltares Aqua Monitor contains satellite imagery from 1984 until today. The choice was made to analyse the data in time batches of 10 years from 1985 until 2005, then in 5 years from 2005 to 2015, and lastly every 2.5 years in the last decade.

A preview of the maps can be seen in Figure 3.11, but the final analysis and conclusions are explained in Chapter 6. The green parts indicate water losses and the blue parts show water gains over time. For the whole collection of figures, see Appendix D.

Figure 3.11: Aqua Monitor water surface changes over the period 1985-2025 (Google Earth, 2025)

3.3. Modelling approach

This section explains the approach for the models used in the report. Firstly, a two-dimensional hydrodynamic model was set up in Delft3D software. The model was designed to simulate flow velocities, water levels, and bed shear stresses in the confluence area where dredging activities take place. Delft3D was selected because it provides a robust framework to simulate complex river systems, while maintaining computational efficiency.

The model setup is described in Chapter 7, including the generation of the bathymetry and computational grid. The hydrological inputs were based on field measurements taken during the campaign of 25–26 September 2025, complemented by discharge data from a one-dimensional HEC-RAS model provided by INA. Model calibration and sensitivity analyses were conducted to examine the influence of roughness and turbulence parameters on the simulated hydrodynamics and to evaluate model robustness. To increase efficiency, simulations were run on a computational cluster available at INA. The resulting Delft3D simulations provided spatially detailed insight into the flow structure, highlighting high-velocity zones, areas of recirculation, and regions with elevated bed shear stresses.

Secondly, a sheet pile model was developed. This resulted in a design that acts as a mitigation strategy against bank erosion. Prior to designing this specific solution, an overview of structural mitigation measures was compiled, and all potential options were evaluated. Subsequently, the design for the selected solution (sheet pile) was created. A flow chart was used to outline the modelling methodology. The flow chart shown in Figure 3.12 is divided into three phases. In the first phase, data analysis, literature research was performed to gain a better understanding of the critical locations and parameters necessary for the design. First of all, geological soil conditions including borehole findings were used to assess the different layers and the accompanying soil parameters. Further, hydraulic parameters including bathymetry were provided by INA to assess water level and river bed formation along the banks and finally, structural standards and regulations, the Eurocode, were used to perform structural verifications regarding the ultimate limit and the serviceability limit state.

In the second phase of the model, a sheet pile type was chosen and the gathered data was used to analyse the earth and hydrostatic pressures. Multiple design methods were reviewed, and finally the simplified Padfield and Mair method was chosen to perform the earth and hydraulic pressure analysis. The procedure for calculating the embedding depth of the sheet pile came from the simplified Padfield and Mair method, and the pressure diagrams for the earth and hydrostatic pressure were analysed in Python. By combining the earth and hydrostatic pressures, the balance of moments and the final embedding depth were calculated. Then, the acting components such as shear, bending, and shear buckling were compared to the resistance of the chosen sheet pile profile to access the safety of the design. The final phase includes structural verification of the profile and design, along with a 2D drawing of the final sheet pile design.

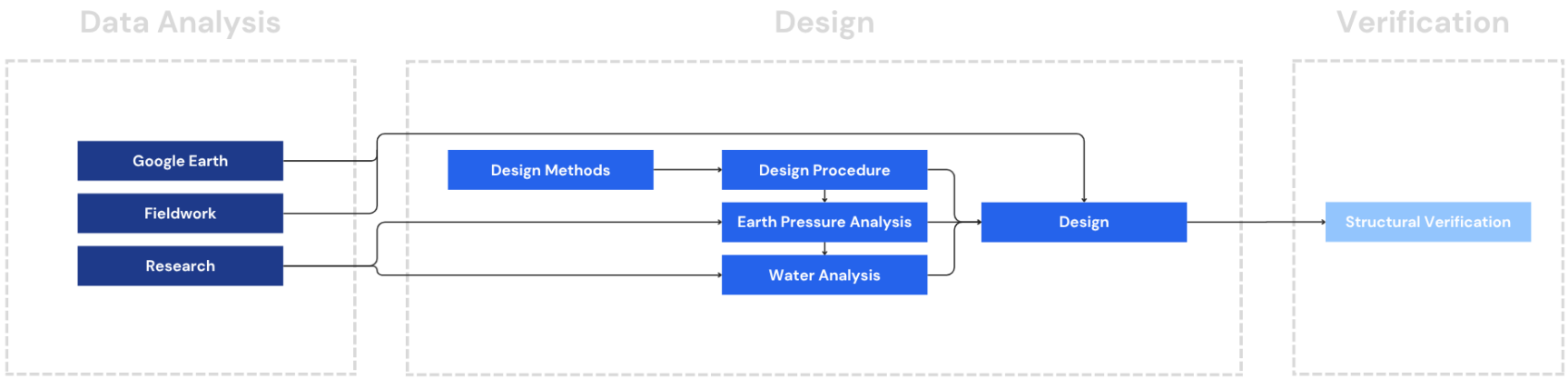

Figure 3.12: Flow chart sheet pile model

4

Stakeholders

Stakeholders play a crucial role in the study, offering valuable insights necessary to answer the research question. This chapter identifies and analyses the key stakeholders involved, presents the methodology for conducting interviews, and summarizes the main findings from these discussions. Finally, the stakeholder analysis is updated to reflect new information and its implications for the study.

4.1. Stakeholder analysis

This section identifies the relevant stakeholders related to mining practices in the delta. The interests and goals of these stakeholders are explained, and a power versus interest matrix is used to illustrate their relevance to the project.

4.1.1. Stakeholders description, interest, and power

All relevant stakeholders are identified for this project based on personal investigations and suggestions by INA staff. The complete overview is listed in Table 4.1 and is discussed in the following sections. Investigation of the relevant parties lead to a list of 8 stakeholders. The stakeholder descriptions are given in Table 4.2, and their interests and goals given in Table 4.3. All stakeholders were contacted to arrange interviews. In Appendix B, the typed out interviews can be found and the summarized results are given in Section 4.2.

Table 4.1: Stakeholders and their roles

Stakeholder	Role
Dredgers	Extraction of sand and gravel from shallow river areas.
Prefectura Naval Argentina (PNA)	Protection of rivers and maritime territory, and functions as coast guard and river police.
Agencia Nacional de Puertos y Navegación (ANPYN)	Oversight of signalling systems, dredging operations, and maintenance of the Main Waterway.
Ports	Handling, storing, and trading of goods and dredged material.
Fishers	Independent fishing activities for local and regional markets.
NGOs	Non-profit organizations advocating for environmental protection and community interests.
Landowners	Owners of riverfront or adjacent lands, may lease property for port or dredging operations.
Filmmakers	Filmmakers documenting trade and social impacts of the Paraná–Paraguay waterway.

Table 4.2: Stakeholder descriptions

Stakeholders	Description
Dredgers	Dredgers extract sand and gravel from the Paraná Guazú, ranging from small independent vessels to organized groups of boats (areneros) and larger hopper ships. They operate mainly in shallow areas where simple extraction methods are possible, transporting the material to nearby ports such as Ibicuy or Brazo Largo.
Prefectura Naval Argentina (PNA)	Prefectura Naval Argentina (PNA) serves as Argentina's coast guard and river police, operating under the Ministry of National Security. It is responsible for protecting rivers and maritime territory, ensuring safety, security, and regulatory compliance. In the Paraná Guazú, PNA plays a key role in monitoring dredging activity and maintaining lawful use of waterways.
Agencia Nacional de Puertos y Navegación (ANPYN)	Agencia Nacional de Puertos y Navegación is the authority in charge of implementing and controlling the signalling system, as well as overseeing dredging and maintenance along the Main Waterway, which includes the Paraná Guazú. As an independent agency within the Ministry of Economics, it ensures navigational safety and operational continuity of ports and waterways.
Ports	Ports serve as key logistical hubs for handling and storing goods extracted or transported along the Paraná Guazú. They provide the facilities where dredged sand is unloaded and traded, connecting local extraction activities with broader commercial markets. Their role is essential in enabling the flow of materials and supporting both regional trade and industrial supply chains.
Fishers	Fishers on the Paraná Guazú depend on the river's abundant fish resources, particularly migratory species such as sábalo, surubí, boga, pacú, and dorado. Most are independent artisanal fishers, selling their catch through middlemen, freezing plants, or informal markets. Although associations exist in the region, they hold little influence in decision-making over river use and management.
NGOs	Non-governmental organizations play a role in monitoring the social and environmental impacts of activities along the Paraná Guazú. They advocate for sustainable river management, community interests, and the protection of ecosystems affected by dredging and trade. Their involvement adds external oversight and pressure on both companies and authorities to adopt responsible practices.
Landowners	The landowners in the area have an interest in the sand mining activities. After all, some of them live in the area and experience negative consequences to their land. Jorge Moriatan is a local landowner that was contacted during the study to tell about his experiences related to dredging.
Filmmakers	Alejo Di Risio is a filmmaker who directed a documentary on the Paraná–Paraguay waterway, focusing on the impacts of trade along the river system. His work highlights the economic and social dimensions of waterway use, bringing public attention to stakeholders and their activities. He was also contacted during this study to provide additional insights into stakeholders and businesses connected to the waterway.

Table 4.3: Stakeholders interest and goal

Stakeholders	Interest	Goal
Dredgers	Access to shallow river areas for sand extraction.	Sell extracted sand to nearby ports and local markets for income.
Prefectura Naval Argentina (PNA)	Safety and security of rivers and maritime territory.	Enforce regulations, monitor dredging, and ensure lawful use of waterways.
Agencia Nacional de Puertos y Navegación (ANPYN)	Oversight of navigation safety and waterway infrastructure.	Implement signalling systems, maintain dredging operations, and secure efficient transport.
Ports	Handling and trading of goods and dredged material.	Strengthen logistical capacity and support regional trade flows.
Fishers	Access to fish resources in the Paraná Guazú.	Sustain livelihoods through artisanal fishing and market sales.
NGOs	Environmental protection and community rights.	Promote sustainable river management and hold stakeholders accountable.
Landowners	Protection of riverfront property and prevention of erosion, flooding, or land loss.	Safeguard land rights and preserve long-term property value.
Filmmakers	Research and documentation of waterway dynamics.	Raise awareness through film on trade, impacts, and stakeholder activities.

4.1.2. Stakeholder's influence

After identifying stakeholders, it is important to evaluate their power and interest in the project. This is visualized using a power versus interest matrix, with power on the vertical axis and interest on the horizontal axis. Analysing this matrix informs strategies to approach specific stakeholders. In addition to interest and power, a support-opposition matrix is analysed to visualize the likelihood that a certain stakeholder will support or oppose the project.

The power versus interest matrix is divided into four parts, illustrated in Figure 4.1. The quadrants represent the power and interest that a particular stakeholder has (low or high). High power and high interest are referred to as the key players, and these will be of most importance to the project. Next, the quadrant with low power and high interest is considered the subject. Those with high power but low interest are determined as the context setters. The context setters are not closely related to the project, but can be of great importance. The quadrant of low power and low interest is recognized as the crowd.

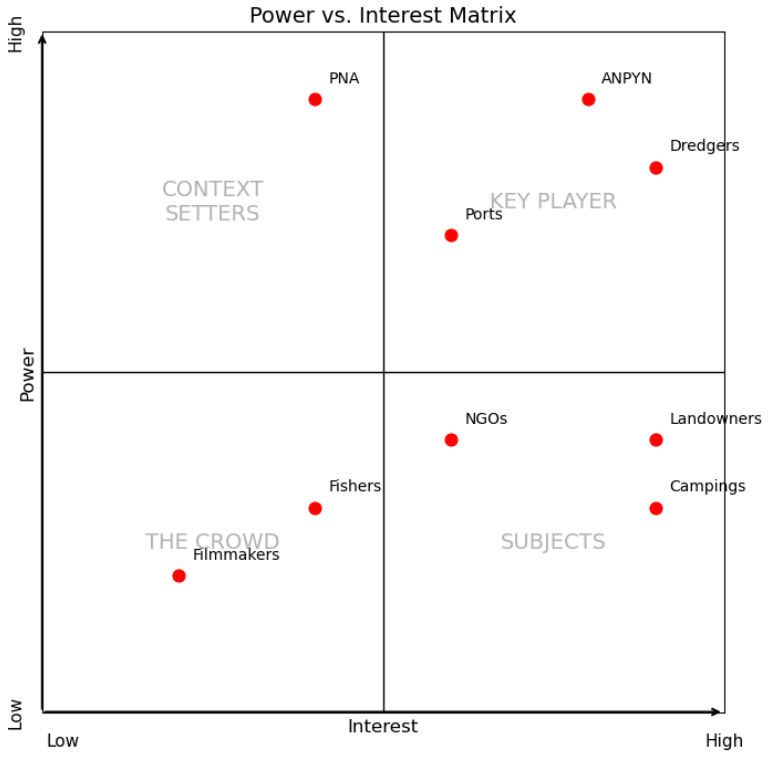

Figure 4.1: Power vs. Interest

The key players, stakeholders with both high interest and power, are of great importance to the project. Among this group are actors with a great economic interest in the dredging activity: the dredgers and the ports. They are commercially organized, which is why their power is also high. Finally, the ANPYN, being the responsible government agency, is an actor of great interest and power. This is the most important group for project success. These stakeholders must be actively engaged and managed through continuous and tailored communication. They should be consulted in decision-making and kept up to date on risks, challenges, and progress. Building strong relationships with them is vital to ensure their ongoing support and alignment with project goals.

Context setters have high power but relatively low interest in the project. Within this group, the PNA can be found. Being a major government organization responsible for safety and compliance with maritime laws, they have significant authority and influence. However, their focus is mainly on guarding the safety on the water, more than supervision of the dredging activities. The context setters are of moderate priority to the project. Since they hold power, it is important to prevent dissatisfaction that could derail progress. The dealing strategy should focus on maintaining their satisfaction without overwhelming them with details. Periodic check-ins and concise reports or briefings can help with this. This ensures they feel respected and considered, as their influence may become critical if project circumstances shift.

On the bottom right of the graph, one can find the subjects, a group that holds high interest in the project but has less power. Here the NGOs, landowners and campings can be found. Because of ideological beliefs or personal concerns, their interest in the project is high. However, due to a limited degree of organization their power is not substantial. This is another group of moderate priority to the project. The stakeholders care deeply about the project but lack significant power to influence its direction. Any enthusiasm from this group can be valuable and should thus be maintained and leveraged if useful. However, it is perhaps more likely for stakeholders in the group of subjects to be opposed to the project. In this case, their high level of interest may manifest as opposition or criticism. Therefore, it is important to actively listen to their concerns and provide information to address any misconceptions or fears. This way, any opposition can be managed and maintained.

Finally, there is the crowd. Stakeholders in this group are characterized by a low power and low interest in the project. The journalists and fishers fall under this group: they are largely unorganized and, although sometimes important, sand mining is not their main concern. This group is the least important to the project's outcomes. Since their involvement is not crucial, one should avoid overloading them with unnecessary details and should instead only monitor them. It is possible to update the crowd on important progress as to prevent disengagement or frustration.

The support-opposition matrix is divided into four parts and a linear trend line is based on the points given to the stakeholders. On the vertical axis, the division between support and opposition is made, while on the horizontal axis, the power is represented. For the degree of power, the power versus interest matrix, in Figure 4.1 was used. The stakeholders support or opposition for the project was based on the interviews held during the field trip and is shown in Figure 4.2.

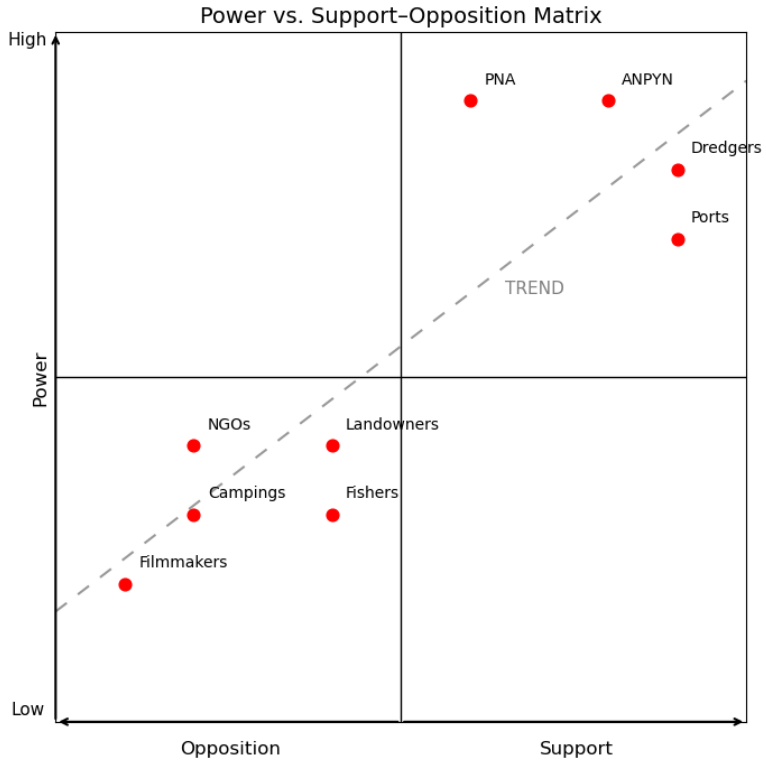

Figure 4.2: Power vs. Support-Opposition

With multiple stakeholders who have different interests and goals, it is of importance to know the competing interests. Among the various stakeholder interests, the focus will be on the competing economic and environmental interests. The first competing interest is the economic growth of the area versus environmental protection. The dredging activities of the Paraná Guazú and Ibicuy stimulate the economic growth of the area and are one of the income streams for dredgers and ports. These economic benefits are prioritized over the environmental protection of the river and the river banks. Environmental protection is of interest to fishers and NGOs operating on the Paraná waterway. Their goal is to minimize the environmental impact of dredging. This leads to a competing interest, as dredging will have effects that come at the expense of the environment.

A second competing interest is safety and regulations versus profits made by dredging activities. For business-related stakeholders, the interest in making profits is of greater value than the safety regulations created by the governmental organizations. The PNA and ANPYN regulate the safety of waterways, which can impose restrictions on the amount of sand a dredger can extract or the frequency limit for dredging activities. This can be a concern, as the regulations will cut profits of ports and dredgers, which lie between the strict enforcement and the loosely regulated operations of dredgers.

Another area of conflicting interests can be summarized by local livelihood versus local development. The dredging of the river will lead to income for the ports and dredgers, which, through taxes, can attribute to development of the region. This can be of interest to local businesses and communities. On the other hand, there is the local livelihood that may be of even greater importance to the community. As mentioned before in Chapter 2, dredging can reduce water quality, fish spawning and land loss, among other things. A reduction of fish in the river will harm food security in the region and is even more problematic for the fishers, since this directly hurts their businesses and livelihood. Likewise, land loss through increased erosion negatively affects landowners, reducing both property value and security.

Finally, a fourth conflict can be identified that deals with property rights on the one hand and public river use on the other. Some stakeholders, such as landowners and ports, have an interest in protecting their private landholdings near the dredging site. After all, protecting their property is of economic interest to them. However, some other actors are more interested in maintaining open access to the waterways and shorelines. This is for instance the case for the fishers: access to the river and its sides is of crucial importance to their businesses. NGOs are likely to engage in this conflict as well, since public use of the river and its resources is tied to community rights and local well-being.

4.2. Interview results

During the fieldwork, 10 interviews were conducted with the stakeholders listed in Table 4.3. Some interviews were set up during the field trip and were not contacted before. Some of the stakeholders who were contacted by email did not respond, namely Puerto Guazú and PNA. The responses were recorded and these raw results are given in Appendix B. In this section, the responses are grouped by theme.

On Wednesday, the 24th of September, interviews were conducted at the local Fisher's club (Club de Pescadores Olivos), the port manager at Puerto Ibicuy, the Mayor of Ibicuy and a landowner in the area of Ibicuy. The caretaker and the landowner showed multiple erosion banks around the river. On Thursday 25 September, interviews were conducted with the Municipality of Zárate, a local sand miner, and a camping owner. The local sand miner showed the mining process on his vessel and in the port and the land owner showed their land. On this day, several drone images were also made. Finally, on Friday 26 September, the plant manager of the YPF dry sand mine and another person from the municipality of Zárate were interviewed.

Table 4.4: Overview of carried out interviews

Date	Occupation	Location	Language
24-09-2025	Caretaker at Fisher's club	6RJF+C7, Ibicuy, Entre Ríos	Spanish
24-09-2025	Port manager at Puerto Ibicuy	6RRC+VC, Ibicuy, Entre Ríos	Spanish
24-09-2025	Mayor of Ibicuy	7R5R+4G Puerto Ibicuy, Entre Ríos	Spanish
24-09-2025	Landowner (Jorge)	7R5R+4G Puerto Ibicuy, Entre Ríos and his private land	Spanish
25-09-2025	Municipality of Zárate	GLO, Av. Rivadavia 751, B2800GLO Zárate Provincia de Buenos Aires	Spanish
25-09-2025	Dredger	Caminera a Ibicuy, Entre Ríos	Spanish
25-09-2025	Camping owner	Ruta 45 Km 5, E2823, Entre Ríos	Spanish
26-09-2025	Plant manager YPF	7XPC+72 Parnacito, Entre Ríos	English
26-09-2025	Municipality of Zárate	Leandro M. Alem 780, Zárate	Spanish

4.2.1. Dredging activities

The nature of the dredging activities was discussed in nearly all interviews and different perspectives came forward. First of all, stakeholders provided many insights on the scale and development of dredging in the Paraná Guazú. The caretaker at the Fisher's Club didn't perceive any increase in recent years, while nearby landowners recalled that the number of dredgers used to be higher, with only two remaining active today. The mayor of Ibicuy confirmed this trend, explaining that most dredging vessels left the Ibicuy after municipal taxes on sand extraction were raised. At the Port of Ibicuy, the administrator remembered that small dredgers, no longer than twenty meters, once handled sand but have since

disappeared; dredging activities there have ceased altogether and moved to a different port (Puerto Constanza). A private dredger entrepreneur described his own ship, the Vizcaíno 978, which has been prepared for operation after years of administrative delay.

Stakeholders also offered insights into the purposes for which dredged sand is used. According to the mayor, river sand is generally used for construction materials and, in some cases, glass production. The port administrator confirmed that the sand once handled in Ibicuy was also directed toward the construction sector. The dredger entrepreneur described a mixed market, with sand used primarily for concrete, but also increasingly sold to the fracking industry when sufficiently fine-grained. The YPF mine manager confirmed that the company uses river sand for fracking purposes, although not from the area of interest.

Overall, stakeholders agreed that construction is the traditional destination of dredged sand. However, multiple stakeholders noted a declining demand for construction sand in recent years, due to the slow-down of public building projects. In contrast, the demand for fracking sand has been growing steadily, as highlighted by the YPF manager. The dredger indicated that selling to YPF is a viable option.

4.2.2. Effects of dredging

Stakeholders expressed contrasting views on the ecological and geomorphological impacts of dredging in the Paraná Guazú. Mostly the impacts on fish populations and bank stability were discussed. The caretaker of the Fisher's Club reported a noticeable decline in fish populations. He did not link this directly to the dredging activities, but instead pointed to contamination from agricultural fertilizers. In contrast, a municipal representative from Zárate questioned the narrative of decline, arguing that complaints about fewer fish reflect generational shifts among fishers rather than an actual reduction. When it comes to riverbank stability, landowners described severe erosion of up to thirty metres per year, which they attributed to the activities of dredging vessels and passing cargo ships. The caretaker added that vegetation removal near the club increased local erosion. In contrast to this, the mayor of Ibicuy downplayed the role of dredging, attributing bank collapses in his jurisdiction to the natural flow of the river. Furthermore, in 2011 there was a quay wall collapse in the Port of Ibicuy, but the port manager claimed that this was an accident and not due to the sand extraction activities.

4.2.3. Dry sand mining

The significance of dry sand mining activities emerged from stakeholder interviews and field observations. Therefore, the topic naturally came up in almost all interviews. Stakeholders consistently underlined the large scale and rapid growth of dry sand mining in the region. The caretaker at the Fisher's Club estimated that around 500 trucks leave the area each month carrying 40–45 tons of sand each, noting that this number has doubled compared to when he started his job 4.5 years ago. The mayor of Ibicuy described an even larger scale, reporting that approximately 350 trucks transport some 9,000 tons of sand daily. These impressions were confirmed by the YPF plant manager, who stated that his mine alone extracts about 120,000 tons of sand per month and that output is expected to increase in the coming years. He also referred to geological surveys indicating sufficient reserves to sustain regional extraction for 88 years. This number was confirmed by the mayor, who added that in areas of intense extraction this would be around 40 years.

Multiple effects of these activities were named by interviewees. The caretaker observed that waste from washing processes flows back into the river, making the water dirtier, while the removal of sand on land reduces drainage capacity and therefore increases flooding risks. He and the mayor both emphasized the damage caused by heavy truck traffic, which worsens road conditions and leads to complaints from locals. The mayor added that judicial interventions have forced authorities to introduce extraction limits and monitoring mechanisms, as uncontrolled mining had raised public concerns.

Stakeholders emphasized that the dominant purpose of dry sand mining in the region is to supply the fracking industry. Both the mayor, port administrator, dredger and the Fisher's club caretaker indicated that most or all dry sand is sold to YPF. The YPF plant manager explained that the sand extracted is transported primarily to Añelo, in the province of Neuquén, where it is used in fracking operations. He highlighted that this sand is very rich in quartz, and thus fine-grained and highly resistant, which makes it suitable for use as proppant, to keep fractures in the shale open during extraction. According to him, these properties are not easily substituted by sand from different locations or other alternatives.

Some stakeholders recalled that also the dry sand was traditionally associated with construction or in some cases glass production, but they acknowledged that these markets have become secondary to the fracking. Part of this is the decreasing demand for construction sand. The port administrator, the YPF mine manager and the dredger all indicated that demand from construction has declined due to the reduction of public building projects. The demand for sand to be used in fracking, on the other hand, is constant according to the dredger and is even increasing according to the YPF manager.

4.3. Updated stakeholder analysis

In Section 4.1, an overview of stakeholders was given and each stakeholder's power, interest and support was determined to create a power vs. interest matrix and power vs. support-opposition matrix. Following the stakeholder interviews, some updates to these matrices were necessary.

First of all, in Section 4.1, the municipalities were not named as a stakeholder. The assumption was made that ANPYN, the institution responsible for keeping the Main Waterway navigable, was the only government organization with interest in the dredging matters. After an interview with the mayor of Ibicuy, it has become clear that this is in fact not true. Municipalities have an interest in the dredging activities and are therefore included in the updated matrices. The interest of the municipality is to prevent hindrance to its civilians and to allow for access to the river and therefore their goal is to balance technical river maintenance (via dredging) with the well-being and daily life of civilians and people in the region.

In Figure 4.3, the updated power versus interest-matrix is shown. After interviewing the port administrator, it became clear that most ports in the area don't handle sand anymore. Therefore, their interest and power has decreased as compared to the first assessment. Secondly, the dredger's power was also reduced, as the dredger explained in the interview that the permit procedure was more difficult than expected. Therefore, their power should be reduced compared to the more powerful government organizations. On the other hand, the mayor shared insights on how tourist's complaints about dredging vessels caused the municipality to raise taxes on the activity. This caused dredging to stop fully in the Ibicuy area, a clear sign that the power of the tourism industry, i.e. the campings, is greater than what was portrayed in Chapter 4. Finally, the power and interest of the municipality are the same as that of the ANPYN.

In Figure 4.4, the updated power vs. opposition-support-matrix can be found. The powers are updated in the same way as in Figure 4.3 and the degree of opposition was changed for the landowners and campings. From the interviews, many concerns about the dredging operations arose, such as sound pollution and erosion. Many voiced their opposition to the dredging clearly, which is why these stakeholders were moved to the left on the opposition/support scale. For the dredgers and ports, the same degree of support still holds, for monetary reasons. The municipality is opposed to the dredging, as can be seen from the mayor's statements on the discontinuation of dredging.

In Figure 4.4, it can be seen that the new trend is flatter than the original one. This is a consequence of the fact that dredging operations have not increased in recent years, as opposed to the expectation, and have in fact been completely stopped on the Ibicuy.

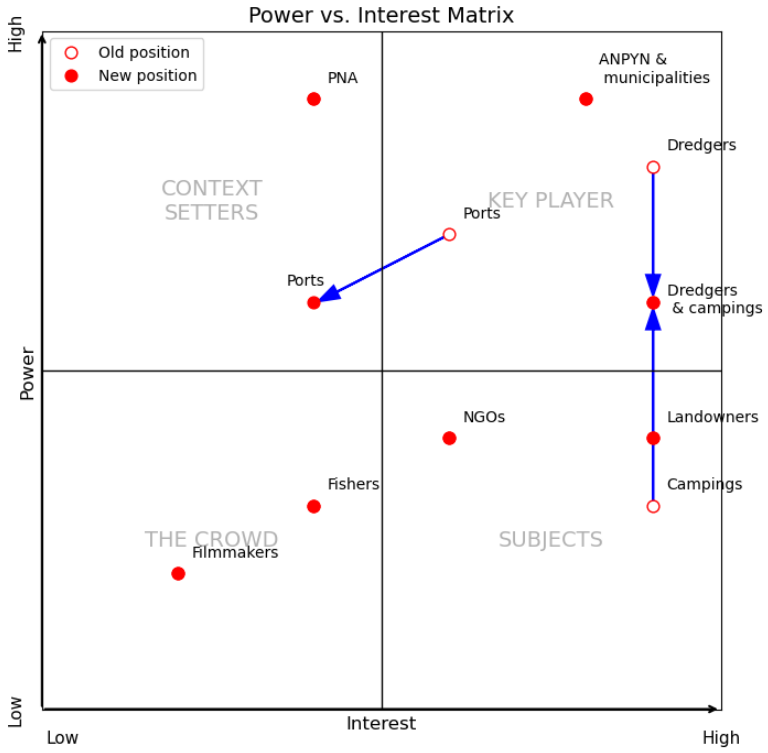

Figure 4.3: Updated Power vs. Interest

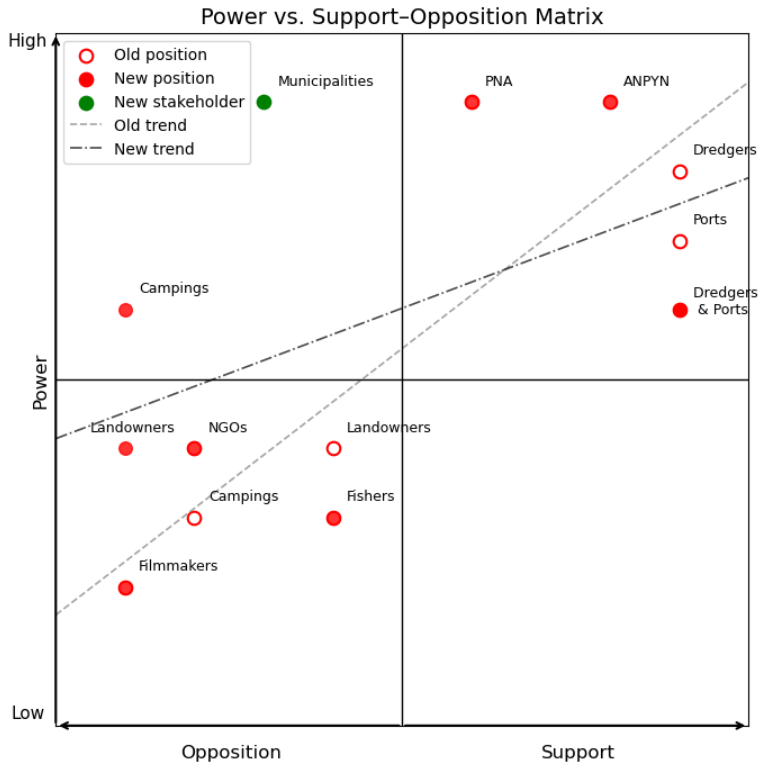

Figure 4.4: Updated Power vs. Opposition-Support

5

Sand extraction

Sand extraction in the Lower Paraná Delta involves both dredging activities in the river and dry mining on land. Therefore, dredging activities as well as dry sand mining practices are considered. The purpose of this chapter is to create an assessment of the extraction quantities and to evaluate the relative importance of both types of sand extraction.

5.1. Dredging activities

This section examines the impact of dredging on the sediment balance of the study area by estimating the volumes extracted from the river. The analysis is based on AIS vessel tracking data and extraction permits submitted to INA.

5.1.1. Vessel positioning information (AIS)

Using MarineTraffic it was found that two dredgers currently operate on the Paraná Guazú between Ibicuy and Brazo Largo: the Comercio Segundo and the E.M. Arroyo N1. The Comercio Segundo has a length of 30 m, a width of 7 m, a draft of 1.3 m, and an approximate cargo hold of 195 m^3. The E.M. Arroyo N1 has a length of 39 m, a width of 8 m, a draught of 2.8 m and an approximate cargo hold of 476 m^3. Using a sand to water ratio of 3:1 for the dredged slurry, the amount of sand dredged is 150 m^3 and 360 m^3 respectively per cargo. The tracks of the two vessels obtained from MarineTraffic are shown in Figure 5.1 and Figure 5.2.

Figure 5.1: Track of the *Comercio Segundo* (Marine Traffic, 2025)

Figure 5.2: Track of the *E.M. Arroyo N1* (Marine Traffic, 2025)

The AIS data for these two vessels is obtained from MyShipTracking, which is used to determine the location of dredging and the average daily number of trips. The dredging location of the two vessels

is shown in Figure 5.3. It can be seen that both dredgers operate in the same area. This can be explained by the bathymetry shown in Figure 5.4, which shows a reduced depth near the junction of the two navigable channels. At this location the flow velocity is lower, causing sediment to settle and thus creating a sandbar. From the AIS data it was concluded that both dredgers make three trips per day.

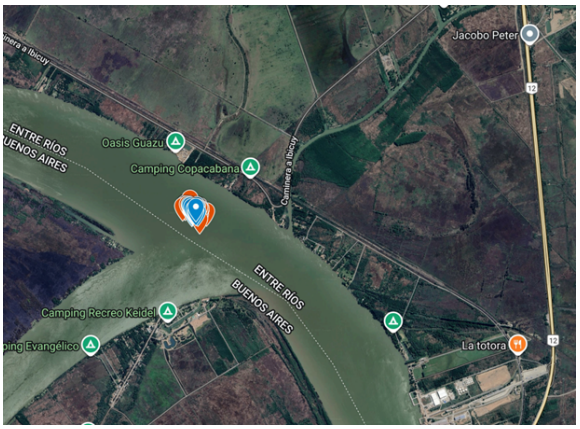

Figure 5.3: Dredging location (Google Earth, 2025)

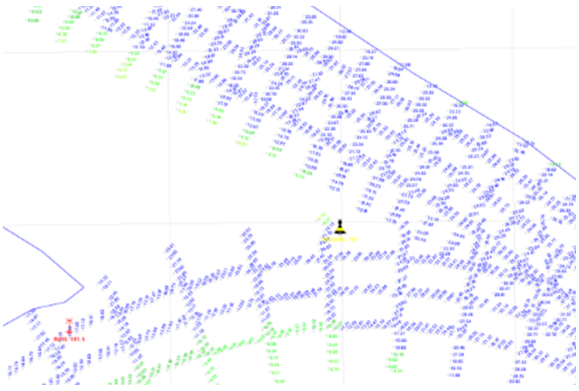

Figure 5.4: Bathymetry (Agencia Nacional de Puertos y Navegación, 2025)

Table 5.1: Sand transport details per vessel

Vessel	Cargo hold [m^3]	Sand volume [m^3]	Trips per day	Volume per month [m^3]
Comercio Segundo	195	150	3	9000
E.M. Arroyo N1	476	360	3	21600

5.1.2. Extraction permits

A total of 33 permits were collected for the Paraná Guazú and 43 for the Ibicuy. On the Paraná Guazú, four permits were issued for channel maintenance, while the remainder concerned sand extraction. For the Ibicuy, all permits were related to extraction activities. The analysis shows that the requested volumes in the Ibicuy are considerably larger than those in the Paraná Guazú. This is, even though the section of the Ibicuy considered here is much shorter in length: Paraná Guazú stretches from km 124.0 to km 232.0, Ibicuy from km 232.0 to approximately km 249.0 for the area of interest (Administración General de Puertos S.A.U., 2023).

It is important to note that the end dates of contracts are unknown. While the requests specify monthly dredging quantities, they do not indicate the duration of the works. As a result, a detailed quantitative assessment cannot be made. For the present analysis, all requests with fixed monthly volumes are assumed to extend over 12 months. The second assumption is to record a single value for the requested volume, when information about monthly or yearly occurrence is lacking. This allows for a comparison between the two river sections of yearly extraction volumes, as shown in Figure 5.5. As mentioned, sand extraction activities on the Ibicuy are large compared to Paraná Guazú, with a maximum recorded yearly volume of almost $4 \cdot 10^6$ m^3.

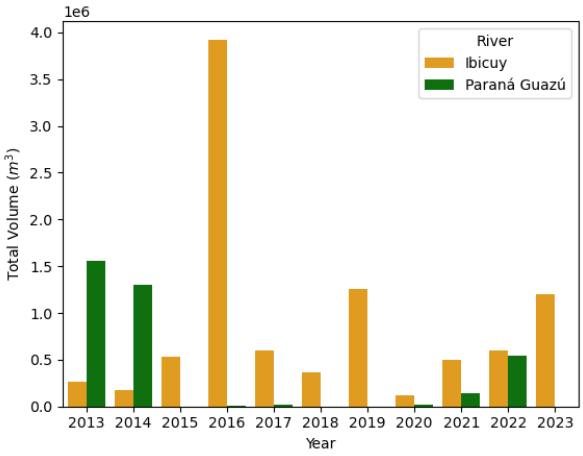

Figure 5.5: Yearly dredging volumes as found in extraction permits

5.1.3. Estimated sand extraction

This section defines the river sand extraction volumes, values which can be useful for the estimation of the sediment balance. Based on the AIS data, permits and stakeholder interviews, the following uncertainties were considered in determining a representative value:

- Not every vessel in the area is equipped with an AIS transponder, meaning that possibly not all active vessels were identified. However, the number of vessels as found by analysis of the AIS data was in agreement with the number of vessels observed during the fieldwork and statements by stakeholders.
- No historical AIS data was available, such that the data was registered for only a short period of time.
- The extraction permits do not mention the duration of the contract.
- Whereas permits imply that most of the activity occurs on the Ibicuy, AIS data and fieldwork observations indicate that the activity on the Paraná Guazú is higher. Furthermore, stakeholders stress that activity on the Ibicuy has ceased, as described in Section 4.2.1.

A rough estimate can be found by calculating the mean annual volume for the total system of interest (i.e., Ibicuy and Paraná Guazú) based on the extraction permits. To make a comparison with the monthly values in Table 5.1, this yearly value is reduced to a monthly value by dividing by 12 months. The described approach yields the following value for dredged sand volumes, based on available permit data:

$$V_{sand,yearly} = 1193923\ m^3 \tag{5.1}$$

$$V_{sand,monthly} = \frac{V_{sand,yearly}}{12} \approx 100000\ m^3 \tag{5.2}$$

Summation of the volumes in Table 5.1 gives a monthly total of 30600 m^3. Considering that extraction permits are surrounded by the uncertainties listed before and considering that permit data of the last 2 years is unavailable, this AIS-based extraction value will be used in the sediment balance. After all, as outlined in Chapter 4, recently almost all dredging activities were stopped on the Ibicuy, and the observations from AIS data align with observations during the fieldwork. A value of 100,000 cubic meters per month therefore does not align with the current situation, which is why the first value is chosen to be representative.

5.2. Dry sand mining

As mentioned in Chapter 4, many stakeholders stressed the relevance of dry sand mining related to fracking for the Lower Paraná Delta region. In this section, context to these claims is given. The history

and development of fracking in Argentina is discussed, followed by the related sand mining. Then, geological properties of the area of interest are looked into as well as the characteristics of dry sand used in fracking. Finally, the effects of dry sand mining are discussed.

5.2.1. Fracking in Argentina

For much of its history, Argentina was regarded a modest oil producer, struggling to meet its own energy demands. This perception shifted with the 2010 discovery of the Vaca Muerta shale formation, located in the Neuquén basin in Patagonia. The Argentine energy company YPF then identified approximately 150 million barrels of recoverable oil in the field, which was welcomed as a new source of hope for economic stability by some, among whom the former president (Krauss, 2011).

The discovery was followed by significant foreign investment. More exploration was done and now it is clear that Argentina possesses the world's fourth-largest shale oil and second-largest shale gas reserves (International Trade Administration, 2025). Today, around thirty companies hold licenses to exploit various areas of the Vaca Muerta basin. The biggest operator is a consortium of YPF, a majority state-owned Argentine energy company, and Chevron, an American energy company. Other players are Tecpetrol, Total, Dow Petrochemical, Petronas, Shell, Gazprom, and ExxonMobil (Foglia, 2023).

The Nuequén basin is located in the provinces of Neuquén, Mendoza, and Río Negro in the South of Argentina and has been an important basin for oil and gas since more than a century. Production started in 1918 and in 2004, 45% of Argentinian oil production and 61% of its gas production came from this area (U.S. Energy Information Administration, 2013). This was done through conventional methods, but after the discovery of the Vaca Muerta shale basin, fracking has become increasingly important for the region and the country. The Vaca Muerta shale consists of finely-stratified black to dark grey shale and lithographic lime-mudstone and is 60 to 520 m thick. Estimates are that the formation contains 16 billion barrels of technically recoverable oil and 8722 billion cubic metres of technically recoverable gas (U.S. Energy Information Administration, 2013). Since Vaca Muerta is a shale reservoir, all oil and gas from this deposit is extracted by fracking.

As seen in Figure 5.6, oil production in Argentina has steadily increased since 2020, driven by a rising production of the Vaca Muerta formations. After the exploration in 2010, oil from Vaca Muerto as a share of total Argentinian oil production has expanded from virtually 0% to 55% today. In addition to that, Vaca Muerta now accounts for 47% of gas supply (International Trade Administration, 2025).

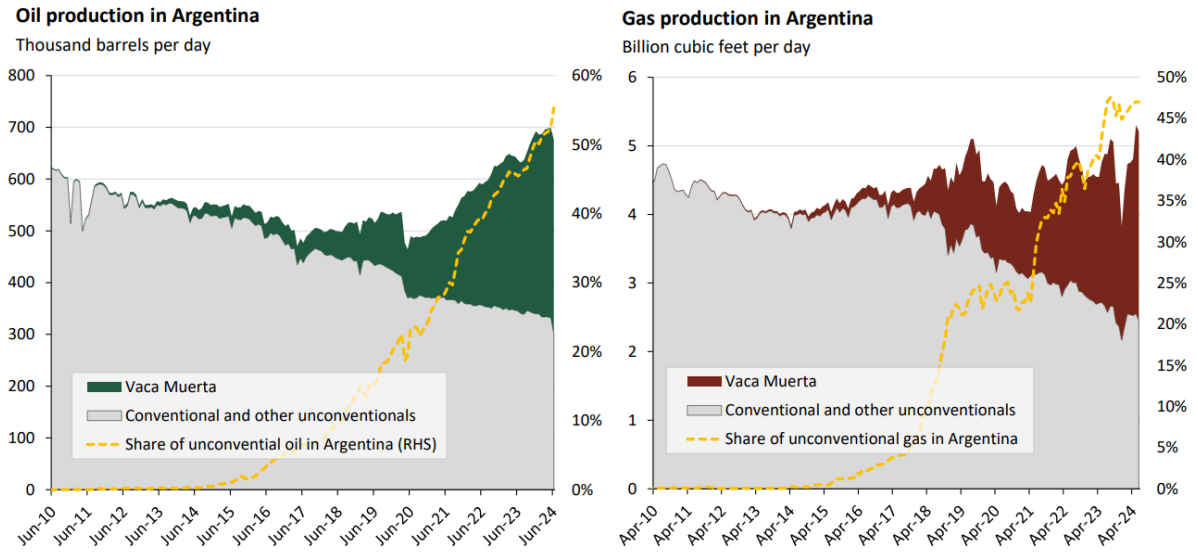

Figure 5.6: Oil and gas production in Argentina (International Trade Administration, 2025)

5.2.2. Sand mining practices

As outlined in Chapter 2, sand is used in fracking practices. The sand used for fracking is mined or imported. In Figure 5.7, the mined silica sand masses as well as the imported masses are given for Argentina. This includes sand used for fracking but also other purposes.

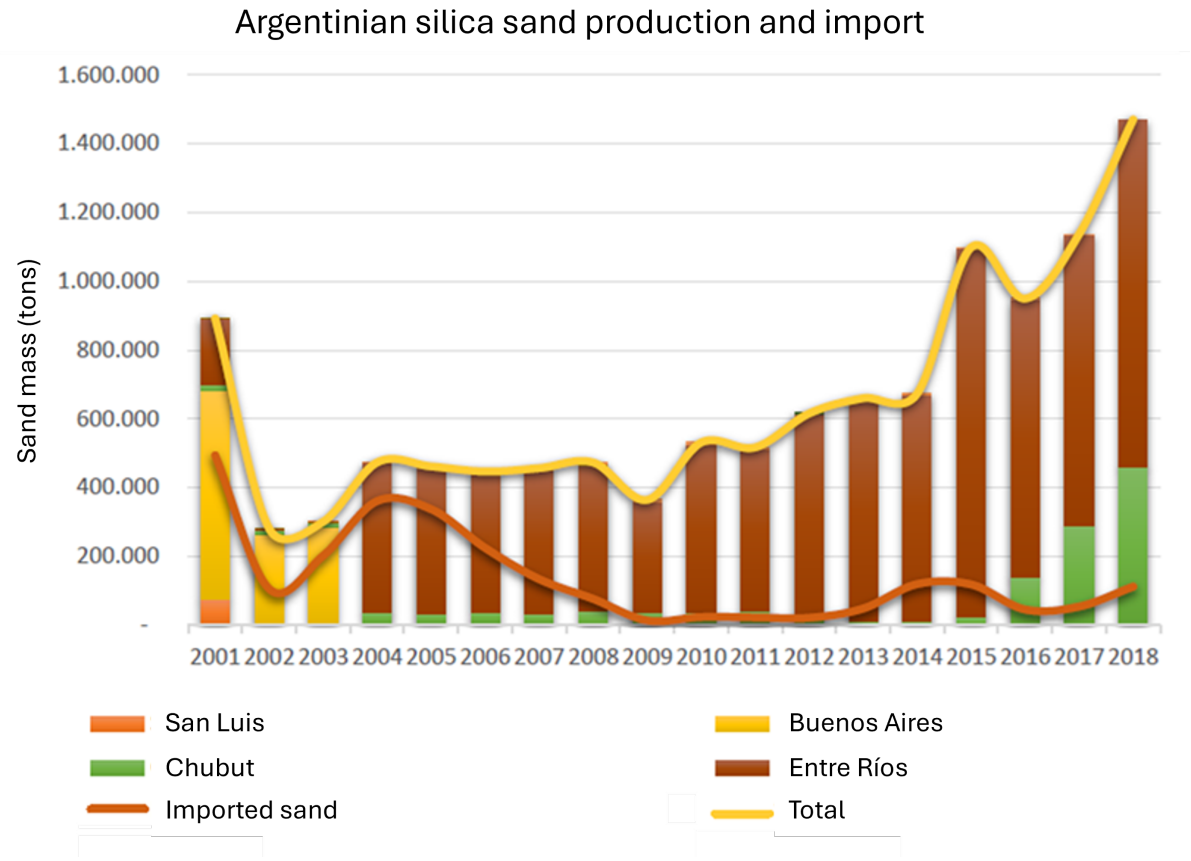

Figure 5.7: Quantities of sand mined in Argentine provinces (Secretaría de Política Minera, 2019)

In 2018, approximately 1.5 million tons of sand were extracted and imported in Argentina, with more than 90% of used sand from national territory. Of the nationally mined sand, 69% are originally from Entre Ríos (Secretaría de Política Minera, 2019). Specific numbers for the period following 2018 are unavailable, but in 2020, the amount of sand needed in Argentina was 3.5 million tons (Novas, 2022).

Historically, silica sand was used as a raw material for the glass industry but since the introduction of fracking, sand miners have found a new attractive market for their product. The exact volumes of sand used for fracking versus the volumes used for other purposes are unknown. However, as seen in Figure 5.7, the rising trend in sand production can be observed only for the past years, after the discovery of Vaca Muerta.

5.2.3. Sand mining in the Lower Paraná Delta

During the fieldwork and by using satellite data, the locations of sand mines in the lower Paraná Delta were identified. A total of 11 locations were found, 10 of which fall within the department of Ibicuy. In Figure 5.8 the locations are shown and in Figure 5.9, the aerial view is given for three sand mines in the department of Ibicuy.

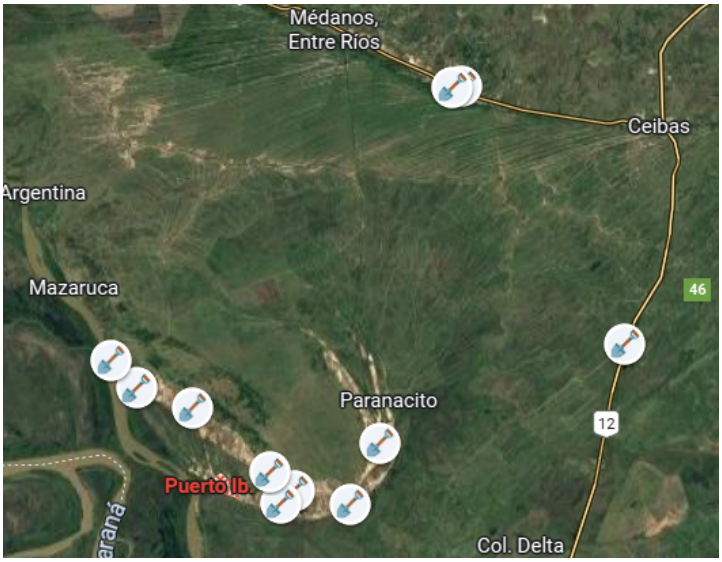

Figure 5.8: The identified locations of sand mines (Google Earth, 2025)

Figure 5.9: Examples of sand mines in the department of Ibicuy (Google Earth, 2025)

Of all departments where sand mining takes place, the most intense sand mining activities are carried out in Ibicuy. Previous reports estimate that 1.250.000 tons of sand were mined in Ibicuy alone in 2022 (Foglia, 2023). This number is comparable to the total national sand mining volume in 2018.

In Ibicuy, Cristamine, Aresil S. A., YPF, La Chola II, NRG Argentina, San Marcos Trading, and QSand are among the companies that operate sand mining facilities. Sand mining companies that have been around for longer originally only sold their product to the ceramics and glass industry, but at present many of them exclusively sell to the oil/fracking sector. Recently, more companies opened mines after the demand for fracking sand started to rise. An example is La Chola II, a company with 50 years of experience in river sand mining, which opened a dry sand mine in 2016: Silicatos Islas del Ibicuy. From here, they transport sand to YPF, the biggest player in Argentina's fracking industry (Foglia, 2023).

Mined sand gets transported by trucks to Añelo, a town in Neuquén that forms the heart of the Vaca Muerta fracking activities. The route from Ibicuy to Añelo is 1283 km long and takes around 20 hours, including a 2 hour delay for handling of goods (Secretaría de Política Minera, 2019). The route is shown in Figure 5.10.

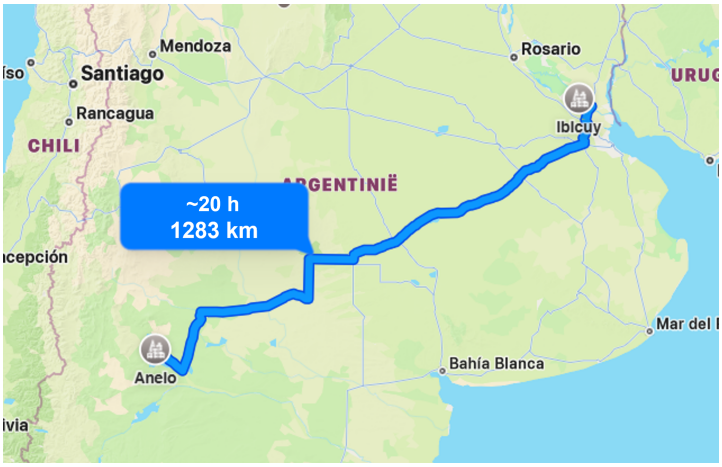

Figure 5.10: The route from Ibicuy to Añelo (Apple Maps, 2025)

5.2.4. Geological conditions

To understand the dry sand mining activities, the characteristics of the subsoil in the Lower Paraná Delta were investigated. This section intends to combine all the available information regarding the subsoil in the investigation area. First of all, as mentioned in Chapter 2, one expects to find relatively soft soils (sands) and very soft soils (clay and peat).

A study conducted by Cavallotto et al. led to a morphological map of the Paraná Delta. In the study, a more detailed geological profile was made for two cross sections, one of which is relevant to the area of interest. The cross section along with the area of interest is shown in Figure 5.11.

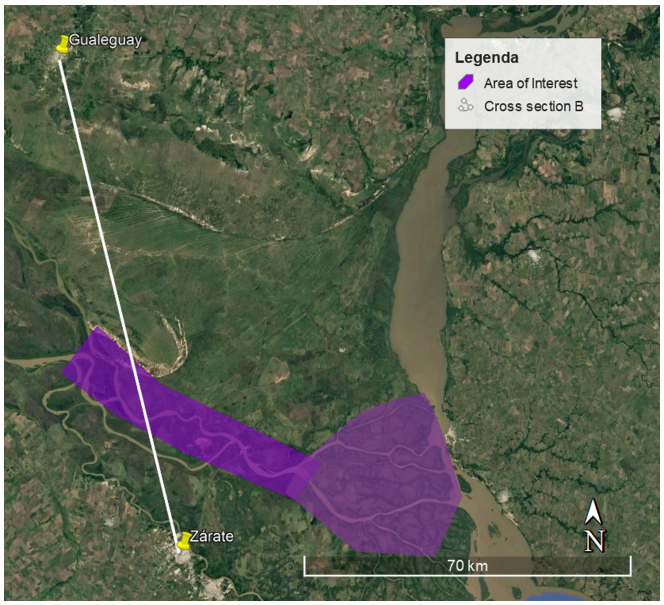

Figure 5.11: Cross section (Google Earth, 2025)

The geological profile of the cross section is shown in Figure 5.12. As can be seen in the figure, the taken cross section was around 80 km long. Of this, 15 km falls inside the area of interest, this zone is marked with purple.

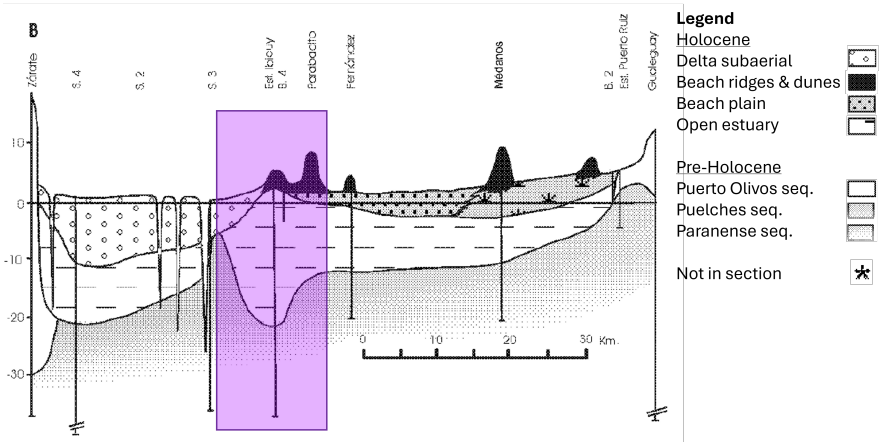

Figure 5.12: Geological profile of cross section (Cavallotto et al., 2005)

- Beach ridges & dunes: This layer consists of ridge-like beach deposits overlain by dunes. The beach deposits have a maximum thickness of 2 m and are composed mainly of well-sorted fine to medium sands with shell fragments. Light minerals represent 97.8% of the sand, almost all of which is quartz (Cordini, 1949). Radiocarbon dating indicates the deposits formed about 6,400–5,500 years ago, during the mid-Holocene. The ridges represent berm deposits formed by coastal progradation toward the northwest, driven by southeast winds and littoral drift. The dunes are up to 11 meters high, especially near Ibicuy, where dune elevations range from 9 to 11 meters and extend 1–2.5 km wide. The dunes consist of well-sorted, fine brown sands composed mostly of quartz (>99%), with minor feldspars and heavy minerals such as magnetite, zircon, staurolite, and kyanite (Cordini, 1949). Thermoluminescence dating shows ages between 2,800 and <500 years old, indicating several phases of dune formation. Their greatest development on the southeast side shows that, like the underlying beach ridges, they were shaped by southeast winds and continue to be reworked by modern activity (Cavallotto et al., 2005).
- Beach plain: The Beach Plain Facies consist of a series of closely spaced beach ridges formed during phases of shoreline retreat and sediment accumulation. The deposits are composed of fine to very fine sands, moderately to well sorted, dominated by quartz (85–90%) with minor feldspars and few heavy minerals (Cordini, 1949). Radiocarbon testing suggests ages between 2,600 and 1,800 years. The presence of both estuarine shells and freshwater species indicates a transition from estuarine to fluvial conditions as river influence increased (Cavallotto et al., 2005).
- Delta subaerial: The subaerial facies of the Paraná Delta developed through the deposition of silty-sandy sediments delivered mainly by the Paraná Guazú and Paraná de las Palmas (Cavallotto et al., 2005). These deposits occur at elevations between 2 m and sea level, with a maximum thickness of 12 m. This is the layer that is drained. Mineralogical analyses show a predominance of quartz with minor plagioclase and K-feldspar, plus heavy minerals such as magnetite, hematite, garnet, zircon, tourmaline (Cavallotto et al., 2005). The life age of the unit is debated: radiocarbon dates suggest origin dates between -150 BC and 180 AD, while other authors propose a later origin around 700–750 AD (Cavallotto et al., 2005).
- Open estuary: The open estuary sediments were deposited during postglacial sea-level rise and were formed at the freshwater–saltwater interface. At the time, seawater flooded the Río de la Plata river valley (Cavallotto et al., 2005). These are olive-green clays to silty clays with thin fine-sand layers, scattered or concentrated shell beds, and fossil content confirming estuarine conditions. The unit is dated to the Holocene, with its base at 6670 +/- 100 years BC, occurring between –22 and –0 m and reaching up to 20 m thick (Vogel & Lerman, 1969).
- Paranense sequence: During the Miocene, large portions of present-day Argentina, Uruguay, Paraguay, southern Brazil, and eastern Bolivia were covered by the Paranense Sea. This was a shallow sea that advanced from the Atlantic into the interior of South America . Its waters left behind marine sediments and fossils and this layer is now known as the Paranense depositional sequence (Tineo et al., 2024).

It is composed mainly of siliciclastic sandstones, mudstones, and bioclastic beds, with thicknesses ranging from a few meters in outcrop to over 100 m. The lower part has mud-dominated offshore deposits with marine fossils, while the upper part is sandier. Studies link the deposits to the Late Miocene (ca. 9.5–6.7 Ma) (Tineo et al., 2024).

In a study conducted by Amato and Busso (2009), a number of boreholes were executed along the Lower Paraná. One of these boreholes was executed near the area of interest in Puerto Ibicuy. The borehole was interpreted and with this the following soil profile was made.

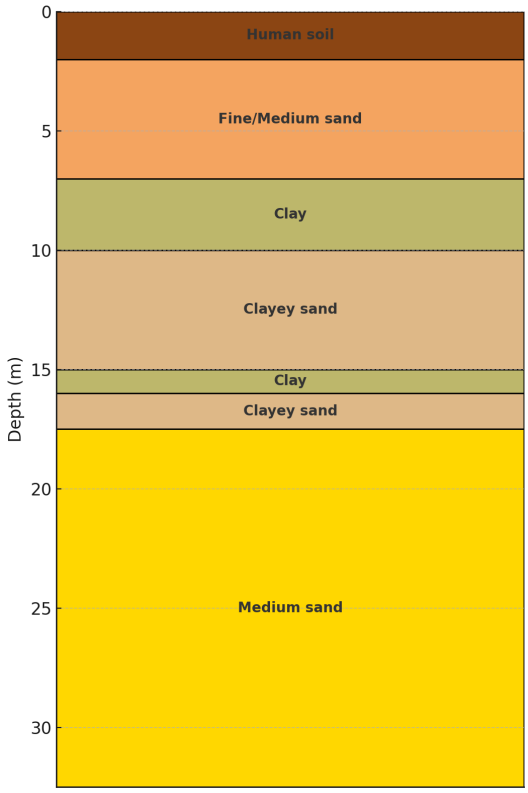

Figure 5.13: Borehole profile in Puerto Ibicuy (Amato & Busso, 2009)

5.2.5. Characteristics of fracking sand

Sand used in the fracking process must meet specific characteristics in order to be used for fracking. Silica sand is mainly required for fracking, which has a grain size between 0.0625 and 2.0 millimetres. The quartz grain content must be higher than 90%.

The specifications for silica sand used in fracking are written down in the international test standard ISO 13503-2:2006. The important aspects are as follows:

1. Size and distribution of the particles
2. Shape of the particles
3. Acid resistance
4. Fracture and compressive strength of the grains
5. Clay and silt content

When it comes to size distributions of the sand particles, the most important requirement is that 90% or more is found within a small particle size range. The size of the particles is less important and can differ per batch. Ten different sizes of particles are described that are suitable for cracking, for which the difference between the lower and higher boundary is constant on a logarithmic scale (Benson & Wilson, 2015).

The shape of the sand particles must be round enough and smooth enough to be applicable. Therefore, the system of Krumbrein, W.C. and Sloss, L.L. is used. This system is shown in Figure 5.14. The norm says that for both roundness and sphericity the value must at least be 0.6. It is important to mention that this procedure is visual and therefore depends on the subjective perception of the person analysing the sample.

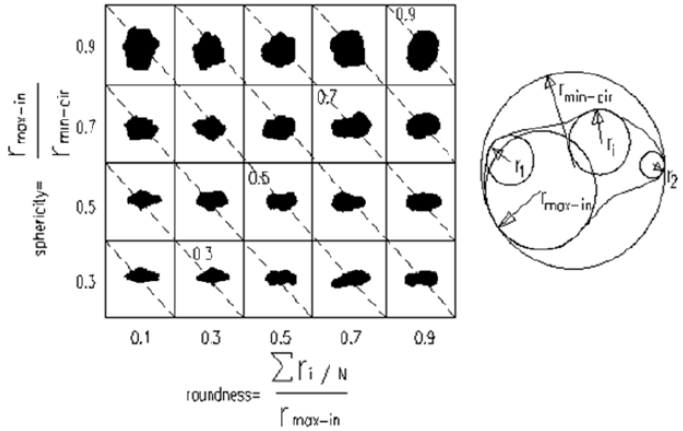

Figure 5.14: Roundness table (Rodriguez et al., 2013)

Acid solubility testing is used to determine the concentration of soluble elements that contaminate the binder. These elements are typically softer materials that can break down and migrate into the artificially created pore system during fracture closure. This process can lead to conductivity issues within the formation. To evaluate this, various acids are used, most of them being hydrochloric and hydrofluoric. These acids dissolve soluble grains such as carbonates, clays, and oxides, while leaving quartz grains intact. Because of this behaviour, industry regulations specify maximum allowable levels of acid-soluble materials that could significantly reduce the permeability of cracks in the wells. For coarser fracking sand with a grain size up to 30/50 mesh, a maximum of 2% acid-soluble content is permitted. For finer sands, this limit increases to 3%, as shown in Table 5.2.

Table 5.2: Recommended maximum acid solubility (Secretaría de Política Minera, 2019)

Particle size (ASTM)	Particle size (mm)	Max. solubility (% by weight)
6/12 to 30/50	1.68/3.36 to 0.30/0.60	2.0
40/70 to 70/140	0.21/0.42 to 0.10/0.21	3.0

For the compressive strength of grains a test is conducted which exerts pressure on the sand particles and eventually sieves the sample to find what percentage of the particles goes trough a certain dimension sieve. This percentage of breaking particles in combination with the known applied pressure tells which pressure the sand can withstand when using it for making cracks. The permeability of the fractures in the oil sources drops rapidly if the percentages of cracking sand particles and clay/silt particles is too high.

When looking at sand from the Lower Paraná Delta, means of transport such as waves and currents in rivers promote the removal of finer or organic particles, thereby ensuring a higher percentage of quartz grains. This is one of the reasons why sand from the Paraná Delta is suitable for fracking. In addition to erosion by water, the action of wind also influences the characteristics of sand. It causes changes in texture and generally makes quartz sand rounder. Furthermore, sand from the Ibicuy region is mostly composed of quartz and the percentage of heavy minerals is very low (0.3%). However, the sand is polluted by iron minerals, and this is one of the reasons as to why the sand is washed before transporting it to the fracking plants (Secretaría de Política Minera, 2019).

5.2.6. Consequences of dry sand mining

The effects of dry sand mining can be diverse. This section combines various reports on dry sand mining as well as knowledge that arises from stakeholder interviews to provide an overview of the consequences that can be linked to this activity.

The most obvious effects due to dry sand mining have to do with the natural environment. As became clear in stakeholder interviews, sand mining leads to the removal of several meters of top soil. This operation requires clearing land of their natural cover: forests or grasslands are removed.

During the interview, the YPF sand mine manager showed two sites where sand mining activities were stopped due to exhaustion of the sand resource. He explained that after mining activities are completed, the areas are left uninterrupted and are thus 'given back to nature'. Figure 5.15 shows the current condition of two former sand mining locations. On the left, activities ceased one year ago and on the right, mining has stopped since four years. The mined areas can be seen in the back of the photos, the sand in the foreground is not part of these sites.

Figure 5.15: The state of 'finished' locations: after 1 year (left) and after 4 years (right)

From Figure 5.15, it follows that the natural cover (grasslands and forests) has recovered within years for this case. This does however not mean that original habitats were also restored. Examples of this can be found in the United States of America: over the past decades, the Dunes Sagebrush Lizard has seen more than 95% of its original habitat in Texas and New Mexico disappear. This is due to the oil industry and the large scale sand mining operations that support it. In 2024, the species was listed as endangered by the U.S. Fish and Wildlife Service (Center for Biological Diversity, 2025). Sand mining leads to permanent removal of habitats, which means that letting natural cover grow back may not be enough for species like these to return.

Beside the effects on natural habitats, the most frequently voiced concerns of stakeholders are the poor conditions of roads, especially the provincial RP45 that forms the entrance to the town, caused by intense heavy truck traffic. These comments were confirmed during the field trip, since many potholes were observed along the entire route.

The poor road conditions are not only uncomfortable but also dangerous. In fact, in 2020 alone, ten people lost their lives on the roads that form part of the sand transport routes. The situation has lead to protesting citizens and to blockages of the national highway 12 (Novas, 2022). Other possible negative effects on people living near the sand mines include noise pollution and light pollution, although these concerns were not raised by stakeholders that were interviewed.

Besides these social concerns, there are also multiple economic effects in the region. In the short term, sand mining can contribute to the economic development of an area. Jobs are created and the government can profit through direct and indirect taxation of the activities. However, since all sand mining activities face a natural end (the YPF mine operator indicated that his mine had resources to

stay open for 8 more years), positive economic effects do not persist in the long term. A closer look at the situation in Ibicuy reveals more economic troubles related to sand mining.

The Argentinian mining codes dictate that so-called 'third-category mines', such as silica sand mines, belong solely to the owner. The government therefore does not receive royalties for exploitation of the areas but instead charges taxes based on volumes (Novas, 2022). Instead, the mayor and YPF mine manager indicated that both provincial and municipal taxes are in place. The transport is taxed and each truck pays a tax based on the mass it carries.

From 2019 until 2023, the provincial government of Entre Ríos chose to not adjust the mining taxes, such that the provincial income from these taxes was approximately stable at 400 million pesos per year. However, this period was marked by high inflation and strong devaluation of the Argentine peso (Bellato, 2025). In December 2019, at the start of the previous administration's term, 400 million pesos equaled approximately 3 million Euros. At the end of their ruling, in December 2023, the same sum was worth 440,000 Euros. The new provincial government tried to strike a deal with fossil fuel companies to secure investments in infrastructure. After this turned out fruitless, taxes were raised by a factor six in May 2025. As of today, trucks pay 2250 Argentine pesos per ton. Both the province and municipality charge taxes on transported sand. However, in 2022, municipal mining taxes were only around one tenth of the taxes the province charged on the activity (Novas, 2022). At 37 million pesos, the municipal taxes are too low to contribute significantly to road reparations.

Besides road reparations there are more costs made due to air and water quality. This is mainly the case because during mining, washing and transport processes, silica-rich sands release airborne crystalline silica particles (silica dust). When the silica dust is inhaled, it can contribute to respiratory diseases like silicosis and lung cancer (Physicians for Social Responsibility et al., 2023). In 2013, the National Institute for Occupational Safety and Health (NIOSH) tested silica concentrations in 11 sand mining locations in the US. They found that 79% of samples exceeded the recommended limit, and in some cases the found concentrations even exceeded limits that hold while wearing protection masks (Foglia, 2023). Effects of silica dusts on nearby communities are a topic of discussion. A 2017 study researched crystalline silica concentrations in homes within 800 m of sand mining activities and concluded that exposure seems unlikely to cause chronic health problems to these communities, because of relatively low concentrations (Peters et al., 2017). However, in January 2021, a ban on fracking sand mining in Winona County, Minnesota, US, was upheld by the Supreme Court. The ban was put in place by the county out of concerns about environmental and health impacts (Physicians for Social Responsibility et al., 2023).

After the sand is mined, it is washed to clean it from unwanted substances such as clay and organic material. For this, large amounts of groundwater are used. In Ibicuy, the sand miners use water from the Talavera formation, which is the same water that flows out of the tap. Sand mining companies are reluctant to share information about extracted groundwater volumes. However, in 2020, an environmental information lawsuit revealed 33 documents with specifics. At the time there were 5 sand-washing installations near Ibicuy that together extracted 400 million liters of groundwater per month from the Talavera formation (Foglia, 2023).

In addition to drinking water competition, the sand washing installations have the capacity to pollute water reservoirs, an effect that is already noticeable in Ibicuy. In June 2022, the local water treatment company reported manganese concentrations of 0.75 mg per liter, whereas the recommended water concentration limit for lifetime exposure is 0.3 mg/L. Further, iron concentrations of 0.93 mg and 1.10 mg were found, an increase of 2200% as compared to the historic value of 0.05 mg. Additionally, flocculants such as polyacrylamide are used to clump together clay particles and other fine suspended solids. Polyacrylamide can infiltrate into the surface and the underground and can break down into acrylamide during drying (Foglia, 2023). The WHO warns that acrylamide is genotoxic and carcinogenic, thus may increase the risk of cancer and is therefore a human health concern (World Health Organization, 2011).

6

Hydrodynamic and sedimentary analysis

This chapter includes the analysis of the hydrodynamic elements of the study area. The extra data acquired from the fieldwork is added together with the data already found to derive an expression of the sediment balance. Lastly, this chapter explores the hydrodynamic effects on riverbanks with the help of satellite data.

6.1. Hydrodynamic analysis

In this section, analysis on the hydrodynamic variables is performed. This includes relations between water elevations, discharge and sediment concentrations - through data sources as described in Section 3.1. Additionally, tidal effects in the study area are considered. A uniform approach is needed to describe water levels and depths of the river. Therefore, these variables will be expressed in terms of a reference level, IGN, which is set by the *Instituto Geográfico Nacional*. It is based on sea level measurements from a tide gauge in Mar del Plata, Buenos Aires province (D'Onofrio et al., 1999). Figure 6.1 gives an overview of the quantities with respect to an arbitrary measurement station.

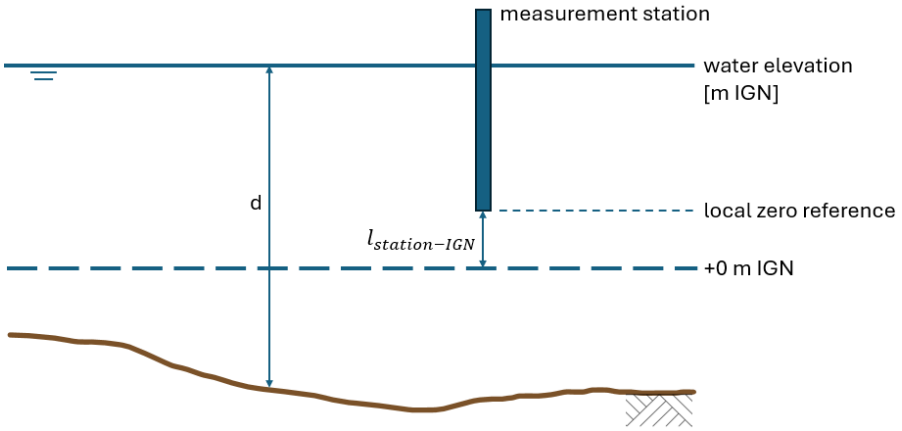

Figure 6.1: Water elevation reference

Here, d is the vertical depth as measured by the ADCP or echosounder. Moreover, each station has a specific distance between its local zero reference and the zero IGN level, which is indicated by $l_{station-IGN}$. Next, all variables should be expressed in terms of IGN level. Defining $wl_{station}$ as the water level recorded in an arbitrary station, water elevations and depths expressed in elevation are defined as follows:

$$we_{station} = wl_{station} + l_{station-IGN}\ [m\ IGN] \tag{6.1}$$

$$d_{el} = we_{station} - d\ [m\ IGN] \tag{6.2}$$

6.1.1. Water elevations and discharge

This section describes the liquid discharge observed in the SNIH measurement stations and relates it to water elevation data. It is relevant to analyse how the discharge of the Middle Paraná partitions over the distributaries of the Lower Paraná Delta, in order to estimate the relative importance of the Paraná Guazú. Downstream of the city of San Pedro, the river splits into two main tributaries, as shown in Figure 3.1. To have an approximation for the discharge distribution between these rivers, the discharge series are given in Figure 6.2a. The discharge data are recorded in Zárate and Brazo Largo. The plots show that the majority of the discharge flows into the Paraná Guazú. Figure 6.2b represents this ratio and plots a linear fit. As there is no significant increase or decrease, the approximation is made that 78% of the total discharge upstream of the confluence flows into Paraná Guazú. Re et al. (2009) report a linearly increasing trend; however, since a larger dataset is used in this study, assuming a constant percentage is considered more appropriate. Note that the contribution of other, smaller tributaries is not considered here.

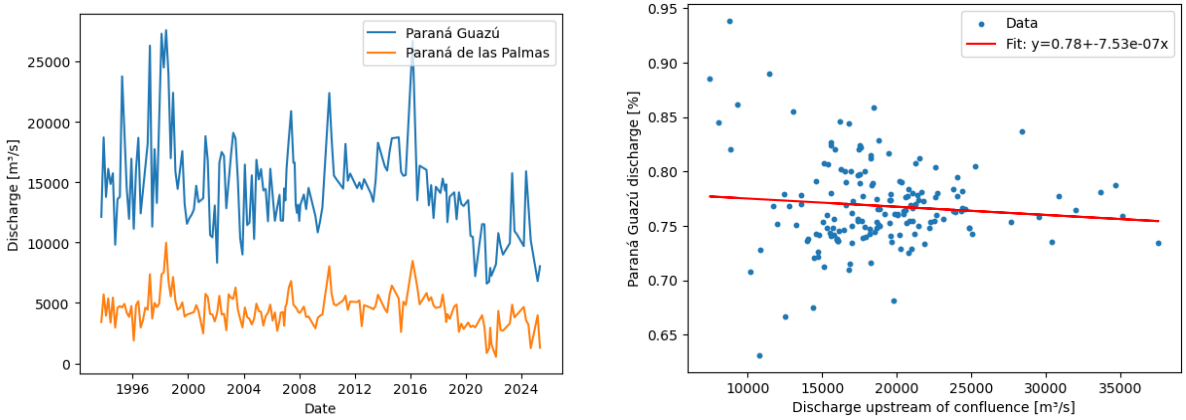

(a) Discharge series obtained from Brazo Largo and Zárate measurement stations

(b) Flow partition, expressed as the share of total flow that streams into Paraná Guazú

Figure 6.2: Comparison of discharge divided between Paraná Guazú and Paraná de las Palmas

The relative importance of the Paraná Guazú in the delta has been established. Considering the study area, the discharge values used for the Paraná Guazú include contributions from both the Ibicuy and, to some extent, the main Paraná channel. At Puerto Ibicuy, no active discharge measurements are available. Brok (2022) reports an approximate river discharge of 1600 m³/s, indicating that the contribution of the Ibicuy branch is relatively minor. Consequently, further analysis focuses on the Brazo Largo station, located downstream.

First, the relationship between water elevation and discharge is examined. Stage–discharge relations are commonly expressed through rating curves, which describe a power-law dependence between these variables. This can be formulated as:

$$Q = a \cdot h^b \tag{6.3}$$

In the expression above, a is a constant and b an index exponent. The relationship between fluvial discharge and water level at Brazo Largo yields a relatively weak correlation with an R^2 of 0.310. This is shown in Figure 6.3. Alternatively, a linear fit was assumed which produced a slightly better result, showing a positive trend with an R^2 of 0.386. In contrast, the El Colorado and Túnel Subfluvial stations exhibit a clear power-law dependence. Power-law fits for these stations resulted in higher R^2-values

of 0.962 and 0.712, respectively, with the El Colorado plot shown in Figure 6.3. Overall, these results suggest that the strength of the water level–discharge relationship decreases as the river flows downstream.

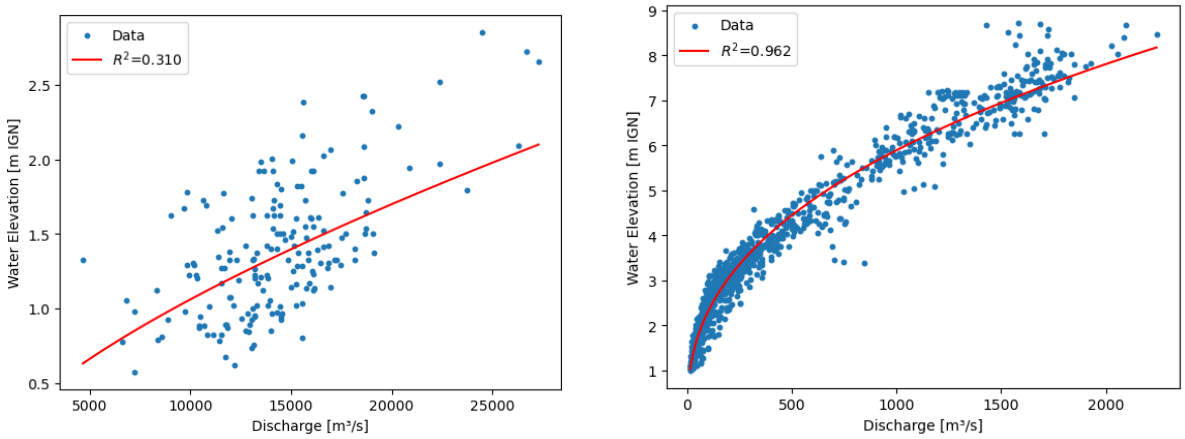

(a) Stage–discharge relation in Brazo Largo

(b) Stage–discharge relation in El Colorado

Figure 6.3: Water elevation–discharge relationships for two measurement stations

6.1.2. Sediment loads

The analysis is extended to sediment concentrations, relating both fine and coarse sediment loads to liquid discharge. Figure 6.4a shows this relation for the Brazo Largo station. The same trend occurs as in the rating curves: in the Bermejo river, fine and coarse sediment discharges are closely related to large flow events through power-law relations. This behaviour is found to a lesser extent in the Lower Paraná, where the correlations are weak. Overall, a power-law fit is a suitable approach to model the relation. The fine sediment concentration is generally higher than the coarse sediment concentration. In addition, the coarse sediment concentration increases more significantly for an increasing fluvial discharge. Note that the R^2 of both relationships is small in comparison to the Bermejo river, for which the same variables are related in Figure 6.4b.

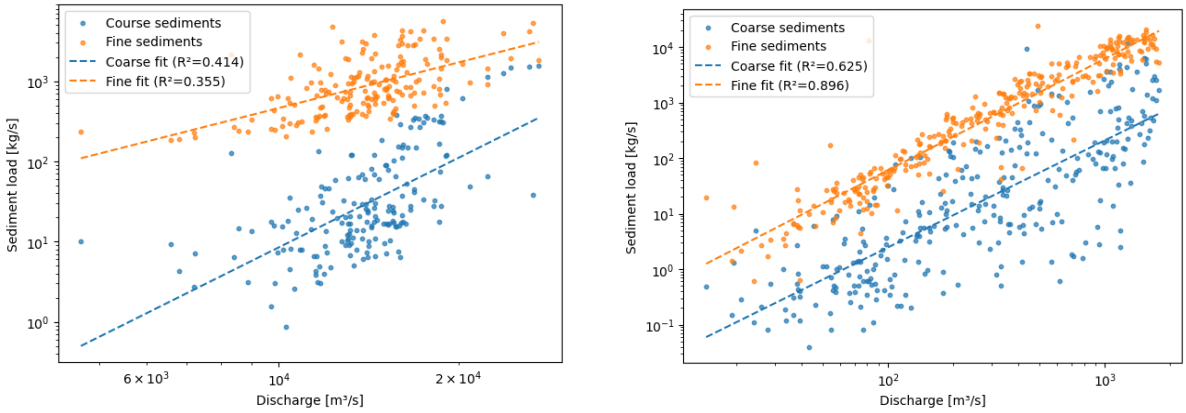

(a) Fine and coarse sediment loads in relation to discharge at Brazo Largo

(b) Fine and coarse sediment concentrations in relation to discharge at Bermejo

Figure 6.4: Fine and coarse sediment loads related to fluvial discharge in two measurement station

The data considered in the previous analysis is recorded approximately every two months over a couple of decades. However, in order to study the balance of sediments in the study area, it is useful to generate time series of sediment loads at a finer resolution. These can provide insight into seasonal effects and sediment flows related to large discharge events. Originally intended for modelling the sedimentological dynamics of the Río de la Plata, Re et al. have developed a methodology for gener-

ating time series of solid discharges. This theory will be applied to the Paraná Guazú under the right considerations.

The first assumption is that the flow of solid sediments in the Middle Paraná can be represented by the sediment flows from Bermejo, disregarding the sediment contribution of the Upper Paraná. Consequently, the flow in the Middle Paraná is regarded as a combination of the fluvial discharge in Santa Fe (Túnel Subfluvial station) and the fine sediment load recorded in El Colorado (see Section 3.1.1). In order to estimate the fine sediment concentration in Túnel Subfluvial, the fine sediment-discharge relation for Bermejo is used as shown in Figure 6.4b. Next, this procedure is applied to more recent data to evaluate the methodology. The most recent, relevantly long interval with continuous data for both measurement stations is 2017 to 2019. A number of assumptions is used to find the time series of fine sediment concentration:

- A base concentration is set for the Middle Paraná to compensate for low inflow periods of the Bermejo. Therefore, fine sediment load data from Itatí and Puerto Pilcomayo stations (SNIH) are studied in the relevant interval. The sum of the mean loads gives a base concentration of 182.96 kg/s.
- To cover the distance between El Colorado and Túnel Subfluvial, a delay of 222 hours is considered (approximately 800 km at a flow velocity of 1 m/s).
- There is compensated for depositions of wash load in the floodplain between the stations by subtracting 10 million tons per year from concentration peaks. This holds for all concentrations above a certain threshold value, which in this case was found to be optimal at 350 mg/l.

The result of this time series is given in Figure 6.5. It is important to note that this relation for fine sediment concentrations is considered useful for the Paraná Guazú as well (Re et al., 2009). The plot shows that the observations are generally higher than the fit predicts in times of low fine sediment loads. Overall, the fit gives a good estimate of fine sediment concentrations, revealing seasonal aspects and relevant concentration values.

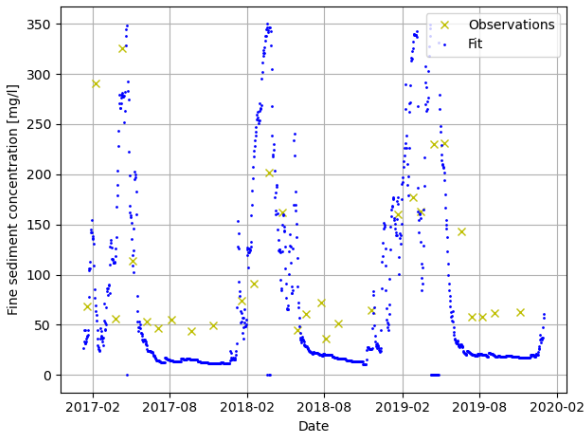

Figure 6.5: Fine sediment concentration time series

Similar to fine sediments, an approach for generating time series of coarse sediment concentrations is based on the Engelund–Hansen formulation (Engelund and Hansen, 1967). This empirical relation predicts the total transport of bed material, which in this case is assumed to consist mainly of coarse sediments or sands. The total volumetric sediment transport rate per unit width is expressed as:

$$q_t = \frac{0.05\, u^2\, h^{3/2}\, S_f^{3/2}}{(s-1)^2\, g^{1/2}\, d_{50}} \tag{6.4}$$

where s is the specific gravity of the sediment, g is the acceleration due to gravity, d_{50} is the median grain diameter, and S_f is the friction slope. The variables u and h represent the flow velocity and the hydraulic

depth, respectively. The value for d_{50} is assumed to be 200 μm (Re et al., 2009). The values for u, h and S_f were gathered by running a one-dimensional hydrodynamic model in HEC-RAS. The model output provided relationships between friction slope, flow velocity, and hydraulic depth as functions of discharge. To generate a time series of sediment transport rates, it was therefore sufficient to obtain a single discharge time series. For this purpose, a recent hydrodynamic simulation of water levels and discharges was used for the Brazo Largo section, located downstream of the confluence of the Talabera and Paraná Guazú rivers. The dataset spans approximately two months with hourly intervals. Using interpolation, time series for the friction slope, velocity, and hydraulic depth were derived from the discharge data. These were then used as inputs to Equation 6.11 to compute the time series of coarse sediment transport rates. The time series of the discharge is given in Figure 6.6 and the corresponding coarse sediment load time series in Figure 6.7.

In comparison to the study of Re et al. (2009), the amount of yearly sediment transport is significantly lower; this estimation yields approximately 1.78 millions tons per year, as opposed to 3.85 million tons per year. This discrepancy is attributed to the difference in friction slope. The HEC-RAS output suggests mean friction slopes of the order of $6 \cdot 10^{-6}$, which is again smaller. In addition, smaller discharge values have been considered, which directly result in smaller flow velocities. The relatively low discharge values are representative for the time frame of this study, and therefore the time series serve as a comparison to the fieldwork. Finally, two methods have been proposed to estimate time series of fine sediment and coarse sediment loads, respectively. These provide estimates of the sediment concentrations encountered in the study area.

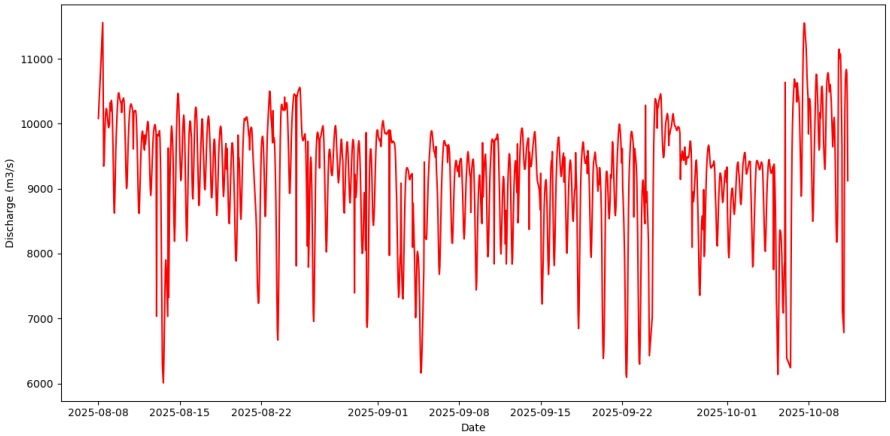

Figure 6.6: Discharge time series from HEC-RAS output in Brazo Largo as input for Engelund-Hansen

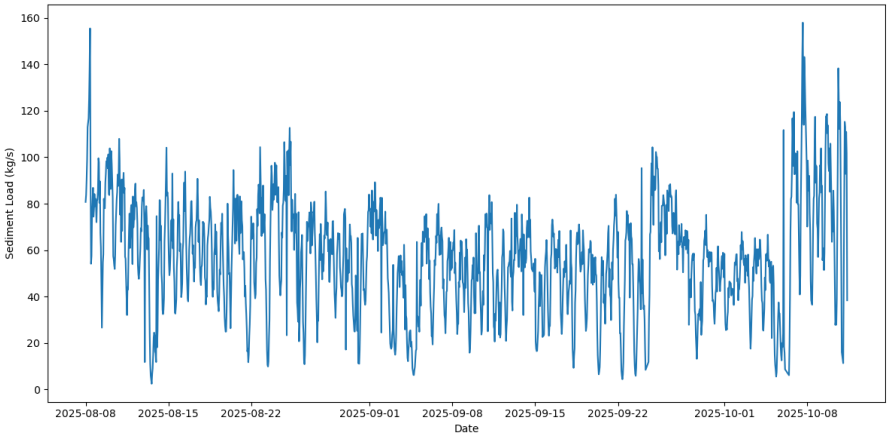

Figure 6.7: Time series of coarse sediment load estimated by Engelund-Hansen

6.1.3. Correlation between variables

As discussed, power-law relationships have been assumed to hold between the variables under consideration. This section describes the correlations encountered during the analysis. The approach to define the relations between measured flow variables is as follows. First, the values in the dataset are logarithmically transformed, after which R^2-values are calculated based on a linear fit on the logarithmic values. This procedure is applied to the variables of all measurement stations as described in Section 3.1.1. Figure 6.18 gives the results for El Colorado and Brazo Largo in the form of correlation matrices. It stands out that correlations in the Bermejo are very high for all variables. This indicates that the power-law assumption is suitable. Subsequently, it was found that correlations for the Paraná Guazú are much smaller. This is also the case for the Zárate station on the Paraná de las Palmas.

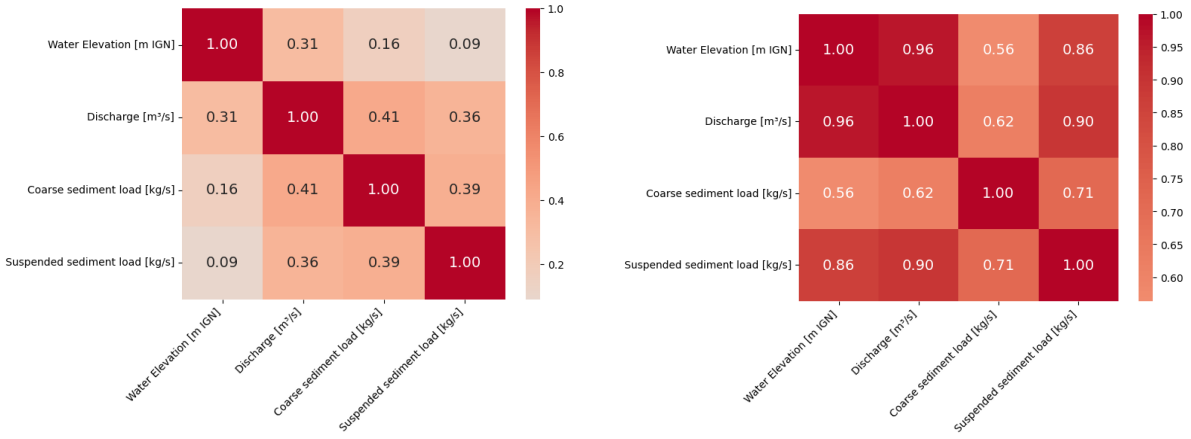

(a) Correlation matrix of log-transformed data in Brazo Largo

(b) Correlation matrix of log-transformed data in El Colorado

Figure 6.8: Comparison of R^2-values at Brazo Largo and El Colorado

6.1.4. Tidal forcing

The tidal wave of the Atlantic Ocean influences the hydrodynamics of the lower Paraná delta. As the tidal wave enters the delta at the Río de la Plata, the tide is damped and phased by friction, channel geometry and branching, resulting in a reduced amplitude and an increase in phase delay. Under normal conditions, the influence of the tide on the Paraná River reaches the city of Villa Constitución, which is located 220 km upstream of the river mouth. For storm conditions, the tide can reach the city of Rosario (Balay, 2018). In order to determine the influence of the tide at Brazo Largo, a harmonic tidal analysis is performed on hourly water level measurements. First, the water level is detrended, such that the mean water level is constant in time. Next, the observed water level time series is decomposed into a sum of sinusoidal components, with each of these components representing a specific tidal constituent. The tidal constituents considered for Brazo Largo are shown in Table 6.1.

Table 6.1: Tidal constituents used to reconstruct the tide (Apel, 1987).

Type	Tidal constituent	Period [h]
Semi-diurnal	M2 (Principal lunar)	12.4206
	S2 (Principal solar)	12.0000
	N2 (Lunar elliptical)	12.6583
Diurnal	K1 (Lunar-solar declinational)	23.9345
	O1 (Principal lunar)	25.8193
Quarter-diurnal	M4 (Overtide of M2)	6.2103

The computed amplitude and phase of the different tidal constituents are shown in Table 6.2. The amplitudes show that the delta has mixed tidal dynamics (semidiurnal-diurnal) dominated by the semi-

diurnal constituent M2 (0.0764 m) and the diurnal constituent O1 (0.0672 m) with contributions from N2, K1 and S2. The overtide (M4) plays a minor role, indicating weak nonlinear distortion and thus a not strongly skewed signal. The relative phase lag of 104° between the M2 phase and the S2 phase, indicates that the S2 tide occurs a few hours after the M2 high tide, resulting in a spring-neap cycle with moderate modulation.

Table 6.2: Computed amplitude and phase

Constituent	Amplitude [m]	Phase [deg]
M2	0.0764	338.51
S2	0.0116	82.10
N2	0.0284	299.34
K1	0.0331	100.66
O1	0.0672	296.74
M4	0.0085	238.09

Figure 6.9 shows the detrended water levels for a period of 1 month compared to the calculated tidal signal at Brazo Largo. The tide does indeed show mixed tidal dynamics with a moderate spring-neap cycle and slight asymmetries. The period of the spring-neap tide cycle is approximately 15 days. The computed astronomical tide has an amplitude of 0.19 m and a tidal range of 0.39 m. By computing the residual water level (r), defined as the difference between the measured water level and the calculated tide, the tidal variance fraction (f_{tide}) can be calculated (see Equation 6.5).

$$f_{\text{tide}} = 1 - \frac{\text{Var}(r)}{\text{Var}(h)} \tag{6.5}$$

The tidal variance fraction at Brazo Largo is 5.71. This means that only 5.71% of the total variance in the observed water levels can be explained by the astronomical tides. The remaining variance ($\sim$94%) comes from river discharge, meteorological effects and non-tidal effects. An estimate of this meteorolocigal tide can be made by looking at the residual water level (r). This yields a meteorological tidal amplitude of 1.05 m and a meteorological tidal range of 2.09 m. Given that the astronomical tidal range is relatively small compared to the meteorological influence, and the tidal variance fraction is only 5.71%.

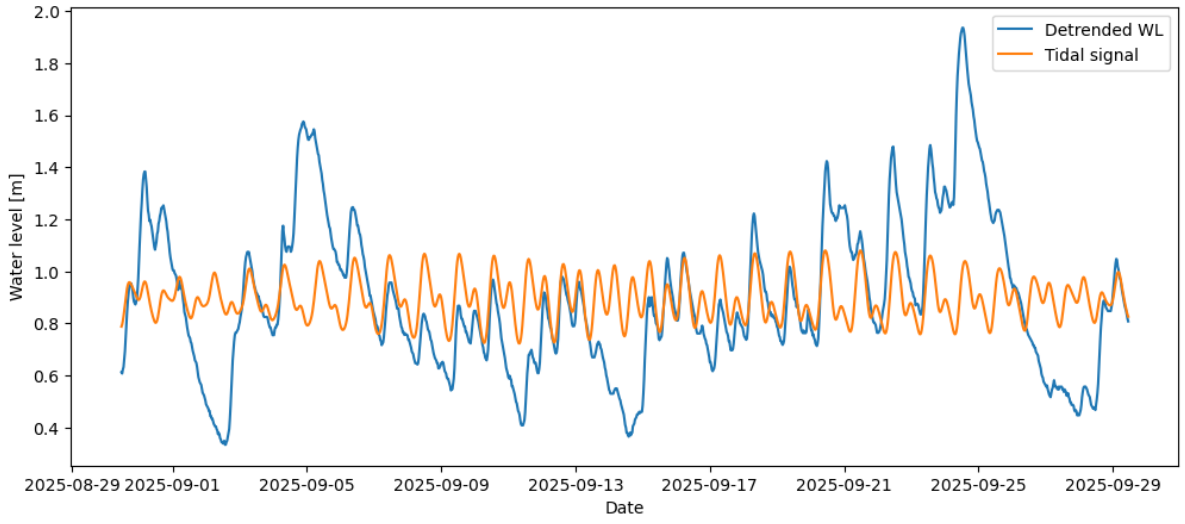

Figure 6.9: Computed tide at Brazo Largo for a period of 1 month.

Although the tidal variance fraction is low, the shape of the tidal signal still provides insight into the potendial sediment import/export. The computed velocity skewness (0.48) and the rising period being shorter than the fall period, suggest a weak flood-dominant asymmetry. This is consistent with the positive M_4/M_2 amplitude ratio (0.11) and the phase difference of 259° between M_4 and M_2, both indicative of flood dominance (Bosboom & Stive, 2023). Therefore, small net landward sediment transport may occur as a result of tidal asymmetry, although its overall effect is expected to be minor compared to the fluvial and meteorological forcing.

6.2. Field work measurements

This section describes the results of the field campaign introduced in Section 3.2. The measurements are compared to the results found in Section 6.1. First, discharge and flow velocities are considered in the sections of interest. Then, measurement samples are processed to desribe grain size distributions, suspended and bed sediment loads. Finally, an explanation is given on longitudinal profiles.

6.2.1. Water level and discharge

Estimates are needed for the discharge of Río Ibicuy and Río Talabera, in order to further study the liquid flows in the Paraná Guazú. These were collected during the fieldwork, as indicated in Figure 3.7 and Figure 3.8. In addition, an overview of all cross sections with discharge measurements is given in Figure 6.10. The indexing of the cross sections is made in chronological order based on the fieldwork. Note that at the confluence of the Ibicuy and Paraná, there is no measurement of the component flowing in from the Paraná. However, this can be estimated by the equilibrium of discharges in the confluence.

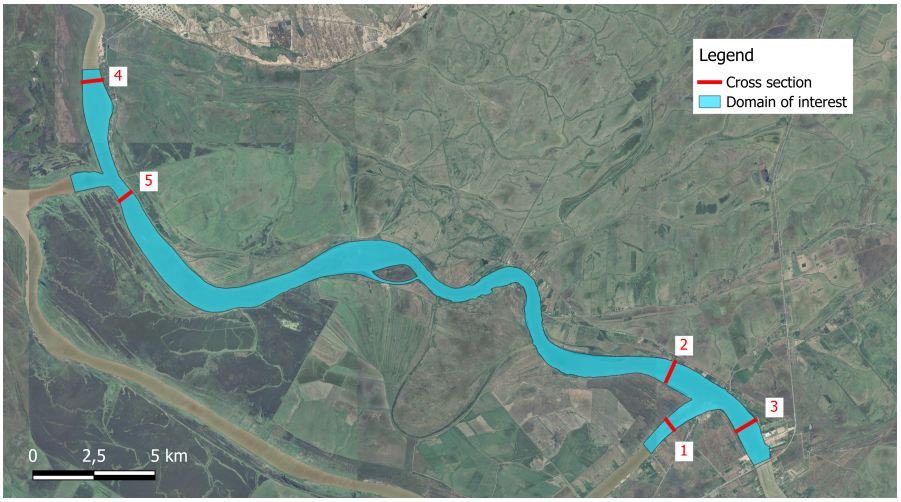

Figure 6.10: Overview of cross sections with discharge measurements (Google Earth, 2025)

The relevant flow measurements of the different cross sections are summarized in Table 6.3. Note that the water levels are recorded on different dates from nearby measurement stations, i.e. Brazo Largo and Ibicuy. Figure 6.11 gives an overview of the evolution of water elevations during the measurement campaign. The values in the table correspond to the location and time of each measurement. For Section 5, the water level is linearly interpolated between the stations. The remaining cross sections are assumed to be close enough to their corresponding measurement station. Also, the flow velocity is a mean velocity taken over the entire cross section of the two measured sections per measurement location. The bathymetries and velocity profiles that result from the ACDP measurements can be found in Appendix E, where the output of the *RiverSurveyor* software is given. Note that of each cross section, only one of the two measured sections is displayed. The water elevations in Figure 6.11 are expressed with respect to the IGN datum. For that reason, elevations at Puerto Ibicuy are consistently higher than at Brazo Largo on the same time instants. During the two measurement days, water levels drop while discharges increase.

Table 6.3: Flow properties of fieldwork measurements in different sections

Section	River	Water level [m IGN]	Mean flow velocity [m/s]	Discharge [m^3/s]
1	Talabera	1.09	0.619	4402
2	Paraná Guazú	1.12	0.507	6562
3	Paraná Guazú	1.10	0.573	10748
4	Ibicuy	0.87	0.445	2901
5	Paraná Guazú	0.82	0.566	6758

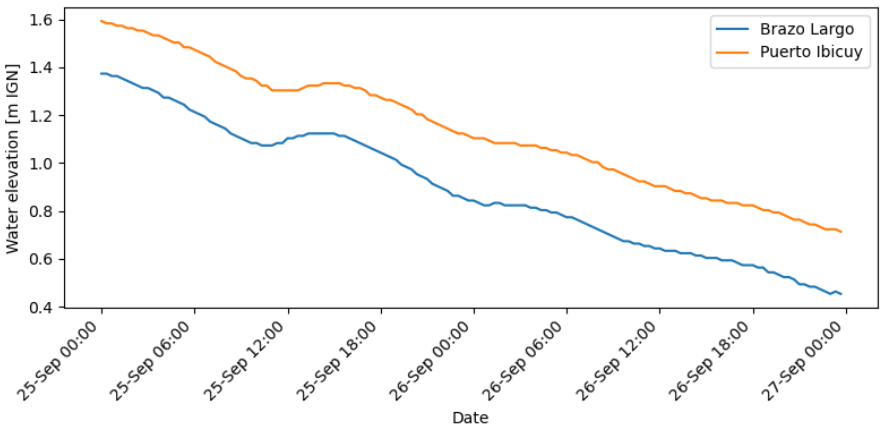

Figure 6.11: Water elevations of Brazo Largo and Puerto Ibicuy during fieldwork

6.2.2. Grain size distribution of bed load samples

During the fieldwork, data was collected on the Paraná River over a period of two days. Seven samples were collected from the riverbed at four different cross-sections. Samples were collected at depths of 10 and 15 metres. The identification numbers of each sample are determined as follows. The first number refers to the location of the cross-section, and the second number refers to a depth of 10 or 15 metres. The locations where the samples were collected are presented in Figure 3.7 and 3.8. Sample 3-1 was quite large, so it was decided to treat it as two different samples (3-1A & 3-1B).

When processing the samples, it was decided to start with a 0.5 mm sieve size for the samples that appeared to be sand and a 0.354 mm sieve size for the other samples. This was done because only six sieves and one residue container fit into the sieving setup. After sieving the samples for 10 minutes, each quantity of sample per sieve was weighed. This was used to calculate a cumulative grain size distribution and the median diameter of the particles. The calculation and processing of the results are described in more detail in Appendix C. The results are presented in Table 6.4 and Figure 6.12.

Table 6.4: Calculated median diameters of samples

Sample	D50 [mm]
1-1	0.080
1-2	0.262
2-1	0.082
2-2	0.210
3-1A	0.075
3-1B	0.075
3-2	0.083
4-1	0.078

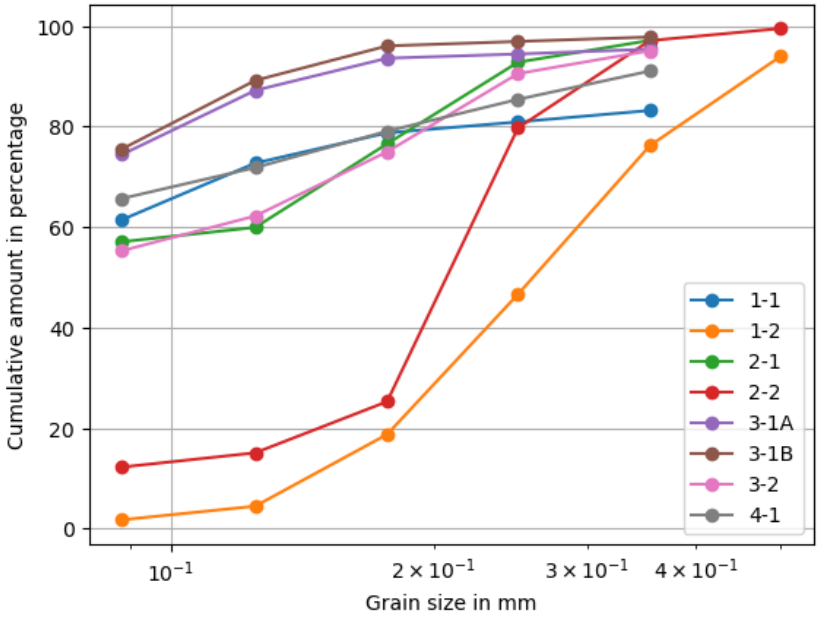

Figure 6.12: Cumulative grain size distribution of bed load samples

Figure 6.12 clearly shows that 1-2 and 2-2 are sand samples and the other samples are clay and silt samples. During the test, possible organic materials were also looked at. When seeing something that could be organic, the sample was tested with hydrochloric acid to see if this was the case. However, no organic particles have been found in the samples.

Figure 6.12, also shows that sand is more frequently encountered at 15 m depth than at 10 m depth. This suggests that coarser sediments tend to occur in the deeper parts of the channel, which are typically subject to stronger flow and higher bed shear stresses. Since there are no sediment samples available in the study area, this cannot be validated directly. Nevertheless, INA has recently recovered multiple samples in the river near the city of Rosario. Two of those samples were taken at a depth of 30 meters. These are presented in Figure 6.13, together with the Paraná Guazú sand samples and a grain size distribution of Ottawa fracking sand. As said in Section 5.2.1, the demand for fracking is increasing throughout the years, raising the question if river sand can also be used for these practices. That's why some data about fracking sand from Section 5.2.5 is combined with the gained data in this Section.

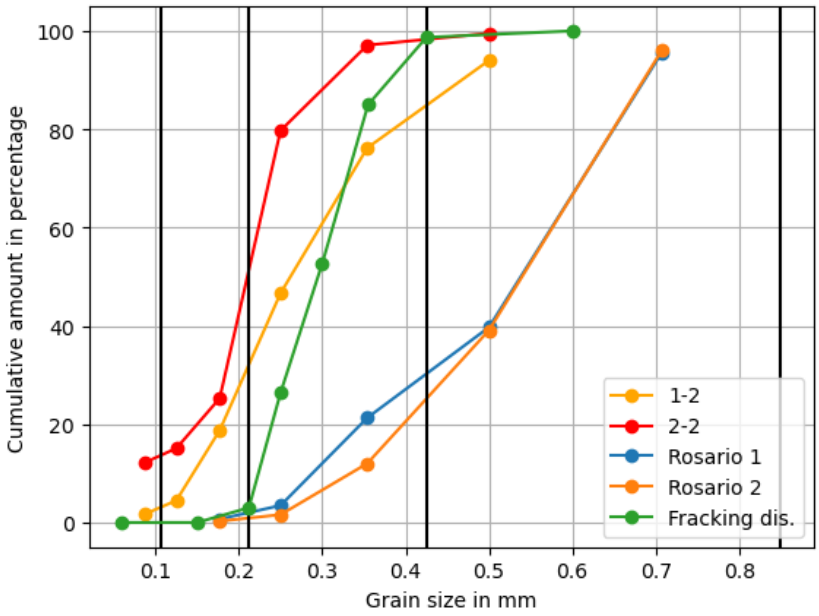

Figure 6.13: CGZD of multiple samples with homogeneous demand lines (Benson & Wilson, 2015)

As can be seen from Figure 6.13, the average particle size of the sand tends to increase with recovery depth. When the findings are related to the requirements for sand used in hydraulic fracturing (fracking), it becomes apparent that even with the observed increase in grain size, the river sand does not meet the necessary specifications. Fracking sand requires a very uniform grain size distribution to ensure consistent permeability and mechanical strength within the proppant pack. At least 90% of the particle sizes must fall within a defined size range, represented by the black boundary lines in the accompanying figure (Benson & Wilson, 2015). Furthermore, this acceptable range tends to widen as the target grain size increases, reflecting a broader tolerance for larger particles. However, the natural river sands under consideration display too much variability in grain size to be classified as suitable fracking sand without additional processing or sieving.

6.2.3. Suspended sediment load

In this section, the measured suspended sediment concentrations and flow velocity profiles are analysed in order to calculate the total suspended sediment flux. The sediment concentrations were obtained by lowering an intake tube connected to a rope and a weight into the water, as described in Section 3.2.2. By assuming a constant angle of the rope at different depths in a cross section and measuring the length of the rope, the depth at which the measurements were taken could be determined. The measured suspended sediment concentrations at different depths are shown in Figure 6.14. This figure shows that for all three cross sections, the suspended sediment concentration is the highest near the bed. Furthermore, cross section 2 shows a steeper profile than cross sections 1 and 3.

The Acoustic Doppler Current Profiler (ADCP) measures the flow velocity and depth across a river cross section by dividing the measurements into vertical bins for every ensemble. These data can be used to create a flow velocity field for the whole cross section, see Appendix E, and velocity profiles for every ensemble along the cross section. These velocity profiles are used to determine the Law of the Wall fit. see Equation 6.6.

$$u = \left(\frac{u_*}{\kappa}\right) \ln\left(\frac{z}{z_0}\right) \tag{6.6}$$

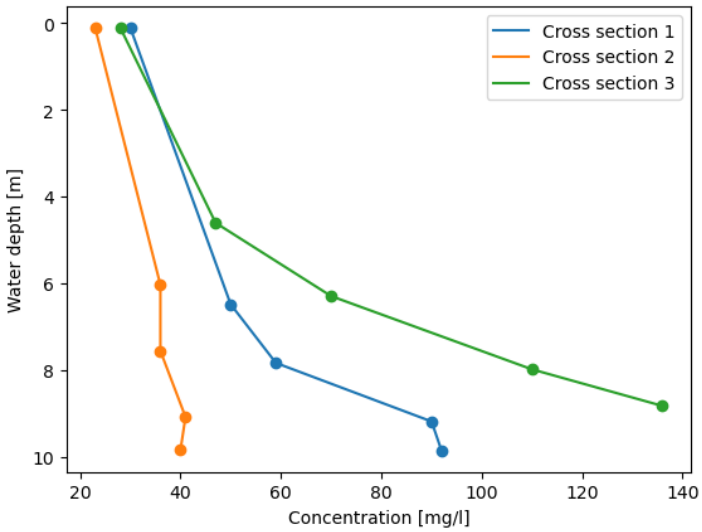

Figure 6.14: Measured suspended sediment concentrations.

The Law of the Wall describes the velocity profile of a turbulent flow near a boundary. Therefore, the log-law is fitted on only the velocity points in the lowest 50% of the water column. Additionally, the Law of the Wall is used to calculate the shear velocity (u_*), which is most accuratly determined from the near-bed region. By fitting only on the lower 50%, the fit is not affected by upper flow deviations such as wind, waves and secondary flow.

The measured flow velocity profiles by the ADCP and the fitted Law of the Wall are shown in Figure 6.15 for the three locations of the concentration measurements. The mean flow velocities for cross sections 1 and 2 are very similar, whereas cross section 3 shows a slightly higher mean velocity.

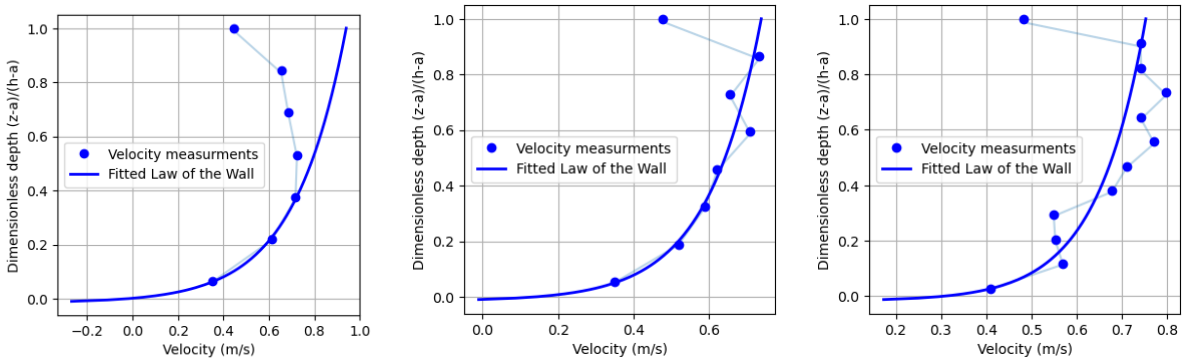

(a) Cross section 1. **(b)** Cross section 2. **(c)** Cross section 3.

Figure 6.15: Velocity profiles with Law of the Wall fit for the three cross sections.

The computed shear velocity (u_*) from the Law of the Wall fit is used to calculate the Rouse number at every ensemble along the cross section; see Equation 6.7. Using this Rouse number it is possible to calculate the sediment concentration (c) at any depth (z) in the water column using the Rouse profile in Equation 6.8.

$$P = \frac{w_s}{\kappa u_*} \tag{6.7}$$

$$\frac{C}{C_a} = \left(\frac{z - z_0}{a - z_0} \cdot \frac{h - a}{h - z} \right)^P \tag{6.8}$$

The reference depth (a) and the near-bed reference concentration (C_a) were based on the lowest suspended sediment concentrations measured for each cross section. By inspecting the Rouse profile at the ensemble where the sediment measurements were taken, the settling velocity (w_s) was determined, as no information on suspended sediment size was available. The Rouse profile for the location at which the suspended sediment measurement in cross section is shown in Figure 6.16. The corresponding velocity profile and Law of the Wall fit are shown in Figure 6.17. The velocity profile measurements show a decreased velocity near the water surface, likely due to wind effects, proving why it is important to fit only on the lowest 50% of the depth.

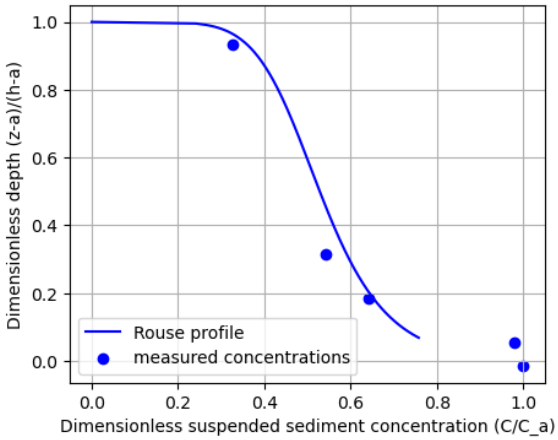

Figure 6.16: Rouse profile for cross section 1.

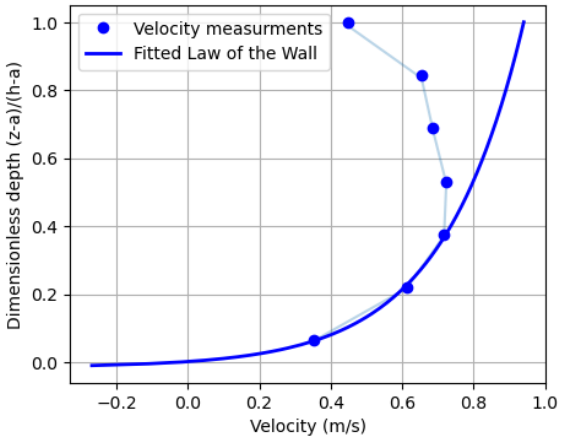

Figure 6.17: Velocity profile with Law of the Wall fit for cross section 1.

As stated above, the settling velocity is determined by fitting the Rouse profile to the measured concentrations. The estimated settling velocities are shown in Table 6.5 for the three cross sections. Additionally, the corresponding sediment grain diameter is given, which is calculated using the Ferguson and Church (Ferguson & Church, 2004) Equation (Eq. 6.9). The submerged specific density (R) is 1.65 for quartz in water and the kinematic viscosity (ν) of the fluid is $1.0 \cdot 10^{-6}$ m^2/s for water at 20 °C. The empirical shape coefficients C_1 and C_2 which reflect viscous and turbulent drag and have a value of 18 and 0.4 respectively.

$$w_s = \frac{Rgd^2}{C_1\nu + \sqrt{0.75\, C_2\, Rgd^3}} \tag{6.9}$$

The lower settling velocity and thus the lower particle diameter for cross section 2, in Table 6.5, corresponds to the steeper gradient of sediment concentration in Figure 6.14. The computed grain diameters all fall within the range of silt.

Table 6.5: Estimated settling velocities (w_s) with diameter (d) per cross section.

Cross section	w_s [m/s]	d [mm]
1	0.0015	0.042
2	0.00035	0.020
3	0.0025	0.054

The suspended sediment flux per cross section is calculated by first multiplying the concentration at any given depth, from the Rouse profile, with the corresponding velocity and a depth increment; see Equation 6.10. This flux per unit width is multiplied by the ensemble width to get the ensemble sediment flux for every point along the cross section.

$$q_s = \int_a^h C(z, \alpha C_a)\, u(z)\, dz \tag{6.10}$$

The total suspended sediment flux for every cross section is calculated by summing the ensemble fluxes. These calculated total suspended fluxes in kg/s are displayed in Table 6.6. For every cross section two different ADCP measurements were taken. The table shows the computed suspended sediment flux based on the velocity profiles of these two tracks and the mean suspended sediment flux for the three cross sections. This mean flux is the value that is used to set up the sediment balance in Section 6.3. To assess the reliability of the measurement concentrations, the estimations are compared to the existing relationship between fine sediment loads and fluvial discharge in Brazo Largo. Figure 6.18a shows the measurements conducted around the confluence. It stands out that discharges are quite small, while the loads of section 1 and section 3 are close to the fit. The fine sediment load measured in section 2 is relatively low.

Table 6.6: Calculated suspended sediment fluxes at different cross sections.

Cross section	Track 1 [kg/s]	Track 2 [kg/s]	Mean [kg/s]
1	127.14	115.61	121.38
2	90.80	61.54	76.17
3	337.44	348.07	342.76

6.2.4. Bed load

This section presents estimates of the total bed load, based on the grain size distribution of the bed samples described in Section 6.2.2. Most samples consisted of clays and silts, while two were classified as sand. This distinction strongly depends on the recovery depth of the bed samples. Considering the variability in bed material composition, a careful selection of the model used to estimate bed load transport is required.

Because the Engelund–Hansen equation was derived for non-cohesive sand-bed conditions, it is only applied to the samples identified as sand (Engelund and Hansen, 1967). The remaining samples, consisting of clays and silts, are cohesive and therefore not suitable for estimation with this method. The equation is repeated here for clarity:

$$q_t = \frac{0.05\, u^2\, h^{3/2}\, S_f^{3/2}}{(s-1)^2\, g^{1/2}\, d_{50}} \tag{6.11}$$

In which:

- u [m/s]: mean flow velocity in cross section (see Table 6.3)
- h [m]: mean flow depth
- $S_f = 10^{-5}$: friction slope, approximated here as the bed slope (López Weibel et al., 2022)
- $s = 2.65$ $[-]$: specific gravity
- d_{50} [μm]: mean grain size, derived from grain size distribution through linear interpolation

Using a channel width B and a volumetric weight of ρ_s =2650 kg/m^3, the total mass transport can then be expressed as follows:

$$Q_b = q_t \cdot B \cdot \rho_s \tag{6.12}$$

Table 6.7 performs the calculation using the corresponding input parameters for section 1, 2 and 3 respectively. Note that for section 3, a value for d_{50} is assumed because the grain size distribution showed that the sample taken at a depth of 15 meters did not contain sand. When comparing the estimated concentrations to historical data, the results appear relatively high. For the given discharge, Engelund-Hansen seems to overestimate the total bed load transport. This is shown in Figure 6.18b.

Table 6.7: Engelund–Hansen input parameters and total bed load

Section	B [m]	h [m]	d_{50} [µm]	Q_b [kg/s]
1	544	13.04	262	18.43
2	917	13.36	210	26.92
3	932	18.60	200	60.32

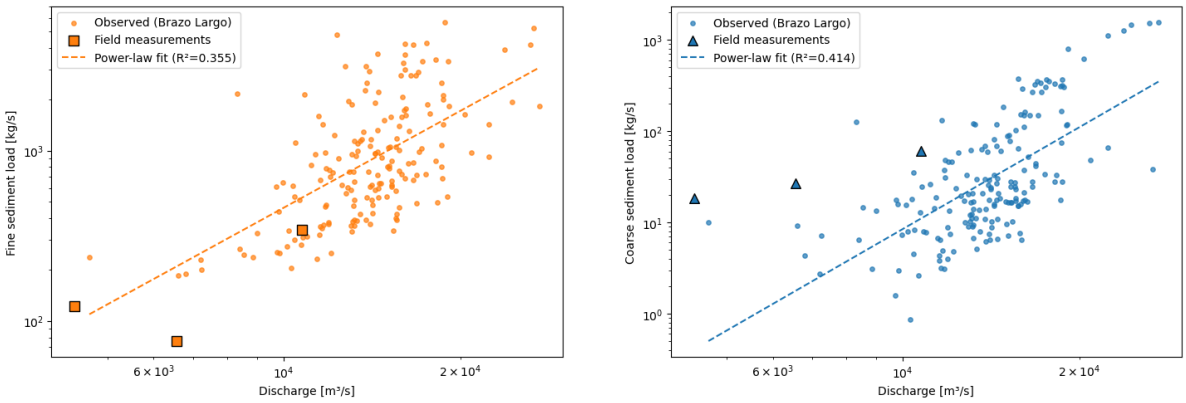

(a) Fine sediment load - discharge relation for Brazo Largo including estimations based on field data

(b) Coarse sediment load - discharge relation for Brazo Largo including estimations based on field data

Figure 6.18: Comparison of estimations based on field measurements to historical data of sediment loads

6.2.5. Longitudinal profiles

To perform analysis on the longitudinal profiles, first the depths were converted to water elevations using the relevant value for $l_{station-IGN}$ for Brazo Largo (see Figure 6.1). Next, the data points were converted to cartesian coordinates such that they could be projected onto a straight line fit through the profile paths. The assumption was made that no major changes occur in the bathymetry perpendicular to the flow direction. The results of this analysis are shown in Figure 6.19. The figure indicates that no significant sand dunes or bed forms are present in the measured profile. In addition, variations in recorded depth are attributed to inaccuracy of the measurement path. For example, the elevation difference for the section between approximately 1000-1500 meters is too large to be caused by regular river flow conditions. Moreover, the dredging location - indicated by the dotted line - experiences an elevation increase on the downstream run. This is unlikely, considering that a dredging vessel was present at the marked location, on the day of the measurements. The exact location is given in Figure 3.9.

No clear results are found in the context of dune migration or bed forms. Nevertheless, the results provide insight in the bathymetry of the confluence and the activity of dredgers. At this section, the bed slope is approximately $8 \cdot 10^3$ m/m, significantly higher than the average slope of the Lower Paraná ($\approx 10^{-5}$ m/m). Also, the vessel dredges at an elevation of around -15 m IGN.

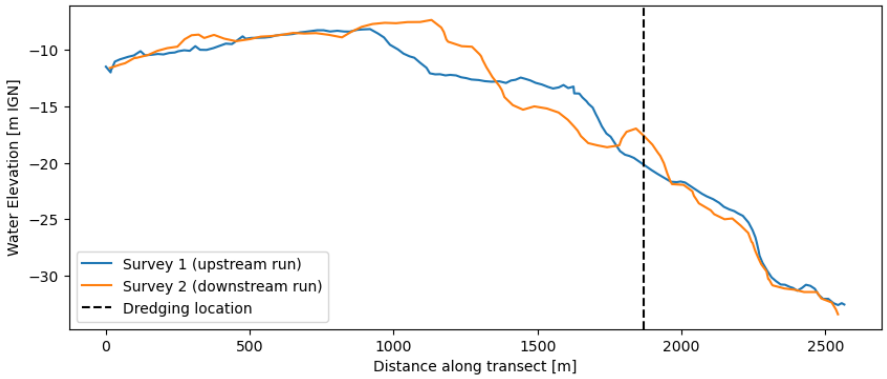

Figure 6.19: Longitudinal profiles over dredging location at confluence of Paraná Guazú and Talabera

6.3. Sediment balance

In this section, the sediment balance of the region of interest will be derived. The control volume around the confluence of the Rió Paraná Guazú and the Río Talabera is shown in Figure 6.20. The boundaries of this volume are defined by the cross sections in which discharge and sediment measurements were taken during fieldwork. These measurements are used to calculate the ingoing and outgoing sediment fluxes. As only measurements of a single day are available, the derived balance will be a momentary assessment of the amount of sediment entering and leaving the area, rather than a long-term sediment balance. However, since one of the main goals of this study is to investigate the effects of sand extraction on the river, a momentary sediment balance can still provide insights into the significance of the amount of sand that is being extracted.

Figure 6.20: Control volume for the sediment balance (Google Earth, 2025).

The computed suspended sediment fluxes from Section 6.2.3 and bed load sediment fluxes from Section 6.2.4 are shown in Table 6.8. From these fluxes, the total sediment flux per cross section is calculated, using Equation 6.13. In addition, the total sediment flux in kg/s is converted to a flux in tons per day, as the calculated flux is only representative of the day the measurements were taken. For all

three cross sections it can be seen that suspended sediment largely contributes to the total sediment flux. For cross section 1 and 3 around 85% of the total flux is suspended sediment. For cross section 2 this fraction is slightly lower with 74%.

$$Q_t = Q_s + Q_b \tag{6.13}$$

Table 6.8: Overview of the computed sediment fluxes.

Cross section	Q_s [kg/s]	Q_b [kg/s]	Q_t [kg/s]	Q_t [tons/day]
1	121.38	18.43	139.81	12079.58
2	76.17	26.92	103.09	8906.98
3	342.76	60.32	403.08	34826.11

The volume of sand extraction estimated in Section 5.1 is 30600 m^3/month. Using a sand density of 1500 kg/m^3, the amount of sand extracted from the river yields 1530 tons/day. Sand extraction in the river can be included in the sediment balance using the following equation:

$$\Sigma Q_{\text{t,in}} - \Sigma Q_{\text{t,out}} - Q_{\text{Dredging}} = \Delta S \tag{6.14}$$

In this equation, dredging is the only sink of sediment identified inside the control volume. There are no additional sources of sediment besides the computed fluxes. From Section 6.2.5 it was concluded that there is no sediment trapped in bars which can act as a sediment source. Local bank erosion is neglected as there is no information available and it is expected to be minimal on a daily scale.

By substituting the sediment fluxes from Table 6.8 and the estimated sand extraction into Equation 6.14, the change in sediment storage (ΔS) can be computed. The change in sediment storage is an indicator of net deposition (if positive) or net erosion (if negative).

$$\begin{gathered} Q_{\text{t,1}} + Q_{\text{t,2}} - Q_{\text{t,3}} - Q_{\text{Dredging}} = \Delta S \\ 12079.58 + 8906.98 - 34826.11 - 1530 = \Delta S \\ -15{,}369.55\ [\text{tons/day}] = \Delta S \end{gathered}$$

Due to the negative change in sediment storage, the deficit must be supplied by sediment already stored in the control volume, which causes bed/bank erosion. However, as the sediment balance is set up closely around the confluence, hydrodynamic effects at the confluence should be taken into consideration when interpreting the sediment balance. The meeting of two flows can create high turbulence and concentration of flow velocities. The increased turbulence enhances the sediment mixing and sediment resuspension, increasing the suspended sediment flux right after the confluence. Higher flow velocities as a result of a confluence, lead to an increased sediment carry capacity, which can potentially lead to scour of the river bed. The sediment deficit may be partly explained by the effects of the confluence still being present in the outgoing sediment flux.

6.4. Hydrodynamic effects on riverbanks

River banks are the separation between the river and the land. Therefore, it is important to evaluate the reaction of this interface to hydrodynamic changes in the river due to sand mining? Wave theory will be applied to estimate hydrodynamic loads, reflecting erosive processes at the banks. In addition to that, one should evaluate the variation of the water level on the river banks, as well as their correlation with bank erosion through the use help of satellite data. These aspects are treated in this section.

6.4.1. Waves, currents and tides

Relevant to the theory of Chapter 2, the situations that contribute to the problem of bank erosion should be investigated. Consequently, the elevation of the water level due to the high astronomical tide, and the elevation of the water level due to the waves will be explained.

The gravitational forces of the astronomical tide yield a change in water level, and are also responsible for tidal waves. These forces are induced by the gravitational pull, in the direction of the moving current. The tidal forcing has been treated in Section 6.1.4. Based on this, the astronomical tide does not contribute enough to the water elevation and wave load impact to be considered in this section.

The other types of waves that can be investigated for this study are wind waves and ship induced waves. Wind waves are produced with help of a striking distance called 'fetch', which happens when the wind blows on the surface of the water, gathering energy which translates into a wave. In order to find the significant wave height of this situation, one takes a sample of wave heights from buoys and takes the average of the highest third waves (Arriaga & Tissier, 2025). But, given that the river is not straight, the fetch or striking distance in the Paraná Guazú is overall quite short, as seen in Figure 1.1. This means that the impact of the wind waves can theoretically only be quite small. Therefore, this impact will not be taken into consideration for the calculation.

The last part of the waves treated in this Section are the ship waves. These are created when ships pass by and push away the water to make way for the boat to go forward. This situation initiates three types of waves: primary, secondary, and propeller wash waves. These can be seen in Figure 6.21 (Antonini, 2025). The impact of the secondary wave is the most promiscuous, as can be seen from the frequency plot below the sketch in Figure 6.21b.

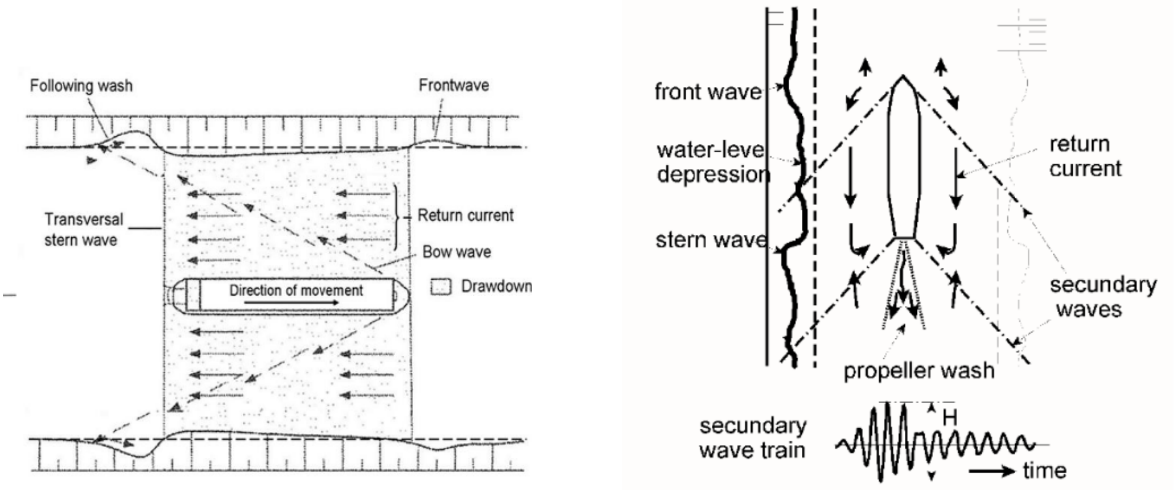

(a) Ship Waves

(b) Propeller Wash Wave

Figure 6.21: Ship waves effect on water and banks (Antonini, 2025)

The effect of current loads on river banks needs to be taken into consideration as well. Using the standard values of the Netherlands and the given facts about the size of the ships circulating and the currents in the Rio Paraná Guazú, one could assume the wave height and current amplitudes for this case. This was reflected once the field measurements were known, as described in Section 3.2. Table 6.9 gives the standard design values for wave heights and currents. The relevant row for this project is the 'Rivers' category. Hinting to the fact that big ships are usually present in the channel, one might take values towards the upper boundary of the table.

Table 6.9: Standard values for wave heights and currents in the Netherlands (Antonini, 2025).

Location	Wave heights [m]		Currents [m/s]	
	Wind waves	Ship waves	Natural current	Return current
Lakes	0.25–1.00	0.10–0.50	0.1–0.5	0.1–0.25
Canals	0.10–0.25	0.25–0.75	0.5–1.0	0.5–1.0
Rivers	0.25–1.00	0.25–0.75	1.0–2.0	0.5–1.0
Small waters	0.10–0.20	n.a.	0.2–1.0	n.a.

6.4.2. Calculation of loads and impacts due to ships

Following the information about tides waves and currents, one might ask how the ship induced waves exerts a force on the river bed. This can be answered with the help of wave theory. The first relevant parameters to take into account are the ship waves in rivers. These are assumed to be between 0.25 and 0.75 meters tall according to Table 6.9. Based on observations during the field trip, the value of 0.25 meter wave height is chosen, and a distance of 100 meters from the boat to the bank, as the cargo ships do not travel with a speed significant enough to reach heights of 0.75 m at the riverbank.

Wave load

In this case, one can calculate the force of the wave, assuming that the wave signal given by the boat is uniform. In the calculation one assumes from the video filmed in the field trip that the wave spectrum coming from the ship includes about 10 repetitions, and that the boat is located 100 meters from the shore. This leaves us with the wave theory of (Arriaga & Tissier, 2025) which states that there are two types of waves you can get energy from:

- Periodic waves
- Random waves

Wave energy is a specific energy and it is calculated per unit of horizontal area [J/m^2]. The equation to calculate wave power for periodic and random waves is given as follows:

$$E_{pw} = \left(\frac{1}{8}\right) \cdot \rho \cdot g \cdot H^2 \tag{6.15}$$

$$E_{rw} = \left(\frac{1}{16}\right) \cdot \rho \cdot g \cdot H^2 \tag{6.16}$$

where:

- ρ is the density of fresh water: 1000 kg/m^3;
- H is the wave height: 0.25 m;
- g is the gravitational constant: 9.81 m/s^2

On a small interval of time, the ship waves can be assumed to be periodic. Therefore, Equation 6.15 can be applied here. Substituting the parameters in the equation yields:

$$E_{pw} = \frac{1}{8} \cdot 1000 \cdot 9.81 \cdot (0.25)^2 = 76.64 \text{ J/m}^2$$

Converting units gives:

$$F_w = 0.766 \,\text{kN/m}$$

There are 6 boats passing by every day and each boat creates approximately 10 ship-induced waves. Accordingly, a dynamic loading system would be required to solve this situation. Due to a lack of

information the implementation of a dynamic loading system is not an option. Therefore, it is chosen to use a slight simplification of the situation by considering a static system.

Summing all the forces for every wave passing by would be incorrect. In order to successfully choose an approach for the static model, the method of cyclic loading assuming a dynamic load factor was chosen. According to dynamic wave loading, a factor of 1.2 to 1.5 can be used to determine the cyclic loading of a wave (Cuomo et al., 2004). This factor depends on the type of structure and soil which is the strongest on a concrete structure, but for a bank made out of clay/sand the value of the factor sits at 1.3. The final value of the ship induced wave load is therefore:

$$F_w = 0.766 \cdot 1.3 = 0.996 \text{ kN/m}$$

Current load

The current of a river can have different effects on the river bank depending on the degree of impact on the bank. A current working directly perpendicular to the bank does not have the same effect as a current moving along the bank. The current going along the river bank creates a different type of load, categorised as shear (Chow, 1959). For the situation of the Paraná Guazú, one may use the shear equation from the Open Channel Hydraulic Book cited above to calculate the force exerted by the current on a vertical structure:

$$F_c = \tau \cdot A = \rho \cdot g \cdot h \cdot S \cdot A \tag{6.17}$$

where:

- F_c: Shear force exerted by the current [N]
- ρ: Density of freshwater: 1000 kg/m^3
- g is the gravitational constant: 9.81 m/s^2
- h: water depth at location [m]
- A: Exposed area [m^2]
- S: River slope [-]

The shear force exerted by a river current on its banks is a critical factor in understanding erosion and bank stability. This force is not uniform along the length of a river channel but varies due to changes in bathymetry and bank geometry.

To be able to calculate the force of the current on the bank, one needs to find the parameters of the equation for the exposed surface area. As the water density (ρ) and the gravitational constant (g) can be assumed to be constant along the channel, the other parameters can differ in function of the chosen location. Since it cannot be known exactly how tall the relevant bank stretch is over the whole area, one could assume a 1 meter riverbank height constant from field work measurements. So A = 1 [m^2] would yield a force illustrated per meter length of the bank. Moreover, the parameter of the river slope (S) is equal to 10^{-5}, as obtained from previous INA research (Instituto Nacional del Agua, 2025). Lastly, the parameter of water depth depends on the bathymetry of the location chosen. These values were obtained during the field trip measurements. Based on a chosen location, one can obtain the water depth via the local bathymetry cross section, and inserting this last parameter into the equation 6.17 above. This can be useful for mitigation strategies regarding bank erosion.

The relevant location for erosion was chosen in Chapter 3, near Camping La Blanqueada. When analysing the current bank conditions, it was seen that the land was highly eroded, some trees were on the verge of being in the water, while others were already sucked up by the river. This is highlighted in the Figure 6.4.2 below taken during the field trip.

(a) Bank erosion La Blanqueada

(b) Bank erosion close-up

Figure 6.22: Bank erosion shots from fieldwork with drone

6.4.3. Implementing Aqua Monitor data

Illustrating the bank damages due to local ship waves, currents and tides is important to understand the local scale. Nevertheless, it makes more sense to add a global scale study of the water gains and losses on top of that in order to sum up the ways water levels can influence the bank erosion. So, in this section the data from the water gains and losses will be explained in more detail.

Recalling the whole period of time available in Section **??**, it is clear that the outer side of the river curves experience a water surface gain (indicated in blue), and the inner sides of the curves lose water, implying sedimentation (indicated in green). For simplicity, the **??** is shown below as well.

The location of the 'La Blanqueada' camping is situated on the outer side of the curve near Puerto Constanza, as seen in Chapter 3, Figure 3.10. The camping's location matches with the blue part of the water gain map, indicating that the water quantity around the shore of the camping has increased. In order to know if this has always been so, or if the water gains in this precise location have been gradually increasing, several maps with closer intervals have been created.

As one can see the blue and green zones stay consistent throughout the years, but when going into detailed time periods they can differ. Variations occur on shorter time periods such as the period 2005-2015, which indicated more water gains than losses in the deltas surrounding the region of interest. Furthermore the flood of 2016 in the Paraná Guazú can also be illustrated through the help of this map, on a time interval of 2015-2017 (see Figure 6.2a).

Figure 6.23: Aqua Monitor water changes 1985-2025 (Deltares, 2025a)

In addition to that, droughts are well highlighted with this application. An example would be the long period of drought in 2022 which led some parts of the Paraná to be left dry, as seen in Figure 6.27. With the Paraná Guazú's significant depths of over 40 meters this was unlikely to happen but still, this change in water quantity did not go unnoticed by the Deltares application. This can be seen on the Figure of 2020-2022. Other periods of time are more or less stable and have nothing to report. For the sake of these explanations the relevant figures can be found in the Appendix D.

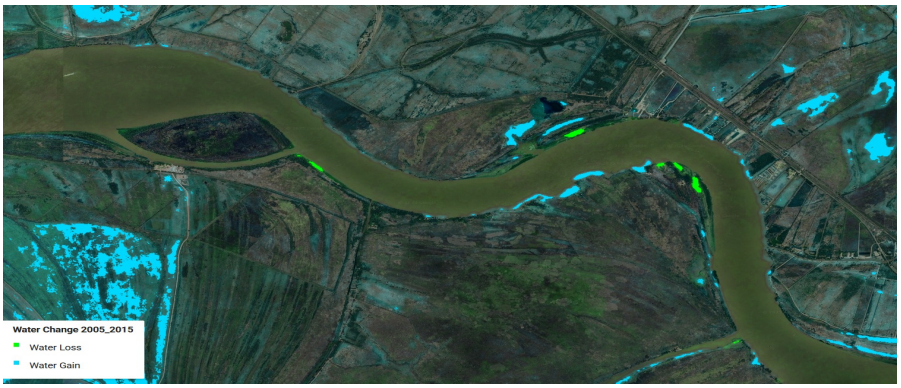

(a) Period 2005-2015 (Deltares, 2025a)

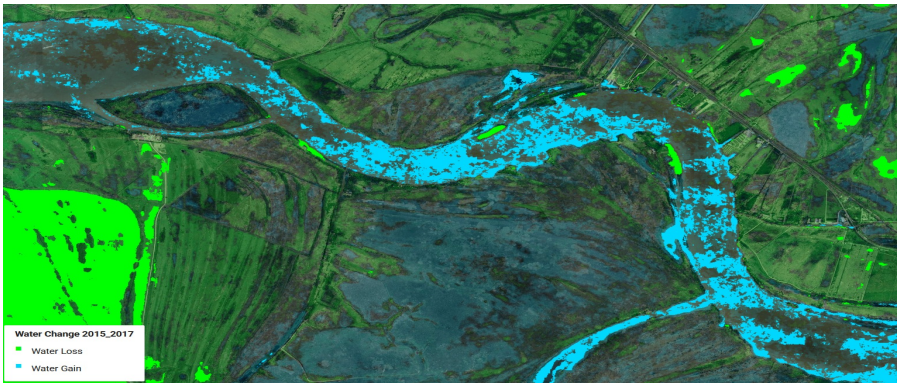

(a) Period 2015-2017 (Deltares, 2025a)

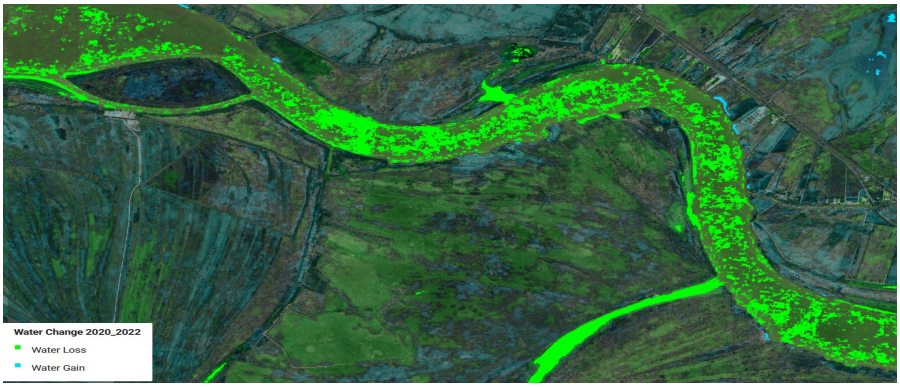

(a) Period 2020-2022

Figure 6.26: Water changes in different periods (Deltares, 2025a)

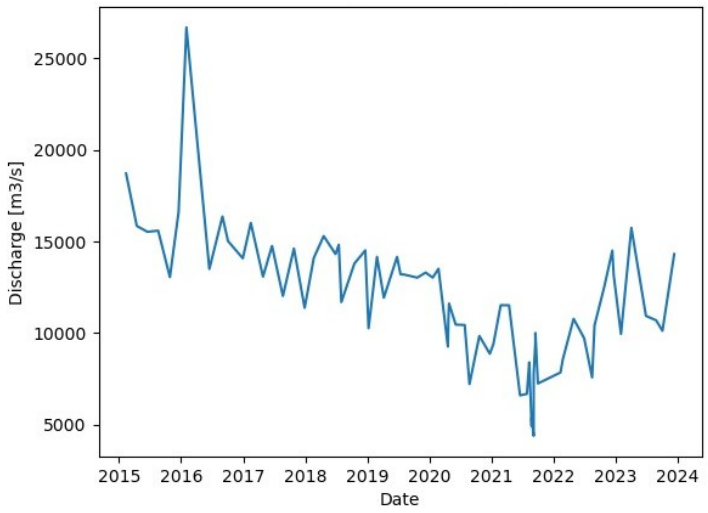

Figure 6.27: Discharge time series in Brazo Largo

6.4.4. Surface area measurements

Using the software's satellite data, one can draw a surface around the area of the camping La Blanqueada in 2022, the most recent available, and then compare it to historical data. This gives a dataset of historical data from 1985 until 2022 but since the satellite images have been improving with time, the only relevant data can be taken from 2003 on.

Thus, it was chosen to take the difference in surface area from 2022 until 2003. Initially, only the East side of the camping was taken into account due to its matching with the drone pictures taken of the area during the field trip as seen in Figure 6.22. Nevertheless on Google Earth it quickly became obvious that the necessity rose to take the West part of the camping in consideration as well since its surface was eroded even further. A summary of the data gathered from this study can be found in Figure 6.28. First the measurement of the East part of the Camping, then the comparison with 2003, 2017, 2018 and then for both sides the added surface lost since 2003.

It is known that there was a flood in 2016 (Equipo de Manejo de Información, 2016). This flood was in return responsible for a significant increase of water quantity and discharge throughout the region, as seen in Figure 6.27. Consequently, this affected certain areas of the channel more than others, in particular the curves of the Paraná Guazú such as Puerto Guazú showed in Figure 6.26. The negative impacts were highlighted when the high discharge and water quantities dropped back to normal, leaving a part of the bank fragile which then contributed to an accelerated bank erosion. This argument can

(a) Surface data for 2022

(b) Surface data for 2017

(c) Surface data for 2018

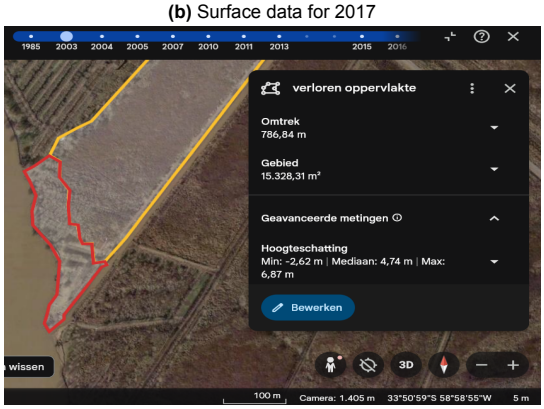

(d) Surface data for 2003

Figure 6.28: Comparison of surface data (Google Earth, 2025)

once again be solidified by the drastic increase of erosion in between those time periods. After this flood event, the rate of erosion decreased again.

Lastly, both sides of the camping and the difference between 2003 and 2022 can be seen below. The leftover piece of land which was present in 2003 but has been eroded since then is also traced as a surface area in a distinct colour (see Figure 6.29). The complete comparison with all accessible historical data was documented in the Appendix D. Moreover, values of the surface areas, perimeters, and further quantifications can be found in Section 6.4.5.

(a) Surface data for 2003

(b) Surface data for 2022

Figure 6.29: Comparison of lost surface data (Google Earth, 2025)

6.4.5. Quantitative Results

The values of these areas can be found in the Table 6.10. It is important to note that the green part of the area is very likely to be dug out by the owner himself to build a channel for the boats. This probably contributes to an acceleration of the erosion around this part of the land.

Table 6.10: Surface changes at camping La Blanqueada in 2022.

Location	Category	Colour	Perimeter [m]	Area [m^2]
East Part	Actual	Yellow	1520.46	88494.30
East Part	Lost	Red	786.84	15328.31
West Part	Actual	Blue	1203.31	71231.39
West Part	Lost	Orange	466.70	8698.71
West Part	Dug out	Green	468.46	7622.01

In addition to that, the lengths of the lost land can be found using the ruler in Google Earth as well. This gives the possibility of illustrating the scale of the erosion, and how much the owners of the camping lost their land in the last decades. In the most extreme case down south east of the camping zone, which can be seen in the Figure 6.29 by the purple lines, and once again in more detail in Figure 6.30.

(a) Length of land 2003

(b) Length of land 2022

Figure 6.30: Comparison of lost surface data (Google Earth, 2025)

The lengths of the measured segments as well as the lost length have been calculated and put in the Table 6.11 below. The loss ratio's of the camping surface are calculated in the Appendix D.

Table 6.11: Loss of land for Camping La Blanqueada in 2022.

Location	Length in 2003 [m]	Total loss in 2022 [m]	Loss per year [m/y]
Section 1	118	73	3.9
Section 2	156	57	3.0
Section 3	276	138	7.3

7

Delft3D model

This chapter presents the setup and application of the Delft3D model developed to understand the flow behaviour in the study area, with a focus on the confluence area where sand extraction occurs. In addition, the model results are used to identify locations along the river that are prone to erosion. The model was set up as a two-dimensional, depth-averaged model in which sediment transport and morphological changes are not considered. The time period simulated is 25 and 26 September 2025, which are the two days at which field measurements were taken. The field measurements from these days are used for boundary conditions and calibration of the model.

7.1. Model setup

In this section, the Delft3D model setup used to simulate the hydrodynamic response of the system is explained. The setup of the model involves defining the computational grid, processing the bathymetry, specifying boundary and initial conditions and finally selecting appropriate physical and numerical parameters.

Since no existing grid was available for the area of interest, the grid was generated using the RGFGRID tool in Delft3D. As a starting point, a land boundary file similar to the one shown in Figure 6.10 was used. By drawing splines with a decreasing spacing towards the confluence, the grid resolution was refined for the region of hydrodynamic interest. This approach ensures that the model captures the flow behaviour at the confluence with high accuracy while maintaining computational efficiency in less critical areas. After generating the grid, further refinements were made to ensure that the grid contains at least 20 cells in a cross section near the confluence and around 10 cells in a cross section far away from the confluence. When generating the grid, it was made sure to limit the aspect ratio to 2.0. The generated grid is shown in Figure 7.1. The generated computational grid has 1044 grid cells in M-direction, 1043 cells in N-direction, and 91706 grid elements. The grid size at the confluence is around 20x20 meters and the grid size at the upstream boundary near Ibicuy is 75x125 meters.

The bathymetry was derived from a Digital Elevation Model (DEM) from 2019, which was provided by INA. This DEM was used to create samples that contain geospatial coordinates and the corresponding depths. Using the QUICKIN tool in Delft3D, these samples were interpolated onto the computational grid. For this interpolation, Grid Cell Averaging was applied with the minimum number of averaging points set to one. Grid Cell Averaging was preferred over Triangular Interpolation as it is computationally less expensive, and more samples were available than grid points (Deltares, 2025b). Lastly, Internal Diffusion was applied, with the number of internal diffusion steps set to 1000, to smooth sharp gradients and fill in missing values. The interpolated bathymetry is shown in Figure 7.2. The maximum depth of 40.403 m occurs just downstream of the confluence.

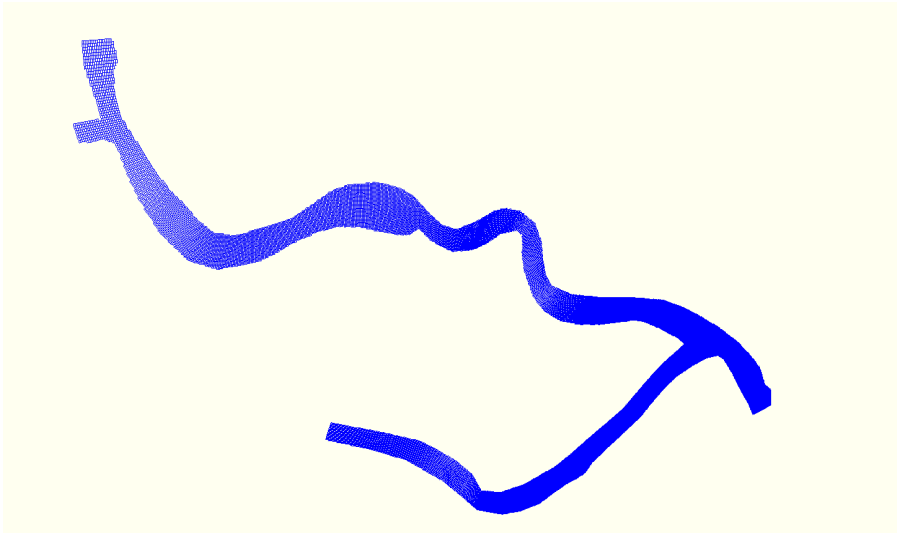

Figure 7.1: Generated grid for the Delft3D model.

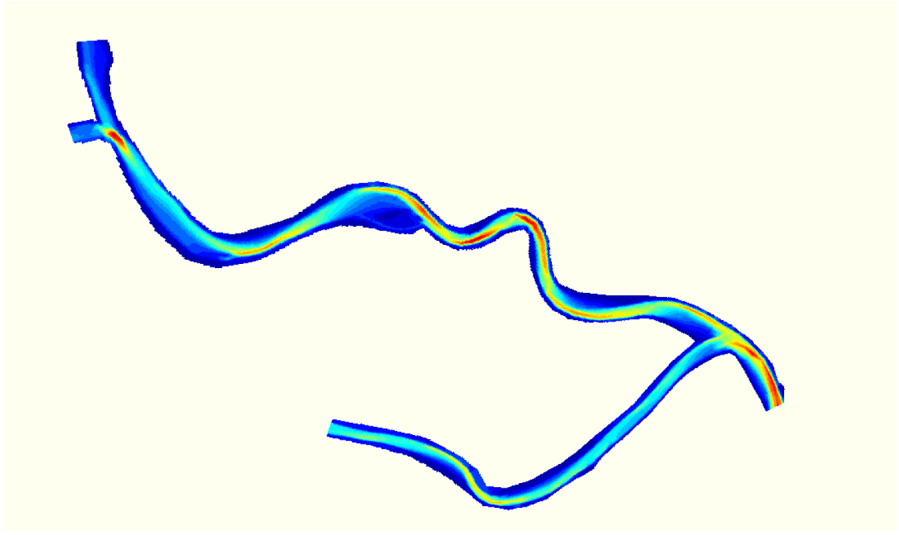

Figure 7.2: Bathymetry Delft3D model.

In order to validate the use of the 2019 DEM for creating the bathymetry, cross sections from the generated bathymetry were compared with measurements obtained by the ADCP during the field campaign. The comparison of the bathymetries of the three cross sections is shown in Figure 7.3. Although the interpolated and measured bathymetries are not exactly the same, the overall shape and depths are very similar, ensuring that the Delft3D simulations accurately represent the current hydraulic conditions.

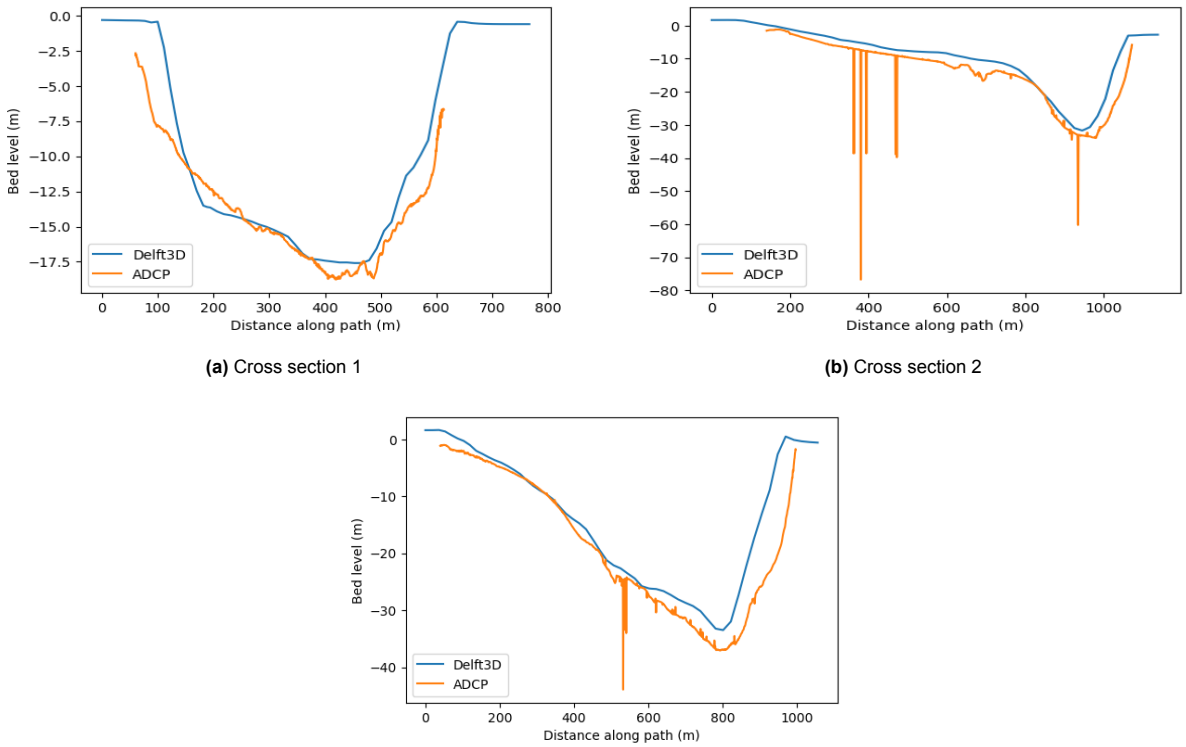

(a) Cross section 1

(b) Cross section 2

(c) Cross section 3

Figure 7.3: Bed levels along three analysed cross sections: (a) Cross section 1, (b) Cross section 2, and (c) Cross section 3.

The computational grid shown in Figure 7.1 has four open boundaries where boundary conditions must be imposed. For the downstream boundary at Brazo Largo, a water level time series with measurements taken every 20 minutes was used, see Figure 7.4. For the other three boundaries at Río Talabera, Río Ibicuy, and Río Paraná, total discharge time series were applied. Since no discharge data were available for these locations, discharge results from a one-dimensional HEC-RAS model at Brazo Largo were provided by INA. Using the discharge measurements from the field campaign, assumptions were made on the percentage of total discharge distributed across the domain. These ratios, derived from Table 6.3, were subsequently multiplied by the Brazo Largo discharge series to determine the appropriate boundary conditions for the remaining boundaries. The three upstream boundary conditions are shown in Figure 7.5. The observed spike in waterlevels and drop in discharge on September 24 is the result of a storm surge in Río de la Plata.

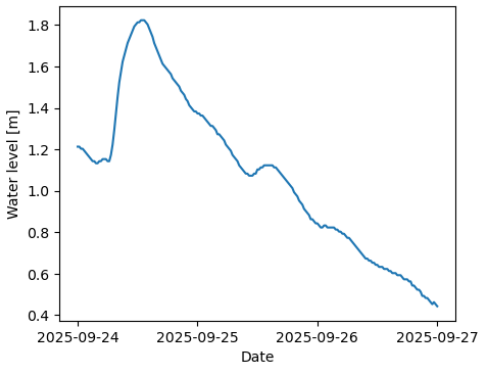

Figure 7.4: Downstream water level boundary condition.

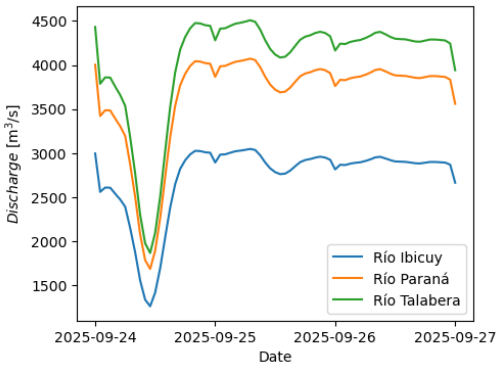

Figure 7.5: Upstream discharge boundary conditions.

For the initial water level, the level was used at the start of the first simulated day (1.213 m). Since the period of interest is 25 and 26 September 2025, the simulation was started on 24 September 2025 to allow for model spin-up.

For the hydrodynamic simulation, a time step of 0.2 minutes was used to ensure that the Courant number remained below 1.0, thereby maintaining numerical stability while remaining computationally efficient. The bed roughness was defined using the Manning equation with a Manning's roughness coefficient (n) of 0.025 in both the longitudinal (U) and lateral (V) directions, which corresponds to moderately rough river beds. In order to account for the secondary flow in river bends and the confluence, a secondary flow coefficient (β_c) of 0.5 was used. This coefficient determines the fraction of shear stress taken into account in the momentum equation due to secondary flow.

The horizontal eddy viscosity and horizontal eddy diffusivity were set to 1 m^2/s and 2 m^2/s respectively. These values were chosen to provide realistic horizontal momentum and scalar transport. Large values for the horizontal eddy viscosity and horizontal eddy diffusivity can lead to excessive numerical smoothing. The Horizontal Large Eddy Simulation (HLES) turbulence model was not activated to calculate the viscosity and diffusivity in the base run because simulations with HLES activated are computationally more expensive. HLES resolves smaller turbulent eddies explicitly, which requires a smaller time step, hence why it is computationally more expensive. Instead, the influence of the HLES turbulence model is evaluated in the sensitivity analysis.

7.2. Model calibration

The Delft3D model was calibrated to ensure that the simulated hydrodynamic conditions accurately represent the real-life flow conditions. The calibration was done by comparing the model's water elevation near Ibicuy to a measured water elevation time series. Additionally, the simulated depth-averaged velocities in the three cross sections near the confluence are compared to the ADCP measurements from the field campaign. The calibration primarily focused on adjusting the Manning roughness coefficient, as this parameter has the highest influence on flow velocities and water depth.

In addition to the initial Manning roughness coefficient (n) of 0.025, the model was tested with roughness coefficients of 0.01, 0.02, and 0.05. The resulting water levels at Ibicuy are shown in Figure 7.6. It can be clearly observed that a higher bed roughness leads to higher water elevations. Of all the values tested, a Manning coefficient of 0.02 was found to result in the most accurate water elevations.

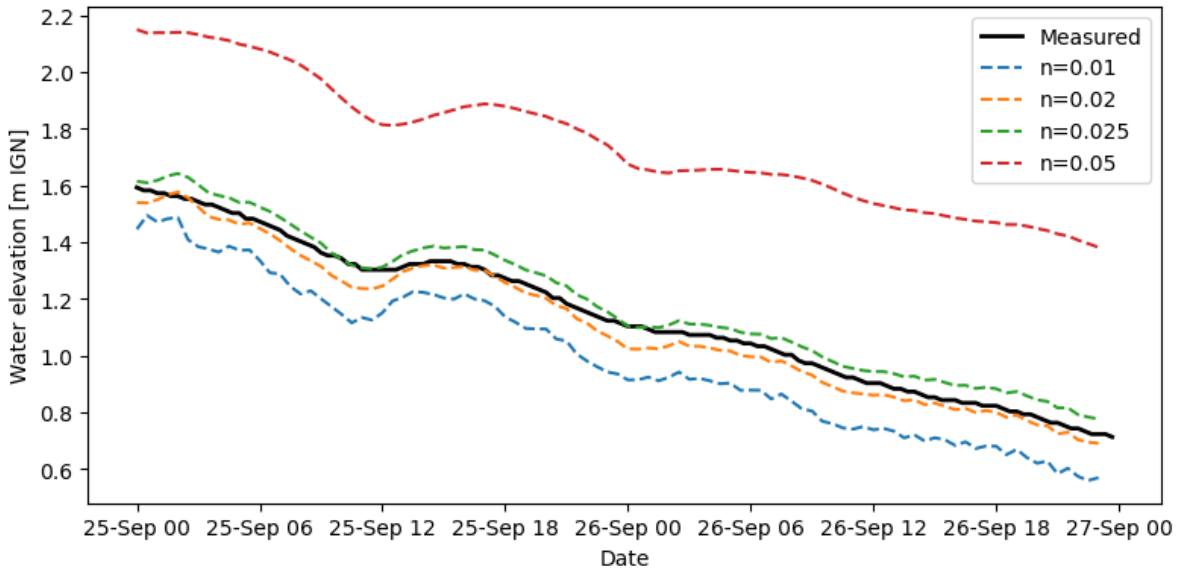

Figure 7.6: Water elevations near Ibicuy for measurements (solid line) and model output (dashed line).

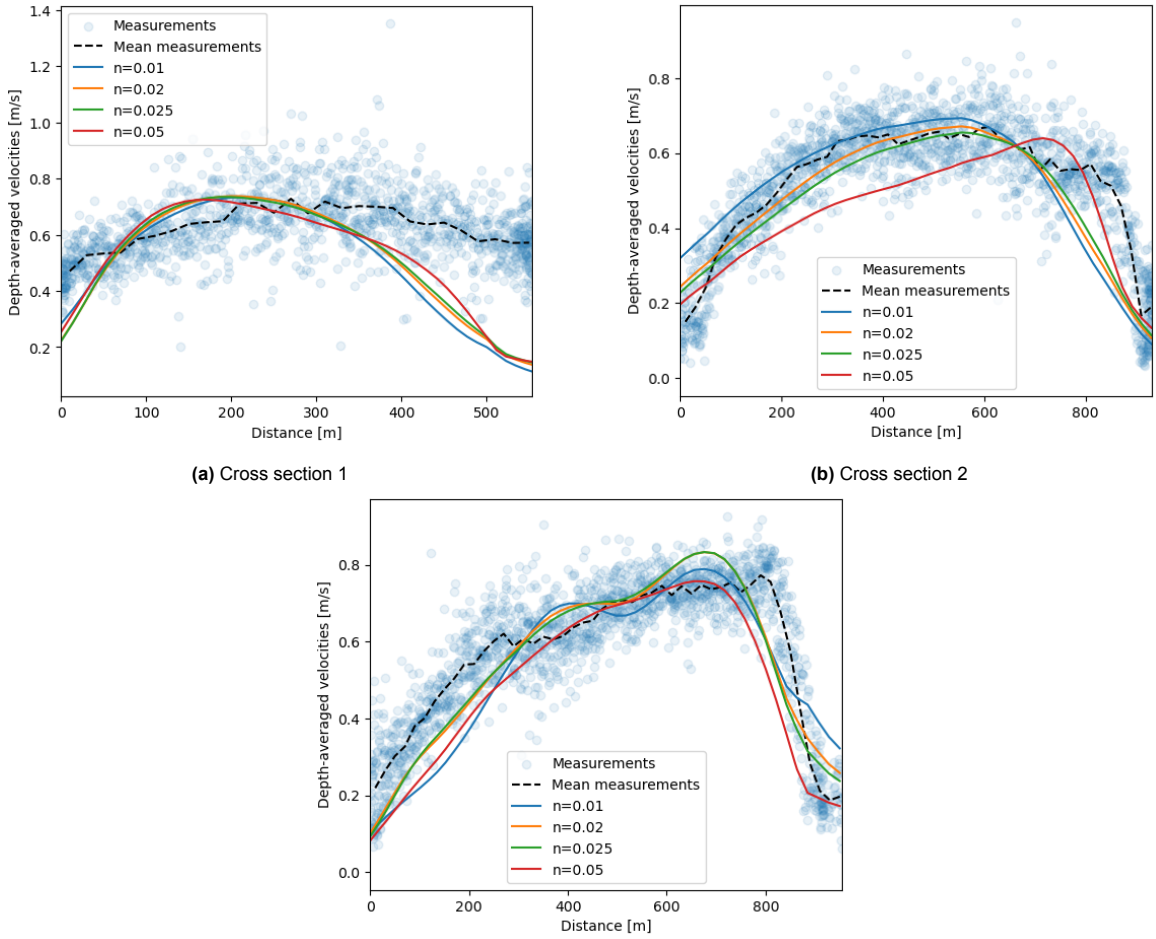

(a) Cross section 1

(b) Cross section 2

(c) Cross section 3

Figure 7.7: Measured and simulated depth-averaged velocities for the three cross sections.

Figure 7.7 shows the measured and simulated depth-averaged velocities for different Manning coefficients. In general, lower bed roughness leads to higher flow velocities. However, the effect of the bed roughness on the flow velocities is less strong than the effect on the water elevation. In addition, different values for the roughness coefficient were found to slightly affect the shape of the depth-averaged velocities profiles. From Figure 7.7 it can be seen that using a Manning coefficient of 0.02 results in realistic depth-averaged velocities for cross sections 2 and 3, both located in the Paraná Guazú. Although the magnitude of the flow velocities is correct for cross section 1 (located in the Río Talabera), the shape of the velocity profile does not match the measured data.

7.3. Model results

The depth-averaged flow velocities in Figure 7.8 show the distinct flow patterns in the confluence area. The highest velocities are concentrated around the outer bends of the channel. These zones correspond to the main flow paths, which is also confirmed by the areas with an increased depth in Figure 7.3. The highest velocities, reaching up to 0.79 m/s, occur downstream of the confluence where the flow of the two channels is concentrated. Lower flow velocities are observed in the inner bends of the channel and at the location at which the two channels meet. The velocity vectors in this latter location indicate flow separation and recirculation.

The bed shear stresses in Figure 7.9 show a behaviour similar to the flow velocities. Furthermore, it can be seen that the bed shear stresses increase just upstream of the confluence in both channels and decrease within or just downstream of the confluence. The increase in bed shear stress is a result of the flow alignment toward the confluence, which accelerates the flow and raises near-bed velocities. The decrease in stresses at the confluence results from the deceleration zone, which is caused by the difference in magnitude and direction of the two streams. The high stress zones along the outer banks, with values exceeding 0.8 N/m^2, indicate areas likely to experience scour. In contrast, the zones with low bed shear stresses at the junction of the two streams, correspond with zones were sedimentation is expected. This is also the location at which sand is extracted, see Section 5.1.

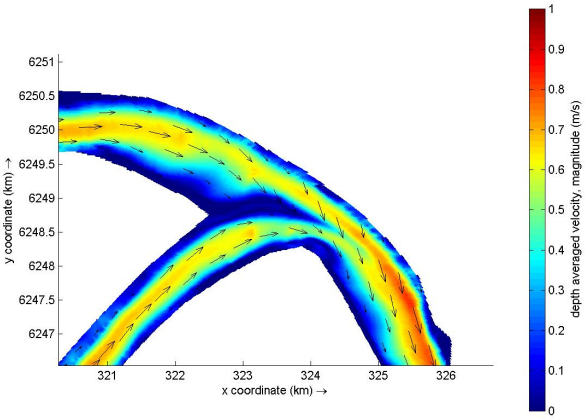

Figure 7.8: Magnitude of the depth-averaged flow velocities at the confluence.

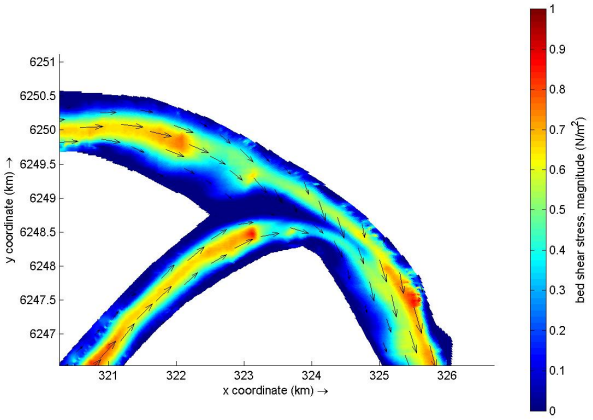

Figure 7.9: Magnitude of the bed shear stress with depth-averaged flow velocities (vectors) at the confluence.

The locations prone to erosion are identified by inspecting the flow velocities for the river stretch upstream of the confluence. The most pronounced acceleration occurs at sharp and narrow bends, where the flow is directed to the outer banks, resulting in increased near-bed velocities and thus increased bed shear stresses. As shown in Figure 7.10, the sharp and narrow bend upstream of the confluence shows a clear concentration of flow velocities near the outer bank, indicating an increased risk of erosion in this area.

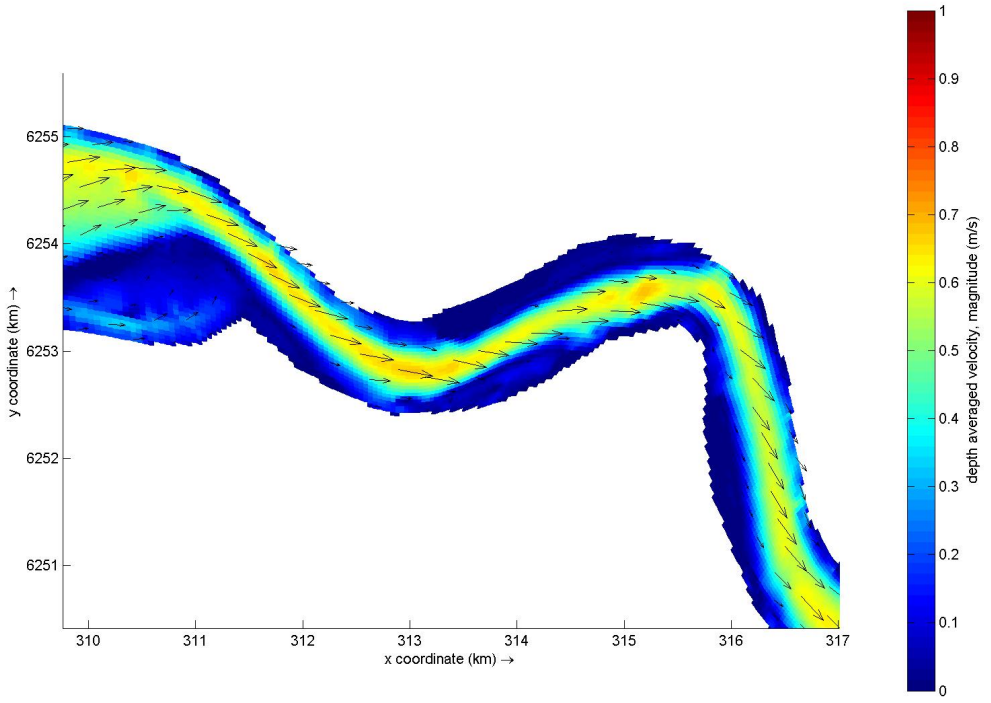

Figure 7.10: Depth-averaged velocities upstream of the confluence.

7.3.1. Sensitivity analysis

The objective of the sensitivity analysis is to assess how key parameters affect the simulated river flow. This is done in order to test the robustness of the model, as the exact value of most key parameters is not known. Inspecting the influence of different key parameters provides insight into the uncertainties related to the model. In Section 7.2 the influence of the Manning roughness coefficient on water level and depth-averaged flow velocities was tested to calibrate the model. In this section, the influence of selected parameters such as the secondary flow coefficient (β_c), the horizontal eddy viscosity and the horizontal eddy diffusivity is discussed. In addition, a simulation was done with the HLES turbulence model activated to assess its impact on resolving turbulent eddies more explicitly.

The secondary flow coefficient used in the base model is 0.5. The influence of this parameter is tested by simulating with both a higher coefficient (1.0) and a lower coefficient (0.1). By inspecting the depth-averaged flow velocity profile in different cross sections of interest, it was found that the shape and magnitude of the profile remained almost identical. For the horizontal eddy viscosity, a viscosity of 5.0 m^2/s was tested besides the used value of 1.0 m^2/s. These values are determined using the Péclet number. From this it was found that the use of a high viscosity leads to more smoothed velocity profiles in the cross sections that do not represent the observed characteristics. Two simulations were performed with an increase in horizontal eddy diffusivity (5.0 m^2/s and 10.0 m^2/s). From this it was found that the influence of this parameter on the model's output is very little. For higher diffusivity values, the model gave an error when simulating. Activation of the HLES turbulence model also did not change the results much, but as it required a much smaller time step (0.05 min), it was computationally more expensive.

8

Mitigation Strategies

This chapter presents solutions to the challenges identified in this study. It begins by comparing structural approaches to address bank erosion. The focus then shifts to Nature-based solutions (NbS), exploring their potential to mitigate the impacts of both dry sand mining and river sand extraction, including their role in reducing bank erosion.

8.1. Comparison of structural solutions

Several structural solutions to mitigate bank erosion are discussed in Chapter 2. These solutions are compared and evaluated in Table 8.1, where the different structural alternatives presented in Section 2.7 are summarized and assessed according to a set of relevant design criteria. The design criteria on which the alternatives are assessed include: installation, price, resistance, versatility, disturbance, water tightness, durability, and sustainability. The scores given for each criterion are based on a scale of –,-,0,+,++.

Table 8.1: Comparison of structural solutions

Method	Installation	Price	Resistance	Versatility	Disturbance	Water tightness	Durability	Sustainability
Sheet pile wall	++	+	+	-	-	0	+	++
Diaphragm wall	–	–	++	++	+	++	++	-
Precast concrete wall	-	-	++	0	++	+	+	–
Auger/Soldier pile wall	+	++	0	+	++	–	-	0

As can be seen in Table 8.1, pile walls score low on water tightness and durability. The area of interest is located in a delta and hence high groundwater levels are to be expected. Therefore, water tightness must be guaranteed. Since the auger/soldier pile walls don't offer this certainty, this option is not further discussed. The diaphragm wall, on the other hand, offers great water tightness but installation is a far bigger challenge for this method. The benefits that the diaphragm wall offers, great resistance and low disturbance being the most relevant ones, do not outweigh the cons: the large amounts of time, space and budget needed to construct them. The same is true for the precast concrete wall: the heavy elements ask for a specialized and expensive installation procedure. The specialized equipment and experience is possibly not available or expensive, which means the precast concrete walls are not a viable option.

As a structural solution, the sheet pile walls are chosen. These elements score high on ease of installation and sustainability (parts can be removed and reused) and price, resistance and durability are also pros of this method. Disturbance is one of the main concerns related to sheet pile walls, but since the area of interest is in a scarcely populated area, this is not necessarily problematic. Another concern is the low versatility: installation is only possible if soils are not too hard. However, since installation will be executed in a delta with relatively soft soil (see Section 2.2), this should not be a major concern for this project.

8.2. Sheet pile wall

Sheet pile walls are widely used in applications such as excavations, waterfront structures, highway structures, flood protection schemes, and bridge abutments (Grabe, 2008). Steel sheet pile walls are particularly common because they offer a wide range of section types and combinations that can be adapted to various design conditions. These profiles provide high moments of resistance while still satisfying the structural requirements (Grabe, 2008). Their main engineering advantages include suitability for use in water, a favourable ratio between steel cross section and moment of resistance, and rapid on-site installation. Collectively, these characteristics make steel sheet piles both functional and economical, contributing to their widespread use (Grabe, 2008).

The primary types of steel sheet pile walls used in practice are cantilever and anchored sheet piles (Brown, 1994). Cantilever sheet piles are typically used as flood or earth retaining walls with heights ranging between 4 and 5 meters (Baxter et al., 2022). Their stability is provided by the resistance of the surrounding ground and foundation soils, as illustrated in Figure 8.1. Anchored sheet piles are used when the heights of cantilever sheet piles is exceeded or when the design is governed by lateral deflections (Brown, 1994). For anchored sheet piles, sufficient horizontal space must be available to accommodate the installation of the anchoring system.

Figure 8.1: Cantilever and anchored sheet pile wall

Sheet pile walls can be constructed from various materials, such as steel, concrete, or wood (Brown, 1994). In this report, steel is selected as its advantages outweigh the disadvantages and make it more suitable than concrete or wood. Although concrete provides a longer service life, it involves higher initial costs compared to steel and the installation of concrete walls is more complex (Brown, 1994). Wooden sheet pile walls are applied for structures of limited height and temporary use (Brown, 1994). As discussed in Section 2.7, the advantages of steel sheet piles make them the most commonly used material, due to their high strength, low weight, long service life, and favourable ratio between cross section and moment of resistance (Brown, 1994).

The sections and interlocks for the steel sheet pile walls are essential to achieve a complete wall, when used for waterfront structures (Baxter et al., 2022). Figure 8.2 presents typical steel sections commonly used in practice, known as U and Z sections. In this figure, the interlocks that provide the sections with their strength are visible. The interlocks of U sections are located on the neutral axis, whereas for Z sections they are placed on the edges. The maximum shear stress occurs on the neutral axis, which means that the interlocks must be welded or crimped to ensure the full moment of resistance is achieved (Kelly, 2018). When sections are exposed to water, water tightness must be ensured. This can be achieved by filling the interlocks with plastic compound materials or applying a preformed polyurethane interlock seal (Baxter et al., 2022). The following paragraph outlines the key steel properties relevant to the design.

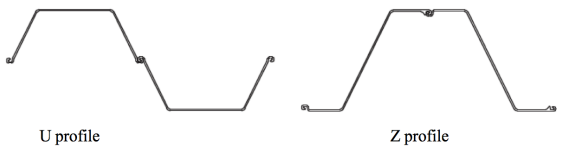

Figure 8.2: U and Z sections (Sheet Piling Group, 2018)

Steel is the material used for the sheet piles. The properties of steel, as a homogeneous material, are briefly introduced in this paragraph. Steel behaves as an elastic material and possesses a favourable strength-to-weight ratio with tensile strengths ranging between 300 and 2000 N/mm^2 (Grabe, 2008). Beyond its general mechanical advantages, understanding the stress–strain behaviour of steel is essential for the design. This behaviour is illustrated in Figure 8.3. The range of elasticity depends on the grade of steel, and the elastic modulus, E, is 210,000 N/mm^2 (Schipper, 2024). In Figure 8.3, $f_{y;d}$ denotes the design yield strength, representing the point at which the stress remains constant, decreases or reaches a strain of 0.2% upon unloading. Furthermore, $f_{t;d}$ indicates the design tensile strength, which varies depending on the grade of steel (Grabe, 2008). The mechanical properties of the steel used for the sheet piles are summarised in Table 8.2.

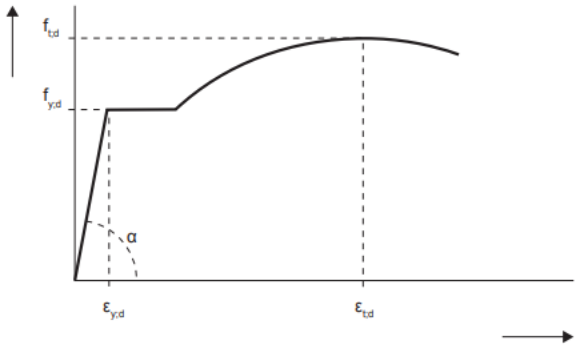

Figure 8.3: Stress-strain relation steel (Schipper, 2024)

Table 8.2: Mechanical properties by steel grade (Baxter et al., 2022)

Steel grade	Tensile strength f_u [N/mm^2]	Yield strength f_y [N/mm^2]	Elongation at failure ε_u [%]
S 240 GP	340	240	26
S 270 GP	410	270	24
S 320 GP	440	320	23
S 355 GP	480	355	22
S 390 GP	490	390	20
S 430 GP	510	430	19

Steel sheet piles are manufactured from hot-rolled sections, produced by heating steel to temperatures between 850 and 1200 °C, above the recrystallization temperature prior to rolling (Samarasekera, 2001). This process allows for the various shapes and larger sizes, which are important for sheet pile applications. Compared with cold-rolled sections, hot-rolled sections generally keep a slightly rougher surface, but are more cost effective as no additional cold-rolling and finishing processes are required (Kalpakjian & Schmid, 2010). A more sustainable alternative for sheet piles is offered by the EPD 'EcoSheetPiles™ Plus' from ArcelorMittal. This section is produced by an electric arc furnace. In this process, 100% renewable electricity and 100% scrap steel are used for production (ArcelorMittal, 2024). Compared to the conventional blast furnace process, CO_2 emissions are significantly reduced, providing a more sustainable solution for steel sheet pile production.

Sheet piles can fail through several mechanisms, primarily flexural, rotational, and deep-seated failure. These failure modes for cantilever sheet piles are shown in Figure 8.4 from left to right. In the design of a sheet pile, these mechanisms must be considered, and corresponding verifications should be performed to check whether the failure mechanisms are acting. The flexural failure mechanism, shown on the left of Figure 8.4, occurs when the cantilever pile fails due to the bending moments induced by earth and water pressure (Brown, 1994). This type of failure develops when the bending action on the wall exceeds the moment resistance of the selected section or the material strength. Rotating failure, occurs when the sheet pile rotates close to its base about a pivot point (Brown, 1994). This mechanism arises from an imbalance between the lateral earth pressure, leading to a structural collapse, shown in the centre of Figure 8.4. The final failure mechanism related to cantilever sheet piles is deep seated failure, as illustrated on the right side of the figure. This mechanism occurs when soil mass around the sheet pile rotates along a failure surface (Brown, 1994).

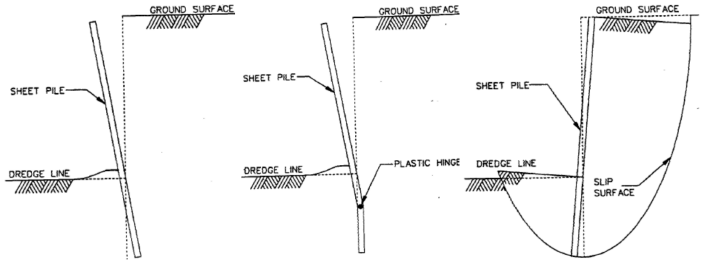

Figure 8.4: Failure mechanisms cantilever sheet pile wall (Brown, 1994)

8.2.1. Geotechnical parameters

For the design, the soil layers including their geotechnical parameters should be known. Section 5.2.4 discusses the geological background of the area, which serves as the basis for defining the soil layers and their parameters. The borehole in Figure 5.13 is considered the most representative source for this analysis. The borehole indicates a top layer with fine/medium sands, underlain by clay/clayey sand, with a bottom layer consisting of medium sand. This aligns with the geological profile shown in Figure 5.12, which describes a transition from beach ridges, dunes, beach plains, and delta sub-aerial facies to deeper open estuaries and marine deposits. The top deposits help to declare the presence of sandy deposits at the top and the layers of clay/clayey sand below correspond to estuarine deposits. The old marine/fluvial deposits were likely compacted and led to the medium sand layer found at the bottom.

Due to the similarity between the borehole and the geological profile mentioned, the layering as shown in Figure 5.13 is deemed representative for the entire study area. Based on this layering, the relevant geotechnical parameters were derived and the results are presented in Table 8.3. These parameters were obtained according to Eurocode 7 (Stichting Koninklijk Nederlands Normalisatie Instituut, 2025). Due to limited knowledge of soil characteristics, conservative estimates were made based on this code. As no explicit information was provided for the top fill layer, conservative parameters were assumed based on typical values for organic topsoil. The soil profile, showing the identified layers and their corresponding properties, is presented in Figure F.1.

Table 8.3: Characteristic values soil

Layer	Soil type	Depth [m]	$\gamma_d\,[\mathrm{kN/m^3}]$	$\gamma_{sat}\,[\mathrm{kN/m^3}]$	$\varphi'\,[^\circ]$	$c'\,[\mathrm{kPa}]$	$c_u\,[\mathrm{kPa}]$
1	Fill	0.0 - 2.0	12	12	15.0	2.5	20
2	Fine/medium sand	2.0 - 7.0	17	19	30.0	0.0	—
3	Clay	7.0 - 10.0	14	14	17.5	0.0	25
4	Clayey sand	10.0 - 15.0	18	20	25.0	0.0	—
5	Clay	15.0 - 16.0	14	14	17.5	0.0	25
6	Clayey sand	16.0 - 17.5	18	20	25.0	0.0	—
7	Medium sand	17.5 - 32.0	18	20	32.5	0.0	—

8.2.2. Hydraulic parameters

In addition to the geotechnical parameters, the design of the cantilever sheet pile wall also depends on the hydraulic parameters. In this case, the wall is located in open water and influenced by the groundwater table. Because of this, hydrostatic pressures acts on both sides of the wall. The water levels of the river and the groundwater may differ, and when this occurs, an excess hydrostatic pressure develops across the sheet pile wall (Grabe, 2008).

In addition, the elevation of the water level is an important parameter in the design. The design water level is determined based on interpolated elevations of the recorded water levels between Brazo Largo and Ibicuy. In Figure 8.5, the corresponding time series of water elevations can be seen, covering a period of four years with time intervals of 20 minutes. As water levels fluctuate over the time, the lowest recorded levels are considered governing, and the design water level is derived from the lower bound of the 95% confidence interval. In this case, the design water elevation is determined to be equal to +0.14 m IGN. Using the measured water elevation on 25 September 2025, the date of the field visit, the ground surface level relative to IGN is defined. This is further explained in Section 8.3.

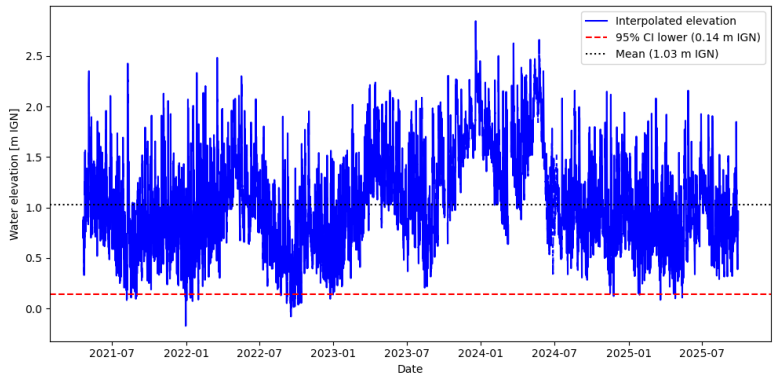

Figure 8.5: Interpolated water elevations between Ibicuy and Brazo Largo

To determine the riverbed level, the bathymetry data from the location analysed in Section 6.4.3 are used. The theoretical background of bathymetry is discussed in Chapter 6. Figure 8.6a presents the bathymetry for the selected location, and the corresponding development of the riverbed can be seen in Figure 8.6b. In this figure, the vertical elevation near the river bank is -1.97 m IGN. Considering the distance between the bathymetry measurement point and the bank, a value of –1.5 m IGN is assumed at the bank and adopted as the representative riverbed level.

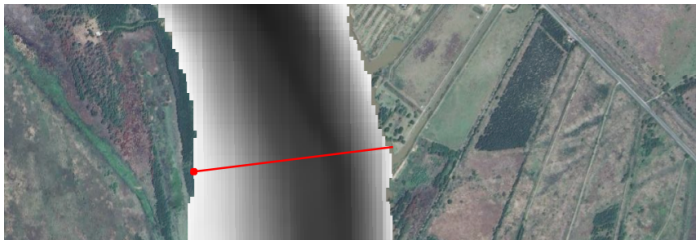

(a) Location of bathymetry

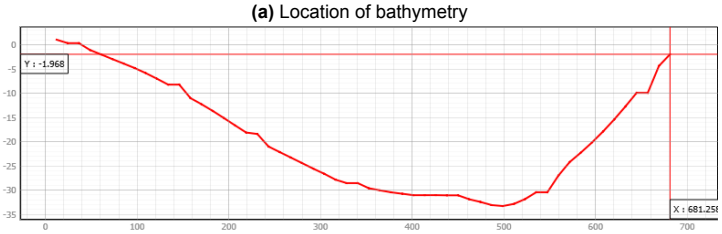

(b) Bathymetry riverbed cross-section

Figure 8.6: Bathymetry analysis

8.3. Design of steel sheet pile

The design of steel sheet piles begins with defining the design location and the problem description to get a clear understanding of the conditions. Once these conditions are defined, an appropriate method is selected to calculate the earth and the water pressures. These pressures are used to balance the moments and iteratively determine the embedding depth of the sheet pile wall. After obtaining the embedding depth based on the moment balance, the sheet pile is verified through structural checks, including bending, shear, and buckling.

To set the balance of moments and determine the embedding depth, the loads acting on the wall must first be defined. The lateral loads that act on the wall consist of soil and water pressures, which are required to compute the corresponding forces. The soil parameters are provided in Section 8.2.1, from which the soil profile and the earth pressures acting on both sides of the sheet pile wall are determined. The hydrostatic pressures resulting from the defined water levels, described in Section 8.2.2, are also considered in the design.

Based on the problem description, a plan is established to calculate the embedding depth of the sheet pile using Python. The procedure begins by defining the soil and water parameters, which are converted into effective stresses, active and passive earth pressures, and hydrostatic water pressures. From these stresses, the resulting forces acting on the sheet pile wall are determined, and a balance of moments is established. By setting the bending moment to zero at the base of the sheet pile wall, the required embedding depth is obtained.

8.3.1. Geometry of the problem

The determination of the critical erosion points along the river is presented in Section 6.4.3. The location analysed in this section forms the location for the design of the steel sheet pile. In Section 6.4.3 the critical point is identified in Aqua Monitor, and photographs taken during the field trip were used to verify the presence of erosion. The total length of this location is 215 meters, as summarised in Table 6.10. The design of the sheet pile wall for this location is based on a cantilever sheet pile. Figure 8.7 presents a sketch of the situation, which was developed using Python.

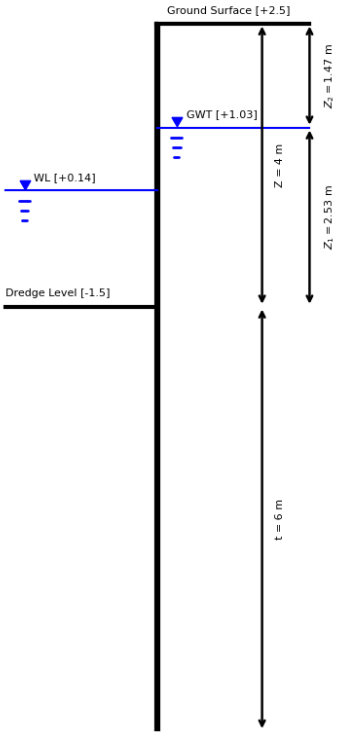

Figure 8.7: Cross-section for sheet pile

In this figure, the retained height of 4.0 meters is denoted by Z, while the embedding depth of the cantilever sheet pile, which must be determined, is represented by t. In Section 8.2.2, the levels of the groundwater table, the water level and the dredge level are defined. The river water level, indicated as WL, is +0.14 m IGN and the dredge level is -1.5 m IGN. The groundwater table, denoted as GWT, is +1.03 m IGN. The ground surface level is derived by comparing the water elevation on 25 September at 14:00:00, obtained from the time series, with the observations. Based on the comparison, the ground surface level is assumed to be 1.5 meters higher than the time series water level of 1.0 m IGN, resulting in a final elevation of +2.5 m IGN.

8.3.2. Method

The design of a cantilever sheet pile can be performed using several classical design methods or through numerical analysis. Common approaches applicable to sheet pile walls include the methods of Bishop, Homberg, Padfield and Mair, Bowles, Day, and Das, as well as the free earth method, the spring-supported beam method, and numerical models such as PLAXIS FEM.

According to Eurocode 7, the design of a sheet pile should be based on the spring-supported beam method (Stichting Koninklijk Nederlands Normalisatie Instituut, 2025). However, due to complexity of this approach, the design of the sheet pile wall is based on the simplified Padfield and Mair method, which provides a representation of the situation. After determining the embedding depth using this method, the depth is verified using the ULS GEO approach, and the final verification is performed in accordance with the ultimate and serviceability limit states defined in Eurocode 3 and Eurocode 7.

The Padfield and Mair method, used in this design, is a graphical procedure shown in Figure 8.8. The right side of the sheet pile represents the active side, while the left side, below the dredge level, represents the passive side. In the simplified representation, an additional resultant force R acts on the lowest point of the sheet pile. This adjustment is introduced because below this point the active and passive zones reverse, creating a more complex distribution. Within the method, plastic soil behaviour is assumed, and the water table level is considered infinitely stiff, meaning that all structural support is provided by the fixity of the soil. To determine the embedding depth, the sum of moments around the lowest fixed point O of the sheet pile wall is set to zero. The unknown embedding depth can be obtained through several approaches. In this analysis, an initial depth is assumed and adjusted iteratively until the moment balance converges to zero. As the method does not account for safety factors, the final embedding depth is increased by 20% to ensure the safety of the design and to resist the force R.

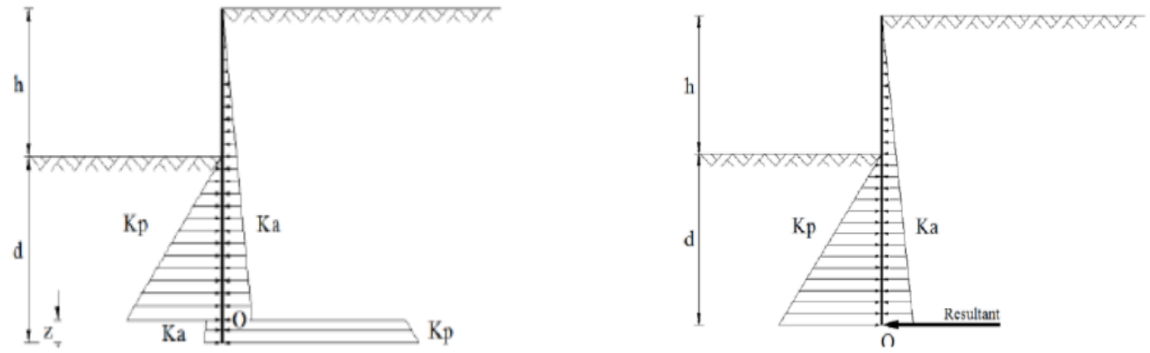

(a) Full method **(b)** Simplified method

Figure 8.8: Padfield and Mair method (Torrabadella, 2013)

8.3.3. Calculation of the embedding depth

The embedding depth of the sheet pile is derived from the balance of moment around the lowest point. The balance of moments should be set to zero, providing the minimal embedding depth. To establish this balance, the pressures that act on the sheet pile are defined and converted into forces. The horizontal pressure acting on the sheet pile is the earth pressure and the hydrostatic pressure. First, the earth pressures are computed using Python, after which the hydrostatic pressures are evaluated and the corresponding forces are determined.

The depth can be defined in multiple ways. The first approach is to keep the depth as an unknown parameter, t. This provides an explicit equation, when moving below the dredge line, for the pressure and resulting forces. As the forces are related to the balance of moments, the roots of the equation are obtained to determine the unknown t. Alternatively, another approach is to begin with an estimated depth and calculate the sum of moments around the base of the sheet pile. Since this balance is generally not equal to zero, an iterative procedure is applied to adjust the depth until the moment balance converges to zero at the lowest part of the sheet pile. In this design, the depth of the sheet pile is based on the second approach. The first value of the embedding depth is taken as 6.0 meters, which can be seen in Figure 8.7.

Effective stress

The horizontal soil pressure can be determined based on the effective stress. The effective stress within the soil is calculated using Equation 8.1. This stress depends on the height of the soil and the unit weight γ of each layer. For soil layers located below the groundwater table, the saturated unit weight must be corrected by subtracting the unit weight of water, resulting in $\gamma - \gamma_w$. Figure 8.1 illustrates the effective stress distribution on both sides of the sheet pile, and the corresponding numerical values are presented in Table F.1.

$$\sigma_z^{'} = z \cdot \gamma \tag{8.1}$$

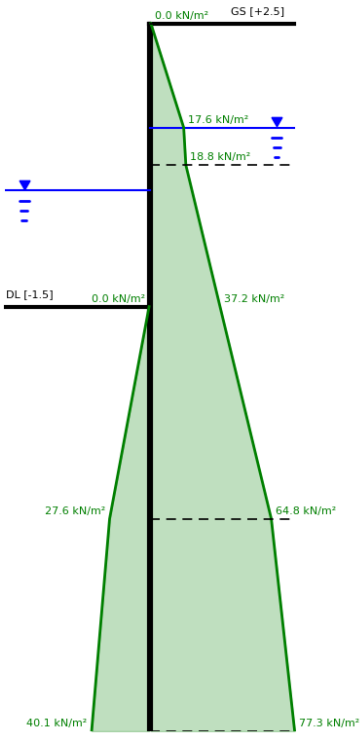

Figure 8.9: Effective stress distribution

Earth pressure and force

The pressure exerted on the wall by the soil is referred to as the lateral earth pressure. This pressure can be determined using the effective vertical stress in combination with the appropriate earth coefficient. Since soil behaviour is largely governed by its natural composition and state, the resulting stresses vary along the profile, similar to the effective vertical stresses. Equation 8.2 presents the calculation of earth pressures for both the active and passive sides. For the active and passive sides, the coefficients $K_{\gamma,a}$ and $K_{\gamma,p}$ are used, respectively.

$$p_{ea,h,z} = z \cdot \gamma \cdot K_{\gamma} \tag{8.2}$$

The active and passive earth coefficients are calculated using Equations 8.3 and 8.4. These equations are derived from Coulomb's theory, where the parameters α, β, and δ, representing the slope of the sheet pile, the slope of the ground surface, and the wall friction angle, are assumed to be zero in this calculation (Grabe, 2008). Under these assumptions, Equations 8.5 and 8.6 are applied to determine the active and passive earth pressure coefficients.

$$K_{\gamma;a;k} = \frac{\cos^2(\varphi' + \alpha)}{\cos^2(\alpha)\left(1 + \sqrt{\frac{\sin(\varphi' + \delta_{a;k})\sin(\varphi' - \beta_a)}{\cos(\alpha - \delta_{a;k})\cos(\alpha + \beta_a)}}\right)^2} \tag{8.3}$$

$$K_{\gamma;p;k} = \frac{\cos^2(\varphi' - \alpha)}{\cos^2(\alpha)\left(1 - \sqrt{\frac{\sin(\varphi' - \delta_{p;rep})\sin(\varphi' + \beta_p)}{\cos(\alpha - \delta_{p;k})\cos(\alpha + \beta_p)}}\right)^2} \tag{8.4}$$

$$K_{\gamma,a} = \tan^2\left(45° - \frac{\varphi'}{2}\right) \tag{8.5}$$

$$K_{\gamma,p} = \tan^2\left(45° + \frac{\varphi'}{2}\right) \tag{8.6}$$

Using Table 8.3, which summarises all relevant soil parameters, the effective angle of internal friction is required to calculate the active and passive coefficients for the different soil layers. The resulting values of these coefficients for each layer are presented in Table 8.4.

Table 8.4: Soil layers and earth pressure coefficients.

Layer	Soil type	Depth [m]	φ' [°]	$K_{\gamma,a}$ [-]	$K_{\gamma,p}$ [-]
1	Fill	0.0 - 2.0	15.0	0.589	-
2	Fine–Medium Sand	2.0 - 7.0	30.0	0.333	3.000
3	Clay	7.0 - 10.0	17.5	0.538	1.860
4	Clayey Sand	10.0 - 15.0	25.0	0.406	2.464

Figure 8.10 provides an overview of the active and passive earth pressure acting on the sheet pile wall. The corresponding numerical values are presented in Appendix F.3. When calculating the earth pressures, it is important to ensure that, at the interfaces of the soil layers, the appropriate earth coefficient is applied and multiplied by the effective stress, σ_z. From the active and passive pressure acting on the sheet pile, the horizontal forces can be determined. These forces are calculated in Python using Equation 8.7, where the earth pressure is multiplied by the height of the corresponding layer. For triangular pressure distributions, Equation 8.7 is multiplied by a factor of $\frac{1}{2}$.

The magnitudes of the forces, derived from both the triangular and rectangular pressure distribution, are computed using Python, and the resulting forces are defined accordingly. Figure 8.10 shows the overall distribution of forces acting on the sheet pile. An overview of the segments, corresponding force magnitudes, and points of application are presented in Table F.4.

$$F_{ea,h,z} = p_{ea,h,z} \cdot h_{layer} \tag{8.7}$$

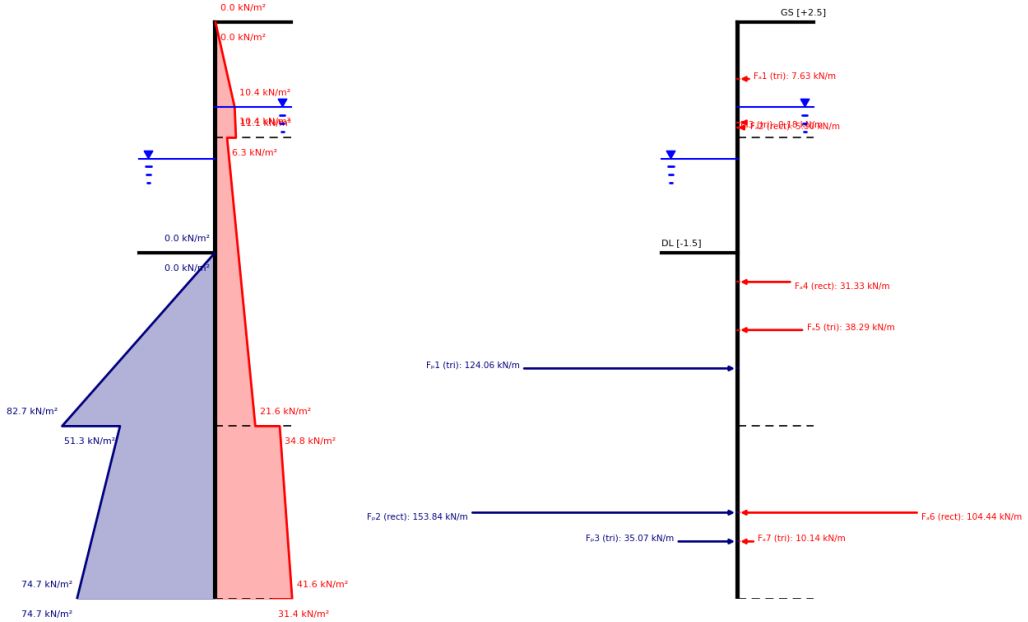

Figure 8.10: Earth pressure active/passive side (left) and resulting force (right)

Hydrostatic pressure and force

The hydrostatic pressure w is also referred to as the pore water pressure (Grabe, 2008). In unconfined groundwater conditions, the pore water pressure at depth z is calculated using Equation 8.8.

$$w = z \cdot \gamma_w \tag{8.8}$$

When an excess of hydrostatic pressure occurs, meaning that the water levels on both sides of the wall differ, an additional pressure acts on the structure. This excess hydrostatic pressure is determined using Equation 8.9. In Figure 8.11, an overview of the hydrostatic pressures and resulting forces are shown. The corresponding numerical values are provided in Table F.5.

$$w_u(z) = w_r(z) - w_l(z) = h_r(z) \cdot \gamma_w - h_l(z) \cdot \gamma_w \tag{8.9}$$

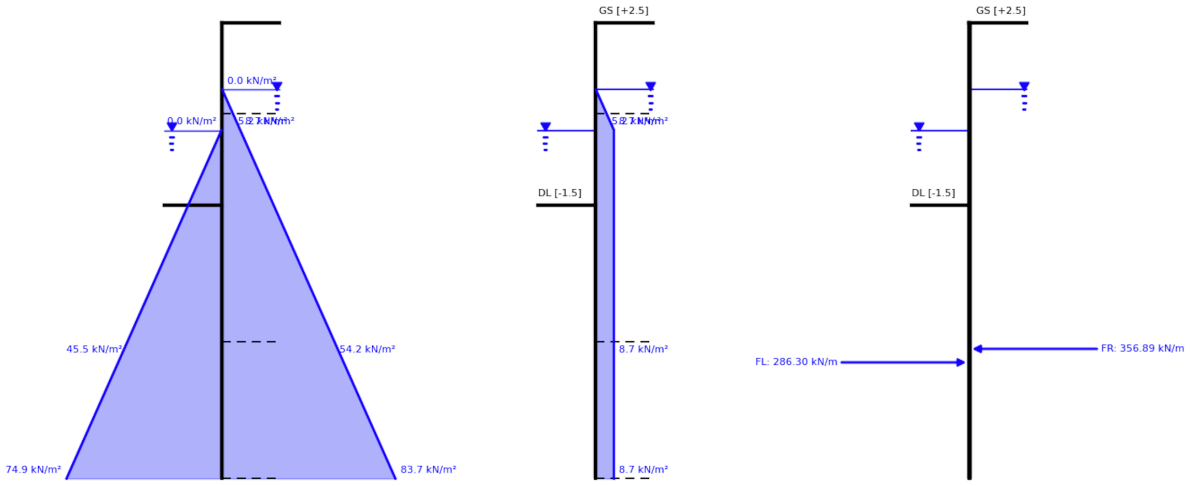

Figure 8.11: Hydrostatic pressure (left), excess hydrostatic pressure (center), and forces (right)

Bending moment

The balance of moments around the lowest point of the sheet pile must be equal to zero, as expressed in Equation 8.10. For an embedding depth of t = 6.0 meters, this point denoted as O is shown in Figure F.4, where the forces resulting from both earth and hydrostatic pressure are illustrated. Based on the acting forces and their arms to point O, the moments are calculated. As shown in Table F.6, the balance of moments for t = 6.0 meters is not equal to zero but 156.3 kNm/m, indicating that equilibrium is not satisfied. Therefore, an iterative calculation is required, increasing the embedding depth until the moment balance equals zero.

$$\sum M_t = 0 \tag{8.10}$$

After an iteration process carried out in Python, the embedding depth was determined to be 7.58 meters. Figure 8.12 shows the forces corresponding to this depth. The calculated forces and moments are presented in Table 8.5, where the resulting moment about point O is 0.051 kNm/m. According to the simplified Padfield and Mair method, the obtained embedding depth found must be increased by 20% to account for the safety factor, resulting in the following final depth:

$$t_{simplified} = 1.20 \cdot 7.58 = 9.09\ m$$

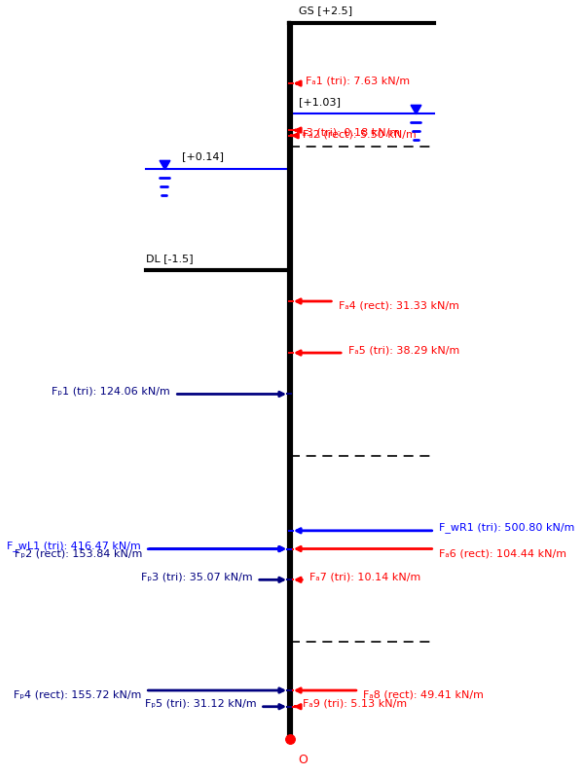

Figure 8.12: Forces for t = 7.58 meters

Table 8.5: Resultant forces, arms, and moments for t = 7.58 meters

Side	Shape	F [kN/m]	z_{base} [m]	M_{base} [kN·m/m]
Active	Triangle	7.63	10.59	80.88
Active	Rectangle	5.50	9.84	54.16
Active	Triangle	0.18	9.75	1.77
Active	Rectangle	31.33	7.07	221.67
Active	Triangle	38.29	6.24	238.98
Active	Rectangle	104.44	3.07	321.08
Active	Triangle	10.14	2.57	26.10
Active	Rectangle	49.41	0.79	38.90
Active	Triangle	5.13	0.52	2.69
Hydro passive	Triangle	416.47	3.07	-1279.17
Hydro active	Triangle	500.80	3.37	1686.78
Passive	Triangle	124.06	5.57	-691.60
Passive	Rectangle	153.84	3.07	-472.98
Passive	Triangle	35.07	2.57	-90.29
Passive	Rectangle	155.72	0.79	-122.59
Passive	Triangle	31.12	0.52	-16.33
$\sum M_t$ (should ≈ 0 for equilibrium)				0.051

8.3.4. Ultimate Limit State GEO

A cantilever sheet pile wall must be designed according to two conditions: the Ultimate Limit State (ULS) and the Serviceability Limit State (SLS). The ULS concerns the most unfavourable loading conditions that may occur during the service life of the structure and ensures the safety of both people and the structure (Baxter et al., 2022). The SLS, verifies the performance of the structure under normal conditions, where its functionality and appearance of the structure are assessed (Baxter et al., 2022). In this section, the ULS GEO verification is performed.

For the design, safety factors corresponding to ULS and SLS, defined in Eurocode 7 GEO must be included. For the analysis, multiple combinations are examined and the most unfavourable case is adopted for the design. Two combinations within Design Approach 1 as specified in Eurocode 7, are evaluated in Appendix F.6. However, for the calculation in this section the most unfavourable combination is taken and further elaborated. Within Design Approach 1, the most critical condition corresponds to Combination 2 (DA1-2). The associated safety factors are presented in Table 8.6, which includes the partial factors for the actions and materials applied to ensure the structural safety of the sheet pile. In this calculation, both hydrostatic and earth pressures are considered permanent loads. Applying this results in a final embedding depth of t = 10.17 meters, as shown in Figure F.7. Table F.11 presents that the balance of moments is -0.063 kNm/m confirming equilibrium.

Table 8.6: Partial factors for actions and material properties

Parameter		Partial factor	1	2
Actions	Permanent, Unfavourable	γ_G	1.35	1.00
	Permanent, Favourable	$\gamma_{G,\text{fav}}$	1.00	1.00
	Variable, Unfavourable	γ_Q	1.50	1.30
	Variable, Favourable[1)]	–	0	0
Material properties	Effective shearing resistance	γ_φ	1.00	1.25
	Effective cohesion	γ_c	1.00	1.25
	Undrained shear strength	γ_{cu}	1.00	1.40
	Unconfined compressive strength	γ_{qu}	1.00	1.40
	Weight density	γ_γ	1.00	1.00

Table 8.7 presents an overview of the ULS analysis. From this overview, it is evident that the ULS combination DA1-2 is the governing case. In the following section, the corresponding bending moments and shear forces are verified with respect to the selected sheet pile profile. The bending moment distributions are illustrated in Figures F.5 and F.8, while the shear force distributions are shown in Figures F.6 and F.9.

Table 8.7: Overview ULS combinations DA1-1 and DA1-2

ULS	Retained height [m]	Embedding depth [m]	Toe depth [m]	Max moment [kNm/m]	Max shear [kN/m]
DA1-1	4.0	7.58	11.6	280.5	220.6
DA1-2	4.0	10.17	14.2	404.4	266.6

8.3.5. Structural Verification ULS

In the structural verification of the cantilever sheet pile, an appropriate profile must be selected and verified in accordance with Eurocode 3 (Technical Committee CEN/TC250, 2007). The verification process begins with the classification of the sheet pile section, after which checks for bending, shear and combined bending and shear are carried out. In these verifications, the requirement is that the applied actions do not exceed the design resistance of the chosen profile, as expressed in Equation 8.11.

$$E_d \leq R_d \tag{8.11}$$

- E_d is design effects of actions;
- R_d is design resistance.

In this section, the AZ 24-700 cross section from ArcelorMittal is verified (Baxter et al., 2022). Since this section is located within the river and is assumed to be exposed to fresh water, a corrosion factor must be considered. This means that the cross sectional properties after corrosion are reduced due to a loss of thickness. According to Eurocode 3, the total thickness loss for a design working life of t_{DWL} is 50 years is calculated as follows:

$$\Delta_t = \Delta_{tfront} + \Delta_{tback} = 0.9 + 0.6 = 1.5\ mm$$

With a thickness reduction of 1.5 millimetres, the cross sectional properties such as height, flange thickness, web thickness, sectional area, elastic section modulus, and plastic section modulus are decreased accordingly. The reduced properties of the section after corrosion are presented in Table 8.8.

Table 8.8: Reduced geometrical and mechanical properties of profile AZ 24-700 (Baxter et al., 2022)

Property	Symbol	Units	AZ 24-700
Overall width	b	mm	700
Overall height	h	mm	457.5
Flange thickness	t_f	mm	9.7
Web thickness	t_w	mm	9.7
Flange breadth	b_f	mm	361
Slant angle	α	°	55.2
Sectional area	A	cm^2/m	163
Elastic section modulus	W_{el}	cm^3/m	2435
Plastic section modulus	W_{pl}	cm^3/m	2810
Moment of inertia	I	cm^4/m	55890
Mass	—	kg/m^2	128
Class	—	—	3

Section classification
The classification of the steel profile determines whether the section behaves elastically or plastically, which is essential for assessing the stability of the cantilever sheet pill during the bending and shear verifications. The classification of the cross section is based on the flange slenderness ratio. Table 8.9 presents the classification limits and the corresponding slenderness ratios for Z and U profiles. Equation 8.12 defines the coefficient that depends on the steel grade.

$$\epsilon = \sqrt{\frac{235}{f_y}} \tag{8.12}$$

- f_y is the yield strength [N/mm^2]

Table 8.9: Section classification

Class	Rotation check	Ratio of b/t_f is less or equal than…	
		Z-profile	U-profile
1	Required	$45\,\varepsilon$	$37\,\varepsilon$
2	Not required	—	—
3	Not required	$66\,\varepsilon$	$49\,\varepsilon$

For cross section verification, the AZ 24-700 profile with the properties listed in Table 8.8 and made of grade S355 GP steel, is classified as Class 3 according to Equation 8.13. Therefore, no additional rotation verification is required.

$$\frac{b}{t_f} = \frac{361}{9.7} = 37.2 \leq 66\epsilon \tag{8.13}$$

Bending
For the bending verification, it is essential that the design bending moment M_{Ed} is smaller than the bending resistance M_{Rd} of the selected profile. The maximum bending moment, 404.4 kNm/m, occurs at the point of zero shear, as shown in Figure F.8. For a Class 3 cross section, the bending resistance is determined using Equation 8.15.

$$M_{Ed} \leq M_{c,Rd} \tag{8.14}$$

$$M_{c,Rd} = \frac{\beta_B \cdot W_{el} \cdot f_y}{\gamma_{M0}} \tag{8.15}$$

- β_B is a factor that accounts for lack of shear force transmission in the interlocks [-];
- W_{el} is the cross section elastic section modulus [cm^3/m];
- f_y is the yield strength of steel [N/mm^2];
- γ_{M0} is a partial factor [-].

Based on the equation above, the bending moment resistance of the cross section is calculated and verified using the following equations:

$$M_{c,Rd} = \frac{1.00 \cdot 2430 \cdot 355}{1.0} = 862.7\ kNm/m$$

$$\frac{M_{Ed}}{M_{Rd}} = \frac{404.4}{862.7} = 0.47$$

Shear
For the shear verification, it is essential that the design shear force, V_{Ed} is smaller than the plastic shear resistance, $V_{pl,Rd}$, of the selected profile. The maximum shear force, 266.6 kN/m, occurs at the base of the sheet pile as shown in Figure F.9. The shear resistance is calculated using Equation 8.17.

$$V_{Ed} \leq V_{pl,Rd} \tag{8.16}$$

$$V_{pl,Rd} = \frac{A_v \cdot f_y}{\sqrt{3} \cdot \gamma_{M0}} \tag{8.17}$$

- A_v is the projected shear area of each web [mm^2];
- t_w is the web's thickness [mm];
- t_f the flange thickness [mm];
- h the overall height of the cross section [mm].

Based on the equation above, the shear force resistance of the cross section is determined and verified using the following equations:

$$A_v = 9.7 \cdot (457.5 - 9.7) = 4343.7\ mm^2$$

$$V_{pl,Rd} = \frac{4343.7 \cdot 355}{\sqrt{3} \cdot 1.0 \cdot 10^3} = 890.4\ kN$$

$$V'_{pl,Rd} = \frac{890.4}{0.7} = 1272\ kN/m$$

$$\frac{V_{Ed}}{V_{pl,Rd}} = \frac{266.6}{1272} = 0.21$$

Combined bending and shear
For the verification of the combined effects of bending and shear, Equation 8.18 must be satisfied. However, when the cross section is classified as plastic, the influence of shear on plastic bending resistance may be neglected, provided that Equation 8.19 is satisfied.

$$M_{Ed} \leq M_{V,Rd}\ ,\ M_{V,Rd} \leq M_{c,Rd} \tag{8.18}$$

$$V_{Ed} \leq \frac{V_{pl,Rd}}{2} \tag{8.19}$$

- V_{Ed} is the design shear force [kN/m];
- $V_{pl,Rd}$ is the design plastic shear resistance [kN/m].

From the following equation, it can be concluded that no explicit verification is required.

$$V_{Ed} = 266.6 \leq \frac{1272}{2} = 636.0\ kN/m$$

Shear buckling
The shear buckling resistance of the cross section must be verified if the condition in Equation 8.20 is met. However, this requirement is not satisfied, as can be seen in the following equations.

$$\frac{c}{t_w} \geq 72 \cdot \epsilon \tag{8.20}$$

$$c = \frac{h - t_f}{sin(\alpha)} = \frac{457.5 - 9.7}{sin(55.2)} = 546.7$$

$$\frac{546.7}{9.7} = 56.4 \not\geq 72 \cdot \epsilon$$

Local effects of water pressure
Due to the geometry of the cross-section, there is a difference in water levels on both sides of the sheet pile, the bending moments should be reduced by transverse local plate bending. Therefore, the cross sectional yield strength is according to Equation 8.21. In this equation, ρ_p is a unitless reduction factor that depends on the slenderness ratio. However, when the difference in the water levels across the wall for Z sections is less than 5.0 meters, this reduction is not required. From the following equations, it can be seen that the difference in water levels is less than 5.0 meters, indicating that the local effects of water pressure on the overall flexural bending can be neglected.

$$f_{y;red} = \rho_p \cdot f_y \tag{8.21}$$

$$\Delta h_w = 1.03 - 0.14 = 0.89\ m$$

8.3.6. Final design

Based on the structural verifications conducted in the ultimate limit state analysis, the minimum embedding depth for the final design of the cantilever sheet pile wall has been determined. As shown in Section 8.3.5, all relevant verifications are satisfied, confirming that the AZ 24-700 profile meets the structural design requirements. Using the final embedding depth established in Section 8.3.3, the minimum depth in the ULS GEO verification is defined as t = 10.17 meters. With this information, the final two-dimensional design of the sheet pile is presented in Figure 8.13.

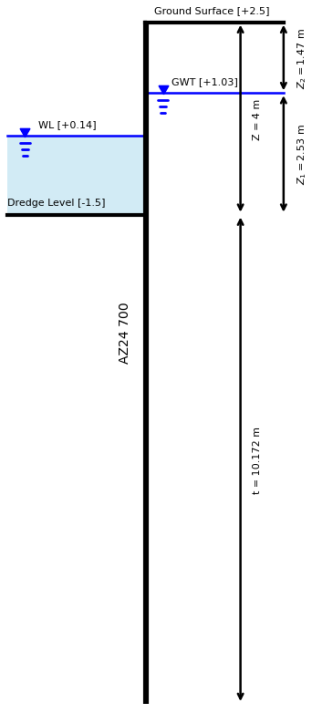

Figure 8.13: Two dimensional design cantilever sheet pile

8.4. Nature-based solutions

As stressed in Chapter 5, natural damage to the ecosystems occurs on locations where dry sand mines are active. Besides that, in Chapter 6 it was explained that riverbank erosion is a common problem in the Paraná Guazú, due to changes of the hydrodynamic parameters of the river. To mitigate these problems, a number of Nature-based solutions is suggested here.

In this section, several NbS are presented to create a cost-efficient, long-lasting, sustainable riverbank. In a first instance, NbS are explained in detail according to the topics of dry sand mining. Following this, other solutions are discussed with aim to mitigate the damage done to river banks. Consequently, when it comes to weighing the different NbS against each other this report makes use of the seven goals of the IUCN which must be achieved as completely as possible. The seven goals are presented in Figure 2.4. Implementations of NbS often face resistance from stakeholders, particularly when these solutions are compared to traditional engineered approaches. From Chapter 2, it was made clear why NbS needed to be introduced without a lot of financial constraints. This chapter works on NbS which are both simple and understandable to all the stakeholders.

8.5. Nature-based solutions for dry sand mining

This section seeks to propose and evaluate Nature-based solutions (NbS) that can effectively address the environmental and socio-economic consequences of dry sand mining. The analysis focuses on developing strategies that harness natural processes to restore degraded ecosystems, enhance landscape resilience, and promote sustainable resource management. In order to provide a comprehensive understanding, the potential advantages and limitations of each proposed NbS is be critically examined. Furthermore, this section will outline the intended implementation strategy including a methodological approach and practical steps required.

8.5.1. Floodplains

Floodplains are low-lying areas around rivers that naturally flood during periods of high water discharge. When managed and restored appropriately, these zones play a crucial role in maintaining riverine ecosystem functions and mitigating the adverse impacts of human activities such as sand mining and land degradation.

In the context of dry sand mining, floodplains could be a Nature-based solution to counteract the degradation of terrestrial and hydrological systems resulting from excessive sand extraction. Dry sand mining frequently occurs in former floodplain areas or adjacent uplands, where the removal of surface materials disrupts soil structure, alters drainage patterns, and reduces the area's natural capacity to retain water. Restoring and reactivating floodplains in such landscapes helps to re-establish the natural hydrological connectivity between surface and subsurface systems. This process promotes groundwater recharge, initiate soil sedimentation and mitigates erosion caused by wind and surface runoff. Moreover, re-vegetated floodplains provide new habitats for native species, contributing to the overall ecological recovery of mined areas. As such, floodplain restoration in dry sand mining zones supports landscape resilience, reduces the long-term environmental footprint of extraction activities, and facilitates a more sustainable post-mining land use.

Restored floodplains offer significant opportunities for local community engagement, livelihood diversification, and socio-economic development. Once stabilized and re-vegetated, these areas can be utilized for sustainable land uses such as flood-resilient agriculture, agroforestry, and controlled grazing, which maintain ecological functions while providing income for local populations. Additionally, floodplains can serve as sites for eco-tourism, recreation, and environmental education, fostering a stronger connection between communities and their natural surroundings. The enhancement of biodiversity and landscape aesthetics further increases the cultural and recreational value of these areas. Moreover, the restored floodplain's role in improving water retention and soil fertility can directly support local food and water security, especially in regions affected by the environmental degradation of dry sand mining. Through community-based stewardship, floodplain restoration can therefore become a catalyst for sustainable rural development and long-term environmental resilience.

8.5.2. Metal-tolerant plants

As mentioned in Section 5.2.6, iron concentrations in the ground water have increased by 2200% since sand mining operations have started. Meanwhile, manganese concentrations are above the recommended concentration limits and polyacrylamide poses a danger to the users' health. Clearly, there is a need for limiting the amount of metal elements and polluters that infiltrate the groundwater.

The use of metal-tolerant plants, such as phytostabilizers and hyperaccumulators, represents an effective Nature-based solution for mitigating contamination and surface runoff in areas affected by dry sand mining. These plant species have the capacity to absorb, immobilize, or stabilize pollutants, including heavy metals and chemical residues from washing processes, within their roots or above-ground tissues. By establishing vegetation on disturbed or contaminated soils, this method reduces the mobility of harmful substances, prevents their leaching into nearby water bodies and the aquifer, and enhances overall soil stability.

In addition to pollutant control, these plants help reduce surface runoff by increasing soil infiltration capacity and root cohesion, thereby minimizing erosion and the spread of sediments. Over time, the vegetative cover contributes to ecosystem recovery, transforming degraded mining landscapes into self-sustaining, biologically active systems. Several plant species exhibit tolerance to moderate metal contamination, conditions which can be associated with post-mining sites. Examples include:

- Phragmites australis (reed): known for high tolerance to heavy metals and ability to stabilize sediments (Popa et al., 2023).
- Typha domingensis (southern cattail): native to wetlands in a delta; capable of taking and accumulating metals (Soliman et al., 2024).
- Schoenoplectus californicus (California bulrush): efficient in reducing nutrient and contaminant loads in water. (L. Idaszkin et al., 2024)
- Spartina densiflora (cordgrass): salt- and metal-tolerant grass found along deltas and coastal zones. (L. Idaszkin et al., 2024)

The Schoenoplectus californicus is naturalised in the Paraná Delta region (Kandus & Malvárez, 2004). For the others species, it is not specifically known whether they already occur in the Lower Paraná Delta.

8.5.3. Vegetated buffer zones

Vegetated buffer zones are strips of land planted with dense vegetation, such as grasses, shrubs, and trees, established between areas of active land use (dry mining sites) and surrounding environments such as settlements, agricultural fields and nature. In the context of dry sand mining, these buffers function as a natural barrier that mitigates the spread of dust, noise, and pollutants generated by extraction activities.

From an ecological perspective, vegetated buffer zones play a vital role in stabilizing soil, reducing wind speed, and capturing airborne particles, thereby improving local air quality and minimizing off-site impacts. The root systems of the plants anchor the sandy substrate, preventing erosion and surface runoff, while the vegetation canopy traps dust and enhances microclimatic conditions by increasing humidity and reducing temperature fluctuations.

In addition to their environmental benefits, buffer zones contribute to biodiversity enhancement by creating transitional habitats that support a variety of species and small fauna. They also serve as visual and acoustic screens, reducing noise and improving the aesthetic quality of the landscape. When designed with native and drought-tolerant species, vegetated buffers require minimal maintenance and can thrive in the disturbed conditions typical of mining landscapes.

Moreover, the establishment of buffer zones can provide socio-economic advantages for local communities through community-based planting initiatives. Overall, vegetated buffer zones represent a cost-effective and multifunctional Nature-Based solution that simultaneously addresses environmental degradation, air quality concerns, and landscape restoration in areas affected by dry sand mining.

8.5.4. Implementation in Ibicuy area

The area shown in Figure 8.14 includes the Cristamine S.A. sand mine (located in the lower right corner) and another sand extraction site located just next to the primary school (Escuela Primaria). These mining activities have a strong influence on the surrounding landscape and local air quality. By changing the orange surrounded area into a floodplain and the blue lines into vegetated buffer zones, these influences could be mitigated.

The restoration approach involving floodplains could be used between the primary school and the Cristamine mine, with the road as its boundary, serving as a floodplain restoration zone (orange area). This solution would be particularly valuable after mining operations have ended, allowing for the area to naturally recover, increasing biodiversity, and providing flood protection and water storage capacity.

In the shorter term, the vegetated buffer solution could effectively reduce dust emissions and protect the local community. Establishing dense vegetation around the primary school would help minimize dust dispersion into the school grounds, improving air quality for the children and teachers. Similarly, implementing vegetated buffers along the main road would limit dust movement caused by sand transportation, improving air quality, visibility and nuisance for nearby residents and road users.

From an economic perspective, these solutions are relatively cost-effective compared to large-scale engineering interventions. Vegetated buffers require moderate initial investment in planting and maintenance but offer long-term benefits in ecosystem services, reduced health costs, and improved landscape aesthetics. Floodplain restoration needs a bigger investment amount. This could be funded through mine closure obligations or environmental offsets, making it a sustainable and financially viable option for the area.

Figure 8.14: Implementation area of possible NbS (Google Earth, 2025)

8.6. Nature-based solutions for bank erosion

Nature-based solutions (NbS) use natural processes and ecosystems to address environmental challenges such as dry sand mining, but also river bank erosion and flood risk. These will be treated in this section. For river bank protection, NbS can include restoring wetlands, planting vegetation, and implementing natural flood management techniques. These solutions not only protect the river banks and infrastructure, but also improve water quality, support wildlife, and create recreational spaces.

8.6.1. Natural flood management

Natural Flood Management (NFM) is an NbS that consists of using natural materials to slow the flow of water through the land and reduce the chance of flash flooding, as well as increasing water storage throughout the landscape (Duncan, 2021). Using NFM upstream means that water takes a lot longer to reach lowlands and downstream areas.

A number of techniques are used in NFM, such as Natural leaky dams. This technique means placing a series of logs across a watercourse to mimic the effect of naturally fallen trees. While it's important not to block the water completely, slowing the flow eases pressure downstream and reduces the risk of flooding, especially after heavy rain. The pathway of the cargo boats found on Marine Traffic is as follows: along the Rio Paraná Guazú, leaving out the Rio Ibicuy, and up until Puerto Ibicuy a few times a year. Since cargo ships require deep, unobstructed channels, leaky dams are only placed in sites away from the main navigation routes. This ensures they do not interfere with shipping while still providing flood protection downstream. This tells that in order to adopt this method in the Rio Paraná Guazú, the logs will have to be placed above Puerto Ibicuy given that these ships would harm the NbS.

8.6.2. Vegetation

Another NbS technique used from which the river banks could benefit is the implementation of vegetation. Sand mining in the delta zones leads to loss of stability of the soil structure, see Chapter 2. This not only accelerates coastal erosion but also diminishes the capacity of these landscapes to retain water and support biodiversity. Bringing trees into the landscape and mangrove forests in degraded coastal and estuarine areas can help reverse these impacts by re-establishing the natural balance between land and water.

Mangroves are fresh and saltwater-tolerant trees and shrubs that are present in intertidal zones, including river deltas and estuaries. Their dense root systems trap sediment, reduce wave energy, and stabilize shorelines, making them an excellent Nature-based solution (NbS) for riverbank protection in coastal water environments. There are different types of mangroves that can serve in diverse situations. Planting mangroves and local vegetation along the riverbanks, particularly in areas with shallower edges. Mangroves are highly effective at stabilizing shorelines due to their dense root systems which trap sediments and reduce wave energy, like those from the cargo ships. If the right trees are planted in the right places, a mangrove creation can go a long way towards managing the flow of water through river catchments (Ferreira et al., 2024). Mangroves are typically found in higher latitude regions than the study area, near the equator, but given the fact that these plants are compatible with the landscape it would be of no harm to integrate them into the mitigation strategies (Ward, n.d.). Figure 8.15a shows a Rhizophora mangle (red mangrove) and Figure 8.15b shows a Avicennia germinans (black mangrove).

(a) *Rhizophora mangle* implementation area

(b) *Avicennia germinans* implementation area

Figure 8.15: Implementation areas of possible Nature-based solutions (NbS) using mangroves

- Red Mangrove (Rhizophora mangle): Excellent for shoreline stabilization due to its dense prop roots, which trap sediments and reduce wave energy. Often used in coastal restoration projects to prevent erosion and create fish habitats (Sprung, 2021), Figure 8.15.
- Black Mangrove (Avicennia germinans): Thrives in saltier environments and has specialized "pneumatophores" (breathing roots) that help aerate the soil.Effective for improving soil salinity tolerance and supporting biodiversity in highly saline areas (Hammond, 2022), Figure 8.15a.
- Casuarinas equisetofilia: is a genus of flowering plants in the family Casuarinaceae, and is native to a lot of regions including Argentina. It enjoys Tropical, Sub-Tropical and Monsoonal regions ("NParks | Casuarina Equisetifolia", n.d.).

The locations where these trees and mangroves would be the most useful, are those where bank erosion is the worst. In this case that would be the outside of the river turns of the region of interest. That would include locations like the land of stakeholders such as the owner of the Camping La Blanqueada, Camping El Trebol, Camping Ipona Guazú, or Oasis Guazú.

8.6.3. Riparian buffer zone

Riparian buffer zones are strips of vegetation planted along riverbanks to stabilize soil, filter pollutants, and absorb floodwaters. These zones can include a mix of trees, shrubs, and grasses, which work together to protect the bank from erosion and improve water quality as an extra benefit (UK Forestry Standard, 2024). The principle is almost the same as for the mangroves, but with different types of vegetation and a bit more in front of the mangrove line. For the riparian buffer zone vegetation, the roots of plants bind the soil, reducing erosion caused by wave action and currents. Vegetation slows overland flow, allowing water to infiltrate the ground and reducing the volume of runoff entering the river (Marshall, 2024). The added value is that in addition to stability, buffer zones also provide habitat for wildlife and create green corridors for biodiversity (Vagheei & Boano, 2025). In Figure 8.16, one can see how one of the local landowners integrated the riparian vegetation zone into his property on the picture taken during the fieldtrip.

Figure 8.16: Riparian buffer zone vegetation

A list of riparian buffer zone vegetation can be found below:

- Willow (Salix humboldtiana): Fast-growing, deep-rooting tree that stabilizes eroding banks, filters pollutants, and provides shade to reduce water temperature (iNaturalist, 2020).
- Cockscomb Coral Tree (Erythrina crista-galli): Nitrogen-fixing tree that improves soil fertility, provides habitat for birds and insects, and helps stabilize banks with its root system (Weeds Australia, 2019).
- Inga Tree (Inga uruguensis): Nitrogen-fixing tree that prevents soil erosion, supports pollinators, and provides food for wildlife (Guia de Plantas Nativas, 2008).
- Junco (Schoenoplectus californicus): This small plant/bush is spiky and is usually located next to water. It grows about half a meter per year and help solidify the soil (Marco, domingo, septiembre 12, 2021).

8.6.4. Deposited Rock Debris as an NbS

When visiting Camping Oasis Guazú, the group saw that mitigation strategies had already been tested. The landowner chose to put rocks on the side of the bank to decrease the erosion process as seen in Figure 8.17. These rocks are used to protect the bank from the high tides and wave impacts from the ships passing by.

Figure 8.17: Local solution Camping Oasis Guazú

According to the owner of the land, this solution has significantly contributed to the decrease of land erosion. As this is not a true natural solution, it could not be interpreted as an NbS like this. Nevertheless, incorporating rocks as a buffer for the current, leaving other vegetation more time to take over and contribute to the stability of the banks, this would be a suitable approach to transition towards a 100% true NbS.

8.6.5. Evaluation of the NbS

The final goal of this section is to integrate these solutions into the landscape, as this could help establish a clearer picture of what can be achieved with these solutions. Table 8.10 presents the grading of various Nature-based solutions (NbS) according to seven key goals, including climate change mitigation and adaptation, disaster risk reduction, economic and social development, human health, food security, water security, and ecosystem degradation and biodiversity loss. Every NbS is classified on a scale of – to ++.

Table 8.10: Grading by the seven NbS goals

	Climate change mitigation and adaptation	Disaster risk reduction	Economic and social development	Human health	Food security	Water security	Ecosystem degradation and biodiversity loss	Overall grading
Floodplains	++	+	0	0	+	+	+	+
Metal-tolerant plants	0	+	+	++	-	+	-	0
Vegetated buffer zones	+	0	++	++	0	0	+	+
Natural flood management	++	+	0	-	0	+	0	0
Mangroves	0	0	0	0	+	0	-	0
Riparian buffer zone	+	0	+	0	+	0	+	+
Rock Debris as NbS	0	0	+	0	0	0	–	0

The results of Table 8.10 show various Nature-based solutions (NbS) across several criteria related to environmental and social benefits. Floodplains show the strongest overall performance, receiving

high ratings (++ or +) in most categories, particularly in climate change mitigation, disaster risk reduction and ecosystem protection. Vegetated buffer zones and mangroves also perform well, especially in supporting human health, food security, and biodiversity. In contrast, options like rock debris and metal-tolerant plants provide more focused benefits on one or two topics. Natural flood management demonstrates strong potential in climate adaptation and water security but is more neutral in other areas. These results highlight that while all NbS options contribute to sustainability goals, some provide broader and more integrated ecosystem benefits than others.

9

Discussion

9.1. Sand extraction volumes, purpose and the demand for sand

Interviews with local stakeholders reveal that dredging activity in recent years has stayed constant in certain parts of the study area. In the Paraná Guazú, two dredging companies are operational, as both AIS data and interview data show, and stakeholders did not speak of a trend in these areas. In Puerto Ibicuy, river sand extraction taxes were increased significantly, leading to the discontinuation of almost all dredging activities on the Paraná Ibicuy. Historic AIS data was not available, but present-day AIS data as well as fieldwork observations confirm that no dredging activities on the Paraná Ibicuy take place anymore. This finding directly contradicts the initial hypothesis suggesting a potential increase in river sand mining. Instead, it highlights the influence of local governance as a powerful regulator of extraction activities.

In contrast, dry sand mining has expanded drastically. Historic data shows the increasing importance of fracking gas and oil from Vaca Muerta since its discovery in 2011. This trend goes hand-in-hand with the trend in mined sand masses in Argentina, increasing from around 500,000 tons in 2011 to 3.5 million tons in 2020. Although sand is also used by the glass and ceramics industry and the exact demand from different sectors is unknown, the upgoing trend in both data sets is a clear indicator that mined sand is used more and more for fracking. This view is supported by stakeholder interviews and previous research (Foglia, 2023) (Secretaría de Política Minera, 2019). The mayor of Ibicuy described the following scale during the conducted interview: 350 trucks that transport 9,000 tons of sand each day. With a total of 260 working days per year, this amounts to more than 2.3 million tons of dry mined sand transported from Ibicuy in 2025. By comparison, the calculated volumes mined from the river section were determined to be equal to 30600 m^3/month, or 587,520 tons per year. In 2022, the dry mined sand mass was 1,250,000 tons in Ibicuy (Foglia, 2023).

The studied geology shows multiple layers of sand containing more than 85% quartz, with some layers showing percentages of more than 99%. Stakeholders also highlighted that sand is very rich in quartz, fine-grained and highly resistant. The literature study showed that sand must be rich in quartz to be suited for fracking. Grain size distributions that were created based on taken bed samples do not meet the fracking specifications related to grain uniformity, but only a limited number of river samples were taken and no dry samples were analyzed. Other factors that contribute to the demand for sand are the deltaic nature of the study area, natural river and wind processes help purify and round the grains, and local government policy. As became clear from stakeholder interviews and the literature analysis, sand extraction taxes have been constant for years in spite of strong inflation and are not enough to compensate for road damage that exists due to the mining activities.

9.2. Hydrodynamic and sedimentary analysis

The hydrodynamic analysis provided insights on water elevations, discharge and sediment concentrations for different locations in and near the study area. With the help of correlation matrices, the relationship between these variables was determined. A couple of results arise:

- Pre-defined functions were used to define relations between water elevations and discharge. Schmidt and Yen (2011) note several limitations related to these rating curves, such as the fact that discharge measurements typically scatter and therefore do not show a unique relation with the stage and the ignorance of underlying physics of the open channel. However, correlations in the Bermejo are high for all variables, indicating that the used power-law assumption is suitable.
- Found correlations for the Paraná Guazú are much smaller, which is also the case for the Zárate station on the Paraná de las Palmas. However, as this river is located in the Lower Paraná Delta as well, this behaviour is expected.
- Analysis of the flow variables has shown that R^2-values tend to decrease, the further downstream the location of measurement is. This result is in agreement with those found by Song et al. (2024), who state that the stage-discharge relationship is considerably affected in the transitional zone and tide-dominated region of the Yangtze estuary.
- The inflow of the Uruguay river should be considered, the variation in elevations that occur due to the presence of this river can cause disturbances in the rating curves. To find out more about factors affecting these relationships, a study of the tide-river interactions was carried out. It follows that the tidal variance fraction is only 5.71%, which indicates that tidal forcing plays a subordinate role relative to other drivers, such as river discharge.

Further, for the sediment-discharge relationship, the differences in correlations in Brazo Largo can be explained through the sources of the variables: whereas the fine sediment concentration predominantly originates from the Bermejo basin, the discharge is dominated by the Paraguay and Paraná. This results in a weak correlation downstream of the confluence of these rivers (López Weibel et al., 2022). Despite the lack of correlation, an attempt to generate time series for sediment concentrations was made. A reasonably good fit was achieved for the sediment loads at Santa Fe, but the considerable number of parameters involved (base concentration, time delay, and threshold) reduces the robustness of the approach. Moreover, the resulting relation is applied to the Paraná Guazú, located hundreds of kilometers downstream. Nevertheless, fine sediment concentrations in the time series were similar to those encountered in the fieldwork and are thus deemed valid.

During the fieldwork, data on flow velocity, discharge, grain size distributions and concentrations of suspended and bed sediments were collected. The water elevations as retrieved from public datasets are consistently higher at Puerto Ibicuy than at Brazo Largo. Further, during the two measurement days, water levels dropped while discharges increased. This appears to contradict the positive correlation between stage and discharge found in public datasets. The discrepancy likely arises since the standard stage-discharge relationship assumes steady flow and acts on longer timescales. In contrast, on short timescales, water levels in the Paraná Guazú are influenced by variations in the Río de la Plata, including backwater effects and transient downstream control. These factors can cause a temporary inverse relation between stage and discharge, leading to the observed short-term response. Jones et al. (2019) confirm that traditional rating curves fail in the tidal zone because of local complexity.

Grain size distribution results reveal that the average particle size of the sand tends to increase with recovery depth. This pattern likely reflects natural sediment sorting processes, where finer particles are carried further by the current, whereas coarser grains settle in deeper or higher-energy parts of the channel. It is important to emphasize that the data supporting this observation were collected outside the area of interest but from near Rosario. However, the Rosario samples are considered representative since they were taken near the study area at a distance of approximately 150 kilometers in the same river. The fact that the Rosario sample shows coarser particles is likely due to the fact that this was taken from a considerably deeper part, at around 30 m depth.

For the suspended sediment concentrations, it was found that this is the highest near the bed, which is typical for suspended sediment. The steeper profile for cross section 2 indicates higher turbulence or finer particles compared to cross sections 1 and 3. Higher turbulence combined with finer particles

causes sediment to stay suspended more easily, which results in a steeper concentration gradient with depth. Combining concentration data with ADCP results yielded the total suspended sediment flux. Similar mean fluxes were found for cross sections 1 and 2, whereas cross section 3 showed a slightly higher mean velocity. This increased flow velocity can be explained by flow concentration as a result of the nearby confluence. The discharges found were quite small compared to the existing relationship between fine sediment loads and fluvial discharge in Brazo Largo, while the loads of section 1 and section 3 were close to the fit. The fine sediment load measured in section 2 was relatively low. In contrast, the flow velocity and bed shear stress simulated by Delft3D are high, which would typically imply higher transport rates. This discrepancy compromises the reliability of the measurement and suggests that the actual inflow into the confluence may have been underestimated, potentially affecting the sediment balance, which was based on mean suspended sediment fluxes.

The calculation of the suspended sediment flux is subject to more sources of uncertainty:

- For each cross section, suspended sediment concentration was measured once and only at one location. Because no information was available on the grain size distribution, the settling velocity for the entire cross section was determined by calibrating the Rouse profile to fit this single measurement and this value was assumed to be representative for all sediment grains in the cross section.
- After plotting the depth-averaged velocities along the three cross sections, the found spread was relatively high compared to the average flow velocity (approximately 30-40% of the mean flow). As the suspended sediment flux is calculated by multiplying concentration by velocity, this uncertainty can lead to a comparable relative uncertainty in the calculated suspended sediment flux.
- Part of the uncertainty may come from short-term flow fluctuations during the measurements and from spatial variability within the cross section that is not fully captured by the ADCP transects.

Uncertainties in the fluxes affect the sediment balance, but in spite of this, the conclusions based off it remain valid. After all, results do not depend on exact sediment values; in fact an order-of-magnitude estimate likely suffices for qualitative insights. Moreover, any underestimation of inflow would only reinforce the limited size and thus impact of dredging.

The results for the bed load transport rate were high compared to historical data. Nevertheless, the result for the downstream boundary at Brazo Largo aligned closely with the discharge–transport relation derived from historical observations. Moreover, the time series of bed load transport estimated for this cross section using the 1D HEC-RAS model was of the same order of magnitude as the Engelund–Hansen estimate based on the fieldwork data. It should be noted, however, that both estimates relied on the same grain diameter, which had not been observed during fieldwork. The main uncertainties in estimating bed load transport stem from the composition of the bed material. The applied Engelund–Hansen equation is primarily suited for sandy beds, but field measurements showed that the Paraná Guazú also contains substantial amounts of fine sediments such as clays and silts. However, sand was indeed present in deeper layers and therefore, the application of Engelund–Hansen remains justified.

From the Delft3D model, it was found that flow concentration of the two streams results in increased flow velocities downstream of the confluence. In this area, the depth-averaged flow velocities reach up to 0.79 m/s compared to the average velocity of 0.6 m/s. The simulated flow field also indicated that at the location of cross section 3 of the sediment balance, the effects of the confluence are still present. From this it seems that the outgoing flux of the sediment balance is affected by the increased flow velocities as a result of the confluence. The bed shear stresses show an increase at the entrance of the confluence for both streams, indicating locations sensitive to scour. Scour of the river bed within the control volume also contributes to the negative sediment balance found. Therefore, when interpreting the calculated negative sediment balance, these factors should be considered in addition to the previously named uncertainties. The bed shear stresses decrease at the junction of the two streams, as a result of the stagnation zone. In this zone the bed shear stresses drop to a value lower than 0.2 N/m^2, leading to deposition of sediment. This also explains why the extraction of sand took place in this location within the confluence. Calibration of the model showed that the simulation does not accurately represent the flow velocities in cross section 1 (Río Talabera). Changing the different parameters in the sensitivity analysis did not resolve this discrepancy. Therefore, it is likely that the bathymetry of the Río Talabera

upstream of the cross section, as derived from the 2019 Digital Elevation Model, is not representative of the current conditions.

9.3. The effects of sand extraction

The effects of sand extraction from the delta area are a key concern of this research. First of all, from the background literature analysis, it became clear that river sand mining can cause bank instability and erosion. This research provided the following insights related to erosion:

- In stakeholder interviews, erosion scales of 30 meters per year were named. Through analysis of satellite data, values ranging between 57 m and 138 m were found for a period of 20 years. This gives considerably lower scales of erosion, between around 3 and 7 meters per year, but is nonetheless significant.
- Erosion was explicitly linked by stakeholders to dredging activities and the passing of cargo ships. The sediment balance can provide insights on the likelihood of these statements. In this calculation, an incoming sediment flux of 20,986.56 tons/day was found. Compared to the estimated amount of extracted sand, equal to 1530 tons/day, it appears unlikely that the net erosion is primarily caused by sand extraction. Even without sand extraction, the system would lack sufficient sediment to balance the deficit.
- From the wave impact study it followed that cargo ships induce waves with a force of 0.996 kN/m. This is a relatively low value and together with the fact that, based on stakeholder data, around six cargo ships per day sail by, it seems unlikely that ship-induced waves contribute substantially to the observed erosion.
- Conversely, in the Aqua Monitor study, a correlation between erosion and flood occurrences was observed. After floods such as the one in 2016, erosion accelerated significantly. The likely explanation for this is that banks become more fragile after a flood and therefore break apart at a faster pace after the flood is gone. Here, it should be noted that climate change increases the likelihood of floods to occur (US Environmental Protection Agency, 2016).
- Natural erosion is a factor that has to be considered. Since the river in the study area meanders, it is expected to have erosion on the outsides of the curves and deposition on the inside of the turns, due to the water with sediment passing by and the differences in flow velocities that occur (Ni, 2025). This behaviour is mostly found in narrow bends where high flow velocities occur at the banks, as shown by the Delft3D simulation. It confirms that the erosion at La Blanqueada camping is a result of this process, considering that high flow velocities occur very near to the bank at this location. Note that this is only described for the camping, but based on the simulation it can be assumed that the effects occur in other locations of the study area as well.

As discussed in Chapter 2, a possible negative effect of river sand extraction is disruption of the river bed. Mining pits are created and later extend in downstream as well as upstream directions. This effect was not found during field work measurement, since longitudinal profiles revealed no significant sand dunes or bed forms. This discrepancy with existing literature can be attributed to the scale of operations: from the sediment balance it follows that dredged volumes (1530 tons per day) are less than one tenth of the sediment influx (20986.56 tons per day). In the lower Mekong river on the other hand, extraction rates are about 8 times greater than the total sand flux entering the delta, triggering sufficient lower bed lowering to cause instability (Hackney et al., 2020).

When it comes to dry sand mining, volumes are considerably larger and therefore effects are also more evident and diverse. First of all there is the truck damage, as became clear from interviews with stakeholders. Many stakeholders complained about the state of the roads, a view that is confirmed by literature and fieldwork observations (Foglia, 2023) (Novas, 2022). Although no research on the exact causes of bad road conditions were done in this report, the extent of truck traffic (350 trucks per day from Ibicuy loaded up to around 25 tons each, as per the mayor of Ibicuy) makes this scenario more than likely. The economic reality in the region is linked to the road damage. As mentioned, the taxes on sand mining activities were kept constant in the years before 2024, so that because of inflation, the provincial income related to the activities was only 440.000 Euros in 2023. This is enough for repaving around 1 kilometer of road that is in ‘fair’ condition, by U.S. standards (Crumb, 2024). The rate was

increased sixfold in 2025, but according to the president of Entre Ríos' tax authority, this still falls short of covering the province's road repair costs (Bellato, 2025).

Another effect of dry sand mining is related to natural habitats: several meters of landscape are removed, including all organisms on it. This has the potential to change habitats for good and have a negative impact on biodiversity; U.S. examples of species that were endangered due to sand mining practices already exist (Center for Biological Diversity, 2025). While visiting the sand mine, it seemed that the natural cover (grasslands and forests) could recover within merely a few years in the study area. It must however be noted that changes to the original natural environment can still be severe: the original soil profile has drastically changed, meaning that even though a new natural cover has emerged, original species might not be able to survive anymore. The literature study has yielded further health-related effects: at high concentrations, silica dust can contribute to the development of cancer, which is a risk for workers at sand mines, but the effects on nearby residents is a topic of discussion.

Finally, washing operations by the sand mines require vast amounts of groundwater: in 2020, 400 million liters of groundwater per month from the Talavera formation was used (Cauce & Humedales sin fronteras, 2022). In comparison, the drinking water cooperation extracts 30 million liters per month in winter and 60 million liters per month in the summer from this reservoir (Foglia, 2023). Considering this scale and the further increase in mining activities since 2020, drinking water scarcity may become relevant in the future. The washing operations furthermore pollute the drinking water, which becomes clear from the fact that manganese and iron concentrations have increased significantly, and manganese concentrations are above limits now.

A number of Nature-based solutions were proposed to protect the delta from the negative effects of sand extraction, such as ecosystem degradation and effects on human health and water security. As mentioned before, erosion in the delta is likely not due to dredging activities. However, since erosion is significant and that dredging activities will possibly increase in the near future, structural mitigation strategies to cope with erosion were still designed. For this, a sheet pile was chosen, however, the design was carried out using the simplified Padfield and Mair method, which represents a simplification of the actual problem.

9.4. Limitations

For the presented study, a number of limitations must be acknowledged. First of all, this research does not engage with future or historic scenarios and therefore conclusions are only valid for the present moment. For example, when determining extraction values, no historical AIS data was available, such that data was only registered for a relatively short period of time (a few weeks). Furthermore, during the fieldwork, data was collected during two days, which means that the full range of historic possible values was not captured. Finally, no future scenarios related to sand mining were taken into account. However, fracking forms an ever greater share of the national production and is viewed by some as critical to the development of Argentina, by driving exports as well as generating foreign currency and investment. The end of the resources is not in sight and in 2025, the number of fractures is expected to increase by 25% as compared to the year before (Barneda, 2025). Given this, it's not unimaginable that in the future, mined sand volumes may increase. Conversely, economic turmoil or sustainable developments might reduce fracking activities. These factors were not considered but have the ability to significantly influence the sediment balance or the reality of dry sand mining in the future.

Moreover, this research focused on the direct effects of sand mining in the lower delta region. However, it must be noted that the purposes of the sand mining, construction and most notably fracking, can have a range of negative effects. In addition to contributing to climate change, fracking poses a danger to children's health, contaminates groundwater, creates noise and air pollution, and triggers earthquakes (Nussbaum, 2024). These impacts might be even more diverse and harmful than the effects of sand extraction in the delta region. But since fracking does not occur in the delta itself, these effects occur in a different area and were hence not considered. This research must therefore not be a read as an analysis of the total effects of sand extraction activities but solely as an analysis of the effects on the delta. Likewise, the research was constrained to a relatively small delta area and therefore, no conclusions on the rest of the delta can be drawn. Incoming sediment or mined volumes likely differ in different parts of the river and thus conclusions may also differ.

Finally, when it comes to the effects on the Lower Paraná Delta, the present study is primarily qualitative in nature. The assessment of sand mining impacts and stakeholder perspectives was largely based on descriptive and interpretative methods. The sediment balance study provided a quantitative analysis of the situation, but conclusions drawn are still qualitative: exact, numeric, conclusions about caused erosion or economic effects are beyond the scope of this study. The fact that limited data on especially sediment concentrations was available also complicated an in-depth quantitative approach. While the qualitative approach allows for an understanding of the relationships between hydrological, morphological and socio-economic factors, it inherently limits the precision with which these relationships can be measured or compared.

10

Conclusion and recommendations

10.1. Conclusion

The sub-questions help formulate an answer to the main research question. The first sub-question was related to sand extraction volumes in the Lower Paraná Delta and the purposes of sand. In the Lower Paraná Delta, river sand extraction has remained relatively constant, while local government intervention has halted dredging in the Paraná Ibicuy. AIS data indicate that current river sand extraction volumes in the region are around 587,000 tons per year, whereas dry sand mining has increased drastically to approximately 2.3 million tons in 2025, about twice the amount extracted in 2022. River sand is mainly used by the construction sector, which currently shows relatively low demand, while most dry sand is extracted for fracking. Overall, sand mining activities show an upward trend, driven primarily by dry sand mining for fracking purposes.

The sediment balance of the relevant section of the Paraná Guazú River was established by quantifying sediment inputs, outputs, and storage within the river reach. During fieldwork, sediment samples were collected at key points along the river, flow properties were measured and the bathymetry was recorded. This method delivered velocity profiles that allowed for estimations of suspended sediment loads, as well as granulometries and discharge data that served as the input for the Engelund-Hansen equation to estimate bed load transport rates. Subsequently, these fluxes enabled an estimation of the net sediment balance. From this, a net negative change in sediment storage of 15,400 tons per day was found. When comparing the estimated dredging volume (1530 tons/day) to the total inflow of sediments (21,000 tons/day) it can be concluded that the dredging activities have an insubstantial contribution to the sediment deficit.

Hydrodynamic analysis shows that stage-discharge relationships are weakly correlated in the study area. This is attributed to variations of the Río de la Plata, which are transient effects that act on different timescales than those under the assumption of steady flow. In addition, the tidal variance fraction of 5.71% suggests that the influence of the astronomical tide is small relative to the meteorological tide. Measurements and simulations record mean flow velocities between 0.5 and 0.8 m/s, of which the upper values are mostly encountered after the confluences in the study area, as a result of the concentration of flow velocities. Finally, meandering effects in the river cause high flow velocities in outer bends that result in bank erosion, which is confirmed by the Delft3D simulation.

Stakeholders suggested high erosion rates in the study area of up to 30 m per year that were attributed to dredging and cargo ships. Satellite data indicate lower rates of around 3–7 m per year. The sand extraction mass was estimated to be 1,530 tons/day and compared to the total net negative sediment flux, it becomes clear that dredging in the area is not substantial enough to cause a significant portion of observed erosion. Ship-induced waves also appear to play a minimal role, as their force is relatively low and vessel frequency is limited. Instead, erosion is strongly influenced by natural factors, including bank instability following floods, which are expected to increase with climate change. The river's meandering behavior, which promotes erosion on outer bends and deposition on inner bends, is another key factor in explaining erosion.

Another possible effect of river sand mining is induced riverbank instability due to lowering of the bed. The scale of sand mining activities together with the observed absence of mining pits indicate that dredging-induced river bank instability is not a concern for the Lower Paraná Delta at present. A socioeconomic effect of river sand mining came forward in stakeholder interviews: dredging vessels cause noise nuisance, which forms a disturbance for people near the river shores. This caused activities near Ibicuy to stop. Dry sand mining has more evident and diverse impacts than river sand mining due to larger volumes extracted. Truck traffic causes significant road damage while taxes have not been high enough to fund repairs. This underscores that political and economic choices have allowed for current poor road conditions to exist. Washing operations demand vast amounts of groundwater that far exceed local drinking water use and can pollute water with elevated manganese and iron concentrations. Finally, large-scale removal of soil alters natural habitats, but the exact long-term effects on biodiversity in the study area do not become clear from this research. Sand mining has the potential to have adverse health effects, but the effects on people in the delta were also not determined.

As mentioned before, the rising demand for sand is driven by fracking activities in the south of Argentina. The specific demand for sand from the Lower Paraná Delta can be explained by the sand characteristics that are needed for fracking activities. Fracking sand must meet strict physical and chemical standards: it typically consists of over 90% quartz, grains must be smooth and round, and the distribution must be relatively uniform. The studied geology shows multiple layers of sand containing more than 85% quartz, with some layers showing contents of more than 99%. Grain size distributions that were created based on taken bed samples do not meet the fracking specifications related to grain uniformity, but only a limited number of river samples were taken and no dry samples were analysed. Other factors that contribute to the demand for sand are the deltaic nature of the study area, natural river and wind processes help purify and round the grains, and local government policy, most notably low taxes. This makes mining in the area economically as well as technically attractive.

A number of observed negative effects call for mitigation measures. To make sure designs align with goals of climate resilience and sustainable development, the focus was on Nature-based solutions. The most relevant Nature-based solutions identified are floodplains, vegetated buffer zones, and riparian buffer zones, as they offer the most benefits for mitigating mining-related impacts. Floodplain restoration helps counteract land degradation and loss of biodiversity from dry sand mining by re-establishing natural hydrological connections and improves groundwater recharge. Vegetated buffer zones capture dust from sand mines, which helps protect nearby communities from air and sound pollution and any resulting negative health impacts. Riparian buffer zones filter pollutants and enhance biodiversity. In addition, all these solutions help reduce erosion. Although erosion in the delta could not be linked to sand extraction activities, the scale is significant and stakeholder interviews show that mitigation strategies are called for. Further, a further increase of dredging activities in the future is likely. Hence, future dredging-induced erosion is possible. As a structural solution to dredging, a sheet pile was deemed most appropriate. A final design, with depth 10.2 meters below the river bed and profile AZ24 700, is structurally sound and can thus help reduce erosion.

Using the answers to the sub questions, the main research question can be answered:
What are the morphological and socioeconomic effects of sand extraction in the Lower Paraná Delta and how can these be managed to secure a sustainable future?

Sand extraction in the Lower Paraná Delta has limited morphological but significant socioeconomic effects. River dredging volumes are stable and contribute only marginally to the sediment deficit, meaning that meandering and flood-induced bank instability dominate erosion patterns. In contrast, dry sand mining has expanded rapidly to supply fracking demand, increasing pressure on natural systems and local communities through groundwater overuse and road damage, reinforced by government policy. A sustainable future for the delta can be supported through applying Nature-based solutions such as floodplain restoration, vegetated buffer zones, and riparian buffers, or through structural measures in the form of a sheet pile.

10.2. Recommendations

As mentioned in the previous chapter, this report should be read as an investigation of current circumstances. However, future research could adopt a broader scope by incorporating both historical and future-oriented data. Long-term monitoring of extraction rates, sediment transport, and hydrodynamic conditions would allow for a more robust understanding of variability and trends in the sediment balance. More continuous AIS data, data on sediment concentrations and hydrodynamic data are necessary for such an analysis. Furthermore, scenario-based modeling, with possible increases or decreases in fracking activity, would make it possible to predict how future developments can influence the socioeconomic effects of sand mining. By extending the modelling approach to a morphological model in Delft3D, the 'turning point' at which dredging volumes are big enough to trigger bank instability and large-scale erosion, could be determined. In addition, tidal effects should be incorporated into the model, considering the significant influence of the Río de la Plata on the hydrodynamics in the Paraná Guazú.

Subsequent studies can also expand on the geographical scope of this analysis to capture the broader dynamics of sand extraction across Argentina. While this study focused on a limited area within the Lower Paraná Delta, similar activities occur throughout the rest of the delta and the country, under different conditions. A comprehensive nation-wide assessment would make it possible to determine whether the findings for the delta are representative. Moreover, this can help link the environmental consequences of sand mining to the impacts of its end uses, particularly fracking. A life-cycle or supply chain analysis would allow for tracing sand from extraction to consumption, thereby quantifying the total socioeconomic and environmental footprint of the sector on Argentina.

Building on this, future research should also aim to inform policy decisions through a broader, quantitative, cost–benefit analysis of sand extraction and its purposes. Such analyses could evaluate not only the direct profits from mining and related industries, but also the long-term costs associated with erosion, biodiversity loss, water degradation, and community impacts. Incorporating this with a nation-wide analysis of the footprint of the sand mining sector would allow for evidence-based decision-making and help put in place more sustainable extraction policies.

References

AcademiaLab. (n.d.). Paraná Delta. Retrieved October 21, 2025, from https://academia-lab.com/encyclopedia/parana-delta/

Administración General de Puertos S.A.U. (2023, January). AGP comenzó la batimetría del Paraná Guazú. Retrieved September 9, 2025, from https://www.argentina.gob.ar/noticias/agp-comenzo-la-batimetria-del-parana-guazu

Agencia Nacional de Puertos y Navegación. (2025, March). La Vía Navegable Troncal. Retrieved September 12, 2025, from https://www.argentina.gob.ar/economia/agencia-nacional-de-puertos-y-navegacion/navegacion/navegable-troncal/la-navegable-troncal

Amato, S., & Busso, A. S. (2009, July). *Estratigrafía cuaternaria del subsuelo de la cuenca inferior del río Paraná* (tech. rep.). https://www.researchgate.net/publication/262497724_Estratigrafia_cuaternaria_del_subsuelo_de_la_cuenca_inferior_del_rio_Parana

Antonini, A. (2025). Lecture 12 - Ships - CIEM4220 Dams, Dikes and Breakwaters.

Apel, J. R. (1987). *Principles of Ocean Physics*. Academic Press.

Apple Maps. (2025). https://maps.apple.com/

ArcelorMittal. (2024). Guidelines - Sustainability of steel sheet piles. https://sheetpiling.arcelormittal.com/sites/default/files/2024-11/AMCRPS_Sustainability_guidelines_EN-2024_web.pdf

Arriaga, J., & Tissier, M. (2025). Lecture 2 - CIEM4000 Base: Hydraulic and Offshore Structures.

Balay, M. A. (2018). Causes and Periodicity of Large Floods in Rio de la Plata: (Flood of 27 and 28 July 1958). *The International Hydrographic Review*, *1*. https://journals.lib.unb.ca/index.php/ihr/article/view/26599

Barneda, D. (2025, April). El fracking de Vaca Muerta está imparable: los números son impactantes. Retrieved October 21, 2025, from https://eleconomista.com.ar/energia/el-fracking-vaca-muerta-esta-imparable-numeros-son-impactantes-n83539

Baxter, D., El Kasimi, A., Hechler, O., Martins, J., Weber, E., White, G., Zillgen, H., & Zück, F. (2022). *Piling Handbook* (9th ed.). ArcelorMittal. https://sheetpiling.arcelormittal.com/sites/default/files/2024-07/AMCRPS_Piling_Handbook_9th_Revision_2022_web.pdf

Bellato, R. (2025, October). Entre Ríos: Frigerio actualizó un impuesto sobre el transporte de un insumo estratégico para Vaca Muerta. Retrieved October 9, 2025, from https://econojournal.com.ar/2025/10/entre-rios-frigerio-impuesto-transporte-insumo-estrategico-vaca-muerta/

Benson, M. E., & Wilson, A. B. (2015). *Frac Sand in the United States—A Geological and Industry Overview* (tech. rep.). U.S. Department of the Interior & U.S. Geological Survey. Reston, Virginia. https://pubs.usgs.gov/publication/ofr20151107

Bosboom, J., & Stive, M. J. F. (2023). *Coastal Dynamics*. Delft University of Technology.

Brok, L. (2022). *Channel Network Morphodynamics in the Lower Paraná Delta* [Master's thesis, TU Delft]. Retrieved September 12, 2025, from https://resolver.tudelft.nl/uuid:5f07f49f-1283-4ff7-9e8e-adc1b74fbe99

Brown, W. D. (1994). *Design of Sheet Pile Walls* (tech. rep.). Washington, D.C. https://www.publications.usace.army.mil/portals/76/publications/engineermanuals/em_1110-2-2504.pdf

Brunier, G., Anthony, E. J., Goichot, M., Provansal, M., & Dussouillez, P. (2014). Recent morphological changes in the Mekong and Bassac river channels, Mekong delta: The marked impact of river-bed mining and implications for delta destabilisation. *Geomorphology*, *224*, 177–191. https://doi.org/10.1016/j.geomorph.2014.07.009

Cassin, J. (2021, January). Nature-based Solutions and Water Security. In J. Cassin, J. H. Matthews, & E. L. Gunn (Eds.), *Nature-based Solutions and Water Security* (pp. 19–34). Elsevier. https://doi.org/10.1016/B978-0-12-819871-1.00018-X

Cauce & Humedales sin fronteras. (2022, October). Arenas para el fracking. https://cauceecologico.org/wp-content/uploads/2022/09/ARENAS-FINAL.pdf

Cavallotto, J. L., Violante, R. A., & Colombo, F. (2005). Evolución y cambios ambientales de la llanura costera de la cabecera del río de la Plata. *Revista de la Asociación Geológica Argentina*, *60*(2).

https://www.researchgate.net/publication/262741595_Evolucion_y_cambios_ambientales_de_la_llanura_costera_de_la_cabecera_del_rio_de_la_Plata?enrichId=rgreq-11484ebb6b5d9feadab55522574bb927-XXX&enrichSource=Y292ZXJQYWdlOzI2Mjc0MTU5NTtBUzoxNTcwMjAwNzAwOTY4OTdAMTQxNDQ0NzkxMTAwNw%3D%3D&el=1_x_2&_esc=publicationCoverPdf

Center for Biological Diversity. (2025, March). Legal Intervention Launched to Protect Dunes Sagebrush Lizard. Retrieved October 9, 2025, from https://biologicaldiversity.org/w/news/press-releases/legal-intervention-launched-to-protect-dunes-sagebrush-lizard-2025-03-12/

Chow, V. T. (1959). *Open Channel Hydraulics*. McGraw-Hill.

Cordini, R. (1949). Contribucion al conocimiento de la geologia economic de entre rios. http://repositorio.segemar.gov.ar/308849217/791

Crumb, K. (2024, February). The Cost of Road Maintenance. Retrieved October 9, 2025, from https://www.strongsactown.org/2024/02/13/the-cost-of-road-maintenance/

Cuomo, G., Allsop, W., & McConnell, K. (2004). Dynamic Wave Loads on Coastal Structures: Analysis of Impulsive and Pulsating Wave Loads. *Coastal Structures*, *2003*, 356–368. https://doi.org/10.1061/40733(147)30

Deltares. (2025a). Aqua Monitor. https://aqua-monitor.appspot.com/

Deltares. (2025b, October). QUICKIN User Manual. https://content.oss.deltares.nl/delft3d4/QUICKIN_User_Manual.pdf

Denchak, M. (2019, April). Fracking 101. Retrieved October 6, 2025, from https://www.nrdc.org/stories/fracking-101

Depetris, P. J., & Griffin, J. J. (1968). Suspended Load in the Río De La Plata Drainage Basin. *Sedimentology*, *11*(1-2), 53–60. https://doi.org/10.1111/j.1365-3091.1968.tb00840.x

D'Onofrio, E., Fiore, M., Mayer, F., Perdomo, R., & Ramos, R. (1999). La Referencia Vertical. Retrieved October 2, 2025, from https://www.ign.gob.ar/content/la-referencia-vertical?utm_source=chatgpt.com

Duncan, R. (2021, September). 5 Easy Ways to Revive Your River: Support nature-based solutions. Retrieved October 16, 2025, from https://theriverstrust.org/about-us/news/five-easy-ways-to-revive-your-river-support-nature-based-solutions

Dunlop, T., Khojasteh, D., Cohen-Shacham, E., Glamore, W., Haghani, M., van den Bosch, M., Rizzi, D., Greve, P., & Felder, S. (2024, March). *The evolution and future of research on Nature-based Solutions to address societal challenges* (tech. rep.). https://www.nature.com/articles/s43247-024-01308-8

Eiselin, M. (2022, March). Verenigde Naties stemmen in met definitie van nature-based solutions. https://www.iucn.nl/nieuws/verenigde-naties-stemmen-in-met-definitie-van-nature-based-solutions/

Engelund, F., & Hansen, E. (1967). A monograph on sediment transport in alluvial streams. Retrieved October 9, 2025, from https://resolver.tudelft.nl/uuid:81101b08-04b5-4082-9121-861949c336c9

Equipo de Manejo de Información. (2016, May). *Argentina - Inundaciones* (tech. rep.). Retrieved October 7, 2025, from https://reliefweb.int/report/argentina/argentina-inundaciones-desde-24-de-abril-al-01-de-mayo-2016

Farber, M. E., Raizboim, I. N., & Farber, M. E. (2024, March). Hydrography of Argentina - El Sur del Sur. Retrieved September 12, 2025, from https://surdelsur.com/en/hydrography-of-argentina/

Ferguson, R., & Church, M. (2004). A Simple Universal Equation for Grain Settling Velocity. *Journal of Sedimentary Research*, *74*(6), 933–937. https://doi.org/10.1306/051204740933

Ferreira, P. F. G., Botelho, I. C. d. S. S., & Mattos, J. d. S. S. (2024). Propágulos de Mangue Vermelho: Solução baseada na natureza (SbN) para a recuperação de manguezais da ilha de Cotijuba, Pará, Amazônia, Brasil. *Research, Society and Development*, *13*(12), e65131247649–e65131247649. https://doi.org/10.33448/rsd-v13i12.47649

Foglia, V. (2023, April). Sed de arena. https://opsur.org.ar/wp-content/uploads/2023/05/Sed-de-arena.pdf

Google Earth. (2025, October). Retrieved October 27, 2025, from https://earth.google.com/web/@0,-1.06609997,0a,22251752.77375655d,35y,0h,0t,0r/data=CgRCAggBOgMKATBCAggBSg0I_____________ARAA

Government of South Australia. (2024, May). Riverbank collapse. Retrieved September 17, 2025, from https://www.sa.gov.au/topics/emergencies-and-safety/types/riverbank-collapse Last Modified: 2024-05-23.

Grabe, J. (2008, July). *Sheet Piling Handbook Design*. https://www.geoset.pro/download/articles/foreign/95_Sheet_Piling_Handbook_Design.pdf

Guia de Plantas Nativas. (2008). Inga uraguensis. Retrieved October 22, 2025, from https://nativas.lanacion.com.ar/

Hackney, C. R., Darby, S. E., Parsons, D. R., Leyland, J., Best, J. L., Aalto, R., Nicholas, A. P., & Houseago, R. C. (2020). River bank instability from unsustainable sand mining in the lower Mekong River. *Nature Sustainability*, *3*(3), 217–225. https://doi.org/10.1038/s41893-019-0455-3

Hammond, N. (2022). What is a Black Mangrove? Retrieved October 22, 2025, from https://www.manggear.com/blogs/stories/what-is-a-black-mangrove?srsltid=AfmBOoqTsPq91Xs6qlwfPytlg7ODKk-_YqobHZmHuWG8WSqtRdopa7Bu

Hiba, J. (2024, August). On the Paraná River, ecological crisis is a threat to its identity. Retrieved September 15, 2025, from https://dialogue.earth/en/climate/on-the-parana-river-ecological-crisis-is-a-threat-to-its-identity/

iNaturalist. (2020). Salix humboldtiana. Retrieved October 22, 2025, from https://www.inaturalist.org/taxa/209991-Salix-humboldtiana

Instituto Nacional del Agua. (2025). Proposal for TU Delft Students: Multidisciplinary Projects.

International Trade Administration. (2025, August). Argentina Country Commercial Guide. Retrieved October 6, 2025, from https://www.trade.gov/country-commercial-guides/argentina-energy-oil-gas

Jones, A. E., Hardison, A. K., Hodges, B. R., McClelland, J. W., & Moffett, K. B. (2019). An expanded rating curve model to estimate river discharge during tidal influences across the progressive-mixed-standing wave systems. *PLOS ONE*, *14*(12). https://doi.org/10.1371/journal.pone.0225758

Kalpakjian, S., & Schmid, S. R. (2010). *Manufacturing engineering and technology* (6th ed). Prentice Hall. https://lib.zu.edu.pk/ebookdata/Engineering/Energy%20System/Manufacturing%20Engineering%20and%20Technology%20by%20Serope%20Kalpakjian,%20Steven%20R.%20Schmid%20.pdf OCLC: 305147413.

Kandus, P., & Malvárez, A. I. (2004, September). *Vegetation patterns and change analysis in the lower delta islands of the Parana River (Argentina)* (tech. rep.). https://link.springer.com/article/10.1672/0277-5212%282004%29024%5B0620%3AVPACAI%5D2.0.CO%3B2

Kelly, P. (2018). Mechanics Lecture Notes: An introduction to Solid Mechanics. https://pkel015.connect.amazon.auckland.ac.nz/SolidMechanicsBooks/Part_I/index.html

Korff, M. (2023, January). *Reader Deep Excavations CIEM2000 unit 3*. Delft University of Technology.

Krauss, C. (2011). Argentina Hopes for a Big Payoff in Its Shale Oil Field Discovery. *The New York Times*. Retrieved October 6, 2025, from https://www.nytimes.com/2011/07/05/business/global/05shale.html

L. Idaszkin, Y., J. Bouza, P., H. Marinho, C., & N. Gil, M. (2024, December). *Trace metal concentrations in Spartina densiflora and associated soil from a Patagonian salt marsh* (tech. rep.). https://www.sciencedirect.com/science/article/abs/pii/S0025326X14006699

Law, B. E., & Spencer, C. W. (1992). Gas in tight reservoirs - an emerging major source of energy. *United States Geological Survey*, *1570*. Retrieved October 6, 2025, from https://www.osti.gov/biblio/6814307

López Weibel, C., Szupiany, R., Latosinski, F., Amsler, M., & Repasch, M. (2022). Sources and temporal dynamics of suspended sediment transport along the middle Paraná River. *Journal of South American Earth Sciences*, *119*. https://doi.org/10.1016/j.jsames.2022.103968

Marco. (domingo, septiembre 12, 2021). Argentina nativa: Junco (Schoenoplectus californicus). Retrieved October 28, 2025, from https://faunayfloradelargentinanativa.blogspot.com/2011/02/junco-schoenoplectus-californicus.html

Marine Traffic. (2025, October). AIS Marine Traffic. Retrieved October 27, 2025, from https://www.marinetraffic.com/en/ais/home/shipid:378648/zoom:6

Marshall, S. (2024, January). Understanding the Vital Role of Riparian Zones. Retrieved October 22, 2025, from https://www.naturetrust.bc.ca/news/understanding-the-vital-role-of-riparian-zones

McNeil Engineering. (2023, March). The advantages and disadvantages of using precast concrete. Retrieved September 23, 2025, from https://www.mcneilengineering.com/the-advantages-and-disadvantages-of-using-precast-concrete-in-structural-engineering/

Ni, S. (2025, April). Why Do Rivers Curve and Meander? Unraveling the Science Behind Nature's Winding Paths. Retrieved October 15, 2025, from https://www.tmparksfoundation.org/single-post/why-do-rivers-curve-and-meander-unraveling-the-science-behind-nature-s-winding-paths

Novas, M. (2022, November). El impacto ambiental oculto del fracking: La minería de arena en Entre Ríos. Retrieved October 7, 2025, from https://aapepyg.com/2022/11/23/fracking_entre_rios/

NParks | Casuarina equisetifolia. (n.d.). Retrieved October 28, 2025, from https://www.nparks.gov.sg/florafaunaweb/flora/2/7/2793

Nussbaum, R. (2024, November). Yale environmental health expert discusses concerns about fracking. Retrieved October 27, 2025, from https://medicine.yale.edu/news-article/deziel/

Orfeo, O., & Stevaux, J. (2002). Hydraulic and morphological characteristics of middle and upper reaches of the Paraná River (Argentina and Brazil). *Geomorphology*, *44*(3), 309–322. https://doi.org/10.1016/S0169-555X(01)00180-5

Padmalal, D., & Maya, K. (2014). *Sand Mining: Environmental Impacts and Selected Case Studies*. Springer Netherlands. https://doi.org/10.1007/978-94-017-9144-1

Peters, T. M., O'Shaughnessy, P. T., Grant, R., Altmaier, R., Swanton, E., Falk, J., Osterberg, D., Parker, E., Wyland, N. G., Sousan, S., Stark, A. L., & Thorne, P. S. (2017). Community airborne particulate matter from mining for sand used as hydraulic fracturing proppant. *Science of The Total Environment*, *609*, 1475–1482. https://doi.org/10.1016/j.scitotenv.2017.08.006

Physicians for Social Responsibility, Science and Environmental Health Network, & Concerned Health Professionals of New York. (2023, October). Compendium of Scientific, Medical, and Media Findings Demonstrating Risks and Harms of Fracking and Associated Gas and Oil Infrastructure. https://psr.org/wp-content/uploads/2023/10/fracking-compendium-9.pdf

Popa, M. D., Simionov, I.-A., Petrea, S. M., Dima, F. M., Patriche, N., Iticescu, C., Oancea, E., & Lacatus, M. (2023). Heavy Metals Accumulation in the Tissues of the Common Reed (phragmites Australis). *Scientific Papers. Series E. Land Reclamation, Earth Observation & Surveying, Environmental Engineering*, (12), 86–91. researchgate.net/publication/376522408_HEAVY_METALS_ACCUMULATION_IN_THE_TISSUES_OF_THE_COMMON_REED_PHRAGMITES_AUSTRALIS?__cf_chl_tk=YWjvV9SKBxzpI7_gmgOaFVC888geGbI18tb9wZprcAU-1760641792-1.0.1.1-42h9vgTSVaKSO8a5ZI.XdqdANvyXboFZmTWNf8JXDUg

Prefectura Naval Argentina. (2025, October). Prefectura Naval Argentina. Retrieved October 27, 2025, from https://www.argentina.gob.ar/prefecturanaval

Re, M., Menéndez, A. N., & Amsler, M. (2009). Metodología para la generación de series temporales de descarga sólida de los ríos Paraná de las Palmas y Paraná Guazú. https://repositorio.ina.gob.ar/handle/123456789/190

Rentier, E. S., & Cammeraat, L. H. (2022). The environmental impacts of river sand mining. *Science of The Total Environment*, *838*. https://doi.org/10.1016/j.scitotenv.2022.155877

Rodriguez, J., Edeskär, T., & Knutsson, S. (2013). Particle Shape Quantities and Measurement Techniques - A review. *Electronic Journal of Geotechnical Engineering*, (18), 30. Retrieved October 6, 2025, from https://www.researchgate.net/publication/237019957_Particle_Shape_Quantities_and_Measurement_Tecniques_-_A_review

Samarasekera, I. V. (2001). Hot Rolling. In K. H. J. Buschow, R. W. Cahn, M. C. Flemings, B. Ilschner, E. J. Kramer, S. Mahajan, & P. Veyssière (Eds.), *Encyclopedia of Materials: Science and Technology* (pp. 3836–3843). Elsevier. https://doi.org/10.1016/B0-08-043152-6/00683-5

Schipper, R. (2024). Material characteristics — Structural Design Essentials. Retrieved October 23, 2025, from https://teachbooks.io/Structural_Design_Essentials/main/basics/steel/material_characteristics_steel.html

Schmidt, A., & Yen, B. (2011, October). Stage-Discharge Relationship in Open Channels. https://www.researchgate.net/profile/Arthur-Schmidt-5/publication/267233546_Stage-Discharge_Relationship_in_Open_Channels/links/5510541d0cf2ba84483d4c99/Stage-Discharge-Relationship-in-Open-Channels.pdf

Secretaría de Política Minera. (2019, October). Arenas para fracking.
Sharip, Z., & Zaki, A. T. A. (2014). The effects of season and sand mining activities on thermal regime and water quality in a large shallow tropical lake. *Environmental Monitoring and Assessment*, *186*(8), 4959–4969. https://doi.org/10.1007/s10661-014-3751-4
Sheet Piling Group. (2018). Sheet Piles. Retrieved October 23, 2025, from https://www.steelpilinggroup.org/steel-piling-overview/sheet-piles/
SNIH. (2025, October). Sistema Nacional de Información Hídrica. Retrieved October 27, 2025, from https://snih.hidricosargentina.gob.ar/Filtros.aspx
Soliman, M. A., Ahmed, D. A., Mansour, K. H., Gharib, F. A., Galal, T. M., & Slima, D. F. (2024). Typha domingensis (Pers.) Poir. ex Steud. Potential to Restore Contaminated Wetlands in Egypt. *Journal of Soil Science and Plant Nutrition*, *24*(4), 8005–8015. https://doi.org/10.1007/s42729-024-02094-0
Song, C., Shao, Q., Chen, X., & Liang, Y. (2024). Evaluating and understanding tide-river interactions based on both physical models and data analysis. *Journal of Hydrology*, *632*. https://doi.org/10.1016/j.jhydrol.2024.130765
Sprung, J. (2021, November). How long does it take for red mangrove propagules to sprout roots? Retrieved October 22, 2025, from https://www.reef2reef.com/threads/how-long-does-it-take-for-red-mangrove-propagules-to-sprout-roots.870580/
Stevaux, J. C. (1994). The upper Paraná river (Brazil): Geomorphology, sedimentology and paleoclimatology. *Quaternary International*, *21*, 143–161. https://doi.org/10.1016/1040-6182(94)90028-0
Stichting Koninklijk Nederlands Normalisatie Instituut. (2025, July). Nederlandse norm NEN 9997-1+C1 (nl) Geotechnisch ontwerp van constructies - Deel 1: Algemene regels.
Technical Committee CEN/TC250. (2007). EN 1993-5 (2007) (English): Eurocode 3 - Design of steel structures.
Tineo, D. E., Pérez, L. M., Brandoni, D., Martínez, S., Bona, P., Brea, M., Noriega, J. I., & Brunetto, E. (2024). Reconstructing the South American Miocene puzzle: An integrated analysis of the Paraná Formation (Argentina). *Journal of South American Earth Sciences*, *147*, 105118. https://doi.org/10.1016/j.jsames.2024.105118
Torrabadella, A. G. (2013). Numerical Analysis of Cantilever and Anchored Sheet Pile Walls at Failure and Comparison with Classical Methods. https://vulcanhammer.info/wp-content/uploads/2021/09/torrabadella.pdf
UK Forestry Standard. (2024). Creating and managing riparian woodland. https://cdn.forestresearch.gov.uk/2024/07/UKFSPG028_Riparian_woodland_web_0108-compressed.pdf
U.S. Energy Information Administration. (2013, June). Technically Recoverable Shale Oil and Shale Gas Resources. https://www.eia.gov/analysis/studies/worldshalegas/pdf/fullreport.pdf
US Environmental Protection Agency. (2016, July). Climate Change Indicators: River Flooding. Retrieved October 7, 2025, from https://www.epa.gov/climate-indicators/climate-change-indicators-river-flooding
Vagheei, H., & Boano, F. (2025). Freshwater riparian zones in a changing climate: A comprehensive review. *Ecological Indicators*, *176*, 113600. https://doi.org/10.1016/j.ecolind.2025.113600
Vogel, J. C., & Lerman, J. C. (1969). Groningen Radiocarbon Dates VIII. *Radiocarbon*, *11*(2), 351–390. https://doi.org/10.1017/S0033822200011279
Ward, R. D. (n.d.). Fig. 6. Latitudinal limits, ecoregions, and location of mangroves in... Retrieved October 28, 2025, from https://www.researchgate.net/figure/Latitudinal-limits-ecoregions-and-location-of-mangroves-in-South-America-Recent_fig7_301732207
Weeds Australia. (2019, March). Cockspur Coral Tree, Cockscomb Coral Tree, Coral Tree, Cockspur, Indian Coral Tree, Fireman's Cap, Crybabytree, Crybaby Tree. Retrieved October 22, 2025, from https://weeds.org.au/profiles/cockspur-coral-tree/
Wester, S. J., Grimson, R., Minotti, P. G., Booij, M. J., & Brugnach, M. (2018). Hydrodynamic modelling of a tidal delta wetland using an enhanced quasi-2D model. *Journal of Hydrology*, *559*, 315–326. https://doi.org/10.1016/j.jhydrol.2018.02.014
World Health Organization. (2011). Acrylamide. Retrieved October 13, 2025, from https://apps.who.int/food-additives-contaminants-jecfa-database/Home/Chemical/5198
WWF. (2019, July). Rising demand for sand calls for resource governance. Retrieved October 15, 2025, from https://wwf.panda.org/es/?346754/Rising-demand-for-sand-calls-for-resource-governance

Xylem. (n.d.). SonTek-M9. Retrieved October 1, 2025, from https://www.ysi.com/sontek-m9?srsltid=AfmBOormWU78QE-PXBFxM_vMD7IV-ip7mEG9r6Rzk4eGyv8vSANzntxp

A

Safety assessment

This appendix presents the risk assessment associated with the procedures that were conducted in the fieldwork as part of the multiple discipline project titled ”Delft University of Technology Sediment Balance in a Sector of the Paraná Guazú River”

A.1. Risk assessment: fieldwork

A.1.1. Hazard identification

This fieldwork involves extensive activities both on and around the water, which inherently present a variety of safety and health hazards. Working in such environments requires continuous awareness and precautionary measures to protect all members of the research team. The most severe hazard associated with water-based fieldwork is the risk of drowning. This can occur as a result of falling from boats, working on unstable or slippery riverbanks, or being caught in strong currents. Proper use of life jackets, safe boarding procedures, and clear communication within the group are therefore essential preventive measures.

In addition to the immediate risks of drowning, environmental and weather-related factors can also impact safety. High temperatures and prolonged exposure to the sun may cause heat stress, dehydration, or sunburn, while sudden changes in weather, such as heavy rainfall, thunderstorms, or strong winds, can rapidly increase danger on the water. Adequate protective clothing, hydration, and weather monitoring should be part of the fieldwork routine.

Contact with surface water may also expose researchers to biological hazards. Natural water bodies can contain bacteria, parasites, or other microorganisms that cause skin infections or gastrointestinal illness. Wearing waterproof gloves, avoiding direct contact with open wounds, and practicing proper hygiene (e.g., hand washing or use of disinfectants after fieldwork) are effective ways to reduce these risks. Another aspect to consider is the safe handling of mechanical and sampling equipment. Working with pumps, sieves, augers, or motorized boats requires attention to mechanical hazards such as entanglement, cuts, or equipment malfunction. Ensuring that all equipment is well maintained and operated only by trained individuals minimizes these dangers.

Finally, the natural environment itself may present additional threats from wildlife. These can range from sharp shells or stinging organisms in the water, to insect bites, snakes, or other animals encountered near the riverbank. Using appropriate footwear, insect repellent, and maintaining awareness of the surroundings can help prevent injuries or allergic reactions.

A.1.2. Risk assessment

The risks associated with this fieldwork vary both in their likelihood of occurrence and in the severity of their potential consequences. Understanding this balance is essential for prioritizing safety measures and ensuring that all critical hazards receive appropriate attention and control.

The risk of drowning, although assessed as having a low likelihood under normal operating conditions, carries extremely severe consequences should it occur. Because of the potentially fatal outcome, this hazard remains a critical concern and must always be treated with the highest level of precaution. Preventive actions such as the mandatory use of life jackets, maintaining clear safety protocols during boat operations, and ensuring all participants are trained in emergency procedures are therefore non-negotiable components of field safety.

Risks arising from weather conditions are more likely to occur and can vary throughout the day. The likelihood of exposure to heat, sun, or sudden changes in weather is considered relatively high, while the potential consequences, ranging from mild heat stress to temporary work interruptions, are moderate. Nevertheless, such risks should be actively mitigated through measures including weather monitoring, adequate rest and hydration, the use of sun protection, and flexible planning to avoid dangerous conditions.

Biological hazards, such as exposure to bacteria or other pathogens present in the water, are generally considered to have a low likelihood of occurrence if proper hygiene and protective measures are followed. However, the consequences of such exposure can be significant, including illness or infection. For this reason, it is vital that all team members remain aware of these hazards and adhere strictly to personal protection and sanitation guidelines, such as using gloves, avoiding contact with open wounds, and washing hands thoroughly after field activities.

Finally, hazards related to mechanical equipment such as cuts, entanglement, or mechanical malfunction, are assessed as having a low likelihood in this specific fieldwork setting. Their potential consequences are moderate, primarily involving minor injuries or temporary disruption of operations. Routine maintenance, proper training, and adherence to safe operating procedures are sufficient to keep this risk at an acceptable level.

A.1.3. Control measures

To minimize potential risks during fieldwork, it is essential that all participants make consistent and appropriate use of personal protective equipment (PPE). Key items include life jackets when working on or near the water, sturdy footwear with sufficient grip to prevent slipping on wet or uneven surfaces, and protective gloves when handling tools, equipment, or biological materials. The type of gloves may vary depending on the specific task, ranging from waterproof gloves for wet environments to cut-resistant gloves when working with sharp instruments.

Equally important is ensuring that every team member is fully aware of the hazards present in the field environment. To achieve this, a comprehensive safety briefing must be conducted before any field activities begin. During this briefing, all risks, safety procedures, and emergency response protocols should be clearly explained, allowing participants to understand both their individual responsibilities and the collective safety measures of the group.

Maintaining proper hygiene also plays a crucial role in minimizing biological risks. Regular handwashing, particularly before eating or after contact with river water, significantly reduces the likelihood of bacterial or parasitic infections. The availability of clean water, disinfectant wipes, or alcohol-based sanitizers should therefore be ensured at all times.

In the event of an emergency, effective communication is vital. All team members must be reachable at short notice to enable rapid coordination and response. For this reason, everyone should carry a charged mobile phone at all times. A clear communication plan, including designated contact persons and emergency numbers, should be established before fieldwork begins.

By combining the proper use of PPE, strong situational awareness, good hygiene practices, and reliable communication systems, the risks associated with water-based fieldwork can be significantly reduced, ensuring a safe and efficient working environment for all participants.

B

Unprocessed interview results

In this appendix, the interview framework for each stakeholder is shown. This consisted of a topic guide with questions. The questions are shown along with the answers in keywords. Finally, the results of unprepared questions are given, these questions were added due to issues raised by the interviewee. In this section, the raw results are given. This means that the answers are shown as they were given by the interviewees. Not all answers are assumed to be true and for interpretation of the results, Chapter 4 should be consulted.

B.1. Caretaker at Fisher's club (Club de Pescadores Olivos)

Name: Eduardo
Role: Caretaker of the club
Date: 24/9/2025
Language of interview: Spanish

Figure B.1: Picture with Fisher's club caretaker

Can you tell us something about the work you do in the Paraná Guazú?

- Club caretaker, responsible for maintenance of the club premises and receives members and guests.

For how long have you been doing this job?

- Since 4.5 years.

What are the changes you have seen over the years when it comes to the river and the fish in it?

- There is less fish than there was before.
- Some years ago: 1 person could catch 15 fish, recently there were 27 people who together caught 6 fish.
- This is due to contamination, fertilizers that are used on the land cause fish to die.
- When the water is low there is more fish than when the water is high. At the time of the interview the water was low, interviewee shows pictures of the entrance road that was fully flooded, now the water is meters lower. With high water, the water is dirtier.

What kind of ships do you see on the water?

- He always sees 1 dredger boat, the name he doesn't recall.
- He sees 10 to 20 cargo ships going by per day.

What do you know about sand mining in this region?

- The dry sand mining is the most important. Around 500 sand trucks per month leave the area, each truck carrying 40/45 tons. This number was half when he started his job 4.5 years ago.
- There used to be 9 sand companies, now 15.
- The dry sand miners work for YPF. It is used for fracking and they can only use the sand from here and Córdoba for that.

Do you know anything about the dredging ships in particular?

- They used to bring sand to the port of Ibicuy, now not anymore.
- The sand from the river is yellow and muddy. It is used for construction.

How many dredging ships do you see? Has this changed over the years?

- The same one has been dredging near the club for a long time, no increase seen.
- Only the dry sand mining activities have increased.

Have you seen any damage to the river banks? Has this changed over the years?

- Yes, interviewee names a few examples.
- There was a collapse at the Ibicuy port 15 years ago.
- For the river banks: vegetation was removed near the club, this increased erosion.

Results of unprepared questions:

- In the case of low water, ships sometimes get stuck upstream. Causes all ships to sail by at the same time, resulting in dirty water.
- A friend of the interviewee recently started a lawsuit because a dredger was operating in an illegal spot.
- Negative effects of dry sand mining: people complain because of the bad road conditions. The sand on the land absorbs water, so the mining has negative effects in case of floods. The sand is cleaned to get rid of organic parts, these parts flow back into the river. This makes the river dirty.

B.2. Portmanager (Port of Puerto Ibicuy)

Name: Matías
Role: Port administrator
Date: 24/9/2025
Language of interview: Spanish

Figure B.2: Picture with port manager of Puerto Ibicuy

What kind of work do you do and for how long have you been in this position?

- Interviewee is the port administrator. He runs the port together with the port manager.
- Since 2020 in this position.
- The port manager changes after every local election and is appointed by the local government. Port administrator stays in place.

Can you tell us something about the port and how it operates?

- Mostly wood is handled.
- They have two docks in the port, one of them is operating at the moment. Wood is handled there. The wood is used for construction and furniture purposes.
- Sometimes rice is handled.
- There were 19 ships in the port in 2024.

How important is the handling of sand for the port?

- They used to handle sand from the dredgers, but not anymore.
- Sand is now handled by Puerto Constanza.

How did the sand handling work? How much sand was it?

- It used to be small dredgers ships, of maximum 20 meters in length. There were two of these boats in the port. These ships are not active in the region anymore.
- They used pools to let the sand settle, water was flushed back in river.
- It was stopped because there were complaints about road conditions, a blame was needed.
- Interviewee does not know exact amounts of sand. The ships pay for the time at the dock, not for volumes.

Did the sand mining activities increase over the last years?

- Since 2-3 years, there is more sand mining from the river.
- Upstream there is no sand mining activities and downstream there is a little.
- Since public construction projects were stopped by the government, the demand for sand is lower.

Can you tell us something about the quay wall collapse that happened here?

- In 2011 the collapse happened.
- A ship left the dock, both ship and wall were heavily loaded. The water movement caused the failure of the wall.
- In 2016 it was restored.
- The dock was in good condition before the collapse.

Results of unprepared questions:

- There is an illegal sand dump just North of the highway 12 bridge.
- The is a dry sand project that transports sand to Vaca Muerta. The dry sand mining is cheaper and high quality.
- The impacts of dredging are not because of mining activities but are due to maintenance of the channel. This does not happen on the Paraná-Ibicuy, but on the Paraná-Guazú river.
- Dredging boats get a permit per sector, there is always maximum 1 boat per zone.

B.3. Plant manager (YPF sand mine)

Name: Enzo
Role: Plant manager
Date: 26/9/2025
Language of interview: English

Figure B.3: Picture with YPF plant manager

Can you tell us something about the work you do?

- Interviewee is the boss of the quarry and is a geologist.

How does the mine work?

- The plant is a sand mine. Sand is excavated and then washed to get the organic material out. Sand is put in tanks, through flocculation the clay parts are separated from the sand.
- The sand is used for fracking to mine shale oil and gas. The sand keeps the cracks open, so that the oil flows out.
- There are 70 people working at the mine.

What are the characteristics of the soil here?

- There is a 5 m deep layer of fine sand. The median grane size is 0.1 mm. The sand here is uniquely fit for fracking.
- It consists for 99.875% of quartz, which makes it a strong sand.

- Below the first sand layer, there is sometimes a clay layer of around 1 meter. This layer is locally concentrated and does not exist everywhere.
- Below this clay, there is more sand that can also be mined. Then there is another clay layer of between 6 to 10 m, gray in color. Finally, there is a thick, 30 to 40 m, sand layer with properties similar to river sand.

What are the benefits of dry sand and sand from dredging?

- The river sand has a similar percentage of quartz.
- The sand from the land is more constant in size and the quality is therefore better.
- If the dredgers are organized better and if they buy a processing plant, it will be cheaper and good quality. Interviewee indicates that his plant would then lose to the competition.

How much river sand is used by YPF?

- Around 30% of sand used by YPF for fracking is from the river, the rest from the land.
- The biggest provided of river sand is located in San Pedro.

How much sand do you mine? Is it more now than it was before?

- 120 thousand tons of sand is mined here each month.
- The demand for construction sand is low, but oil demand is high.
- Sand mining for fracking is a growing business.
- This mine can keep on operating for 8 to 10 years more, then the sand is gone. Study showed that there is 88 years of inland sand still available in the region.
- Next year, more sand will be mined than this year.

Where does the sand go to?

- The sand goes to Añelo, the center of fracking in Argentina.

How is the sand transported?

- Trucks are used. It takes 1 day to transport it to Añelo.
- There is an interest in moving to river transport. This is cheaper and the mine is located 200 m from the river.
- Due to limited availability and infrastructure problems, this is not yet realistic.

Results of unprepared questions:

- The permits for dry sand mining hold for 3 years, then have to be renewed again. No amounts are specified in the permits, but taxes are paid per volume unit mined.
- The price for a cubic meter of sand is relatively constant if expressed in US Dollars.
- There are only a few locations in Argentina where sand for fracking is mined. In many places the characteristics and minerals are not fit for fracking. There are 6 mines in this region.
- An alternative to sand for fracking is not available or to be expected. Ceramic sand was used but was too expensive.

B.4. Municipality of Zárate

Name: Daniela
Role: Municipality employee
Date: 24/9/2025
Language of interview: Spanish

Can you tell us something about the permits related to the dredging on the river?

- Interviewee indicates that she is not responsible for these permits. She shares contact details of colleagues that are involved in this.

- A new interview with these colleagues is planned for Friday 26/9/2025.

Name: Damian
Role: Municipality employee
Date: 26/9/2025
Language of interview: Spanish

Can you tell us something about the permits related to the dredging on the river?

- Interviewee indicates that the permits are handled by the province, not the municipality.

Do you know anything about a decrease in fish on the river?

- Fishers claim there is less fish, but this is due to a generational shift. She has not seen proof of there being less fish in the river.

B.5. Mayor of Ibicuy

Name: Ezequiel Maneiro
Role: Mayor of the municipality of Ibicuy
Date: 24/9/2025
Language of interview: Spanish

Figure B.4: Picture with mayor of Ibicuy

Can you tell us something about your work with the river?

- The jurisdiction of the municipality over the Paraná covers from KM 190 to KM 210.
- The municipality taxes the people that work on the river, such as the dredgers.

Are there any dredging boats active in your part of the river?

- There were, but the sand extraction vessels affected tourism, especially the sounds. The tax to extract sand from the river was increased. Almost all ships then stopped their business.
- In general, these ships moved to Paranácito.
- Only the Lojda company remained, they operate on the side of Buenos Aires province.
- The decision was made because the activity did more bad than good, didn't provide jobs, and was bad for touristic activity.

What is the sand used for?

- The extracted river sand was used for construction and glass.
- The dry sand travels 1500 km to Añelo and is used for fracking there.
- They did tests with the sands near Añelo, but it needed too much washing and processing, it was more expensive.

Did the citizens experience any other problems due to the river sand extraction?

- In the Paraná – Guazú there were no complaint reports.
- There were some collapses of river banks, but this was because of water natural flow. There's a curve.
- Only the Lojda company remained, they operate on the side of Buenos Aires province.

How does the permit/taxing system work for the dredgers?

- The taxes are applied depending on which side of the river the material was extracted. This causes conflicts between the two provinces of Buenos Aires and Entre Ríos.
- In the Guazú River, there is maintenance dredging, there are some shallow parts in the zone.
- The vessels used the excuse of not having enough depth to mine and claimed they extracted less than they did.
- Now, the taxes depend on the boat capacity, not the extracted volume.

Can you tell us more about the dry mining that is done in the area?

- The proportion of dry sand extraction versus river sand extraction is 9 to 1.
- The people complain about the truck traffic and state of the highways. They are used by 350 trucks, 9000 tons/day.
- The judiciary forced the government to get involved: do controls, plan and regulate. Now there's a limit to extract, approx. 2 – 3 m. Before, there wasn't.
- A study by the La Plata National University calculated that, at this rate, the dry sand would last 88 years. In some other areas the rate is higher, so there it would last 40 years.
- They also wanted to investigate how much time the soil would take to recover, but they couldn't find this information.

Are any mitigation measures considered at the moment?

- For the river sand mining not, since the increase of taxes solved the problem.
- For the dry sand mining: there are some ideas about carrying the sand by water to the Bahia Blanca Port, because there are complaints about the state of highways, the RN 45.

Results of unprepared questions:

- The soil profile is: 1 layer of sand (2.5 – 3m), 1 layer of clay (0.5m), 1 layer of sand (2.5 – 3m).
- The sandy material from the Ibicuy River comes from the Gualeguay River, in the center of the province of Entre Rios. This material is different from the Paraná Guazú.
- There are some boats with a 36 cubic meter capacity, they make 16 trips per day. The middle size boats have 400 to 600 cubic meter capacity. The biggest belong to Lojda and can have 1000 cubic meters. These are pure sand volumes, not the mixture of sand and water.

B.6. Landowners

Name: Jorge and Marcelo
Role: Owners of land next to the river
Date: 24/9/2025
Language of interview: Spanish

What is your experience with regard to the river?

- There is a lot of erosion. This is caused by big cargo ships and dredging boats.
- The erosion here is 30 m per year.

Do you ever see dredging ships on the river?

- Yes, they know of two dredgers on the river.

- There used to be more dredgers on the river.

What are the effects of dredging you see?

- The dredgers cause erosion together with the cargo ships and make the water dirty. In 2005 there was an erosion of 4 Ha.

B.7. Dredger

Name: Daniel
Role: Sand miner on the river
Date: 25/9/2025
Language of interview: Spanish

(a) Aerial view of the ship with drone

(b) Group picture

(c) Ship ground view

Figure B.5: Suspended load field trip

Can you tell us something about the work you do in the Paraná Guazú?

- I am the owner of the ship and this port. At the moment we are making the port ready to start with our sand mining activities. With a small cutter we are dredging out our harbour and I am replacing some parts in my ship.
- If we start operating we will do two trips a day.

For how long have you been doing this job?

- We went to this location 2 years ago.
- Before that I have been working for 3 years to get the permits. Getting the permits was a lot of work. The government is extremely slow.
- Before this place, we have dredged at a different location
- You need to get permission from three different parties, the prefectura, the municipality and the county.

Are you operating by yourself or are you working for an organization?

- I am a private entrepreneur.

Do you do this work every day, throughout the whole year?

- Every normal day we work here. (not on the weekends and special days)

Can you walk us through your regular work day?

- When we are fully operating, we go mining twice a day and about 20 trucks come to us to get sand. at the entrance of our harbour is a weighing bridge where we weigh how much sand the truck takes with him.

How much sand can your ship carry?

- Around 600 cubic meters of sand.

Where do you leave the sand after mining it?

- After mining the ship will travel back to our harbour. There, it will mix the sand with water and pump it through a pipe to a big field which is surrounded with dikes and a channel.
- The channel is used to get the water back in the river.
- From this place is the sand transported with trucks to buyers.

What happens with the sand after you leave it there?

- The sand is mostly used for construction works (mostly concrete)
- The demand for sand for construction works has dramatically reduced because of government policy, so now we also sell sand to be used in the fracking process.
- For the fracking process must the sand be very small grained.

Can you tell something about the ship you are using?

- The ship is called the Vizcaino 978, she was build in the 50's. The ship has always been used for sand mining. I bought her a few years ago.
- Trough a pipe is the sand sucked from the riverbed. This is done with an hydraulic pump. then it goes to the highest point, in this point is some of the material poured back into the river because its to fine material (clay and silt).
- the sand goes from this point over a slide. On the slide the workers on the ship can open several entrances from which it falls into the sand storage. This continues till the storage is full
- Then the ship will sail back to the port and mix the sand with water where this slurry is pumped to the shore.

How is the price of sand at the moment?

- The price of sand for construction works has been quite constant true the years (not talking about the inflation differences), but the demand has been less and less.
- The price of sand for fracking has more fluctuations but the demand is always quite high.

B.8. Camping owner

Name: Unknown
Role: Touristic operator
Date: 25/9/2025
Language of interview: Spanish

Do you have any bank erosion on your land?

- Yes, we used to have a lot of bank erosion. Our dog fell into the river once because of it.
- But now we have put rocks on our riverbeds to stop the erosion. This works quite good.

Figure B.6: Local erosion solution

C

Laboratory data

In this appendix the laboratory data will be illustrated in detail. Here, one can find all the results and Figure corresponding to the data which is referred to in the report.

C.1. Bed load samples

The bed load samples collected were all weighed before they were put in the oven. There are 7 samples collected at 4 different locations. The first three locations are the cross sections around the extracting point in the bifurcation of the Rio Paraná Guazú with the Rio Talabera. For these three cross sections two samples were taken from the soil, one at 10 meters depth and one at 14-15 meters depth. The last sample was taken at 10 meters of depth in the cross section upstream close to the Puerto Ibicuy. The Figure C.1 shows all the samples on the weighing scale before they were put in the oven as shown in Chapter 4 3.

C.2. Recapitulatory table

In this table, the details about the samples can be found for all cross sections.

Table C.1: Measurement of saturated and dry weights for samples

Sample			
1-1	400.4	282.1	88.4
1-2	360.1	320.8	109.0
2-1	410.1	317.6	117.1
2-2	454.9	404.0	92.5
3-1-A	365.8	285.3	106.7
3-1-B	332.2	248.2	101.5
3-2	527.8	368.8	99.1
4-1	507.0	332.1	89.7

C.3. Bed load samples pictures

Therefore, the Figures of the samples on the weighting scale are included as references.

(a) Sample 1-1

(b) Sample 1-2

(c) Sample 2-1

(d) Sample 2-2

Figure C.1: Samples from Bed Load Part 1

On the following page, one can find the second part of the samples from the bed load.

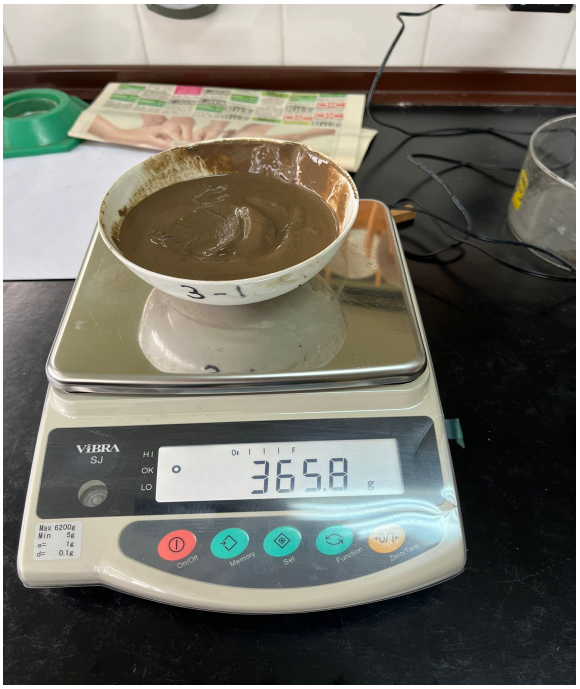

(a) Sample 3-1-A

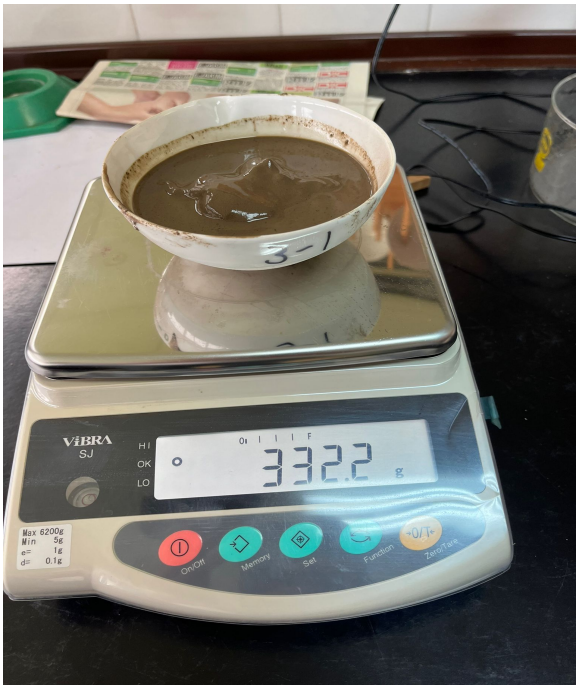

(b) Sample 3-1-B

(c) Sample 3-2

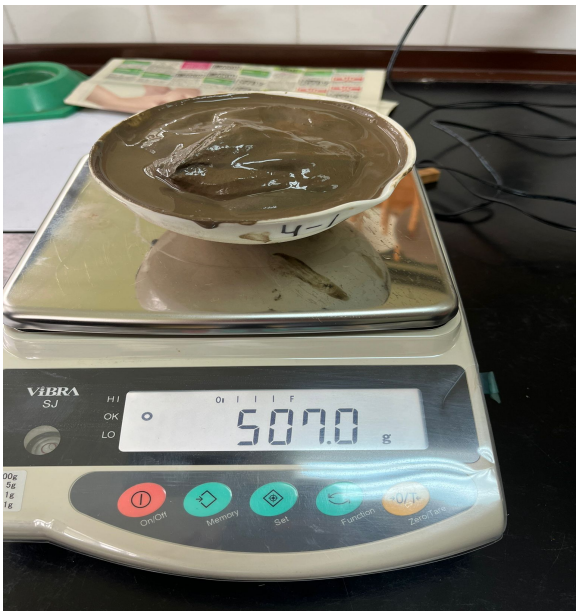

(d) Sample 4-1

Figure C.2: Samples from Bed Load Part 2

C.4. Sieving data tables

Table C.2: Cumulative grain size distribution of samples

Sieve size	1-1	1-2	2-1	2-2	3-1A	3-1B	3-2	4-1
0.50		94.0		99.52				
0.35	83.2	76.2	97.15	97.11	95.40	97.82	95.10	91.05
0.25	80.9	46.6	92.81	79.74	94.44	96.94	90.53	85.42
0.18	78.7	18.8	76.57	25.28	93.60	96.05	74.98	79.08
0.13	72.7	4.5	59.94	15.09	87.20	89.18	62.21	71.83
0.09	61.5	1.8	57.09	12.25	74.45	75.56	55.31	65.70
0.06	25.5		27.12		27.51	25.66	26.76	23.36

Table C.3: Cumulative grain size distribution of Rosario samples

Sieve size	Rosario 1	Rosario 2
0.71	95.53	95.97
0.50	39.72	39.11
0.35	21.29	12.01
0.25	3.46	1.59
0.18	0.69	0.27
0.13	0.17	0.16

Table C.4: Cumulative grain size distribution of perfect Ottawa fracking sand (Benson & Wilson, 2015)

Sieve size	Ottawa fracking sand
0.60	100.0
0.43	98.7
0.36	85.0
0.30	52.7
0.25	26.4
0.21	3.0
0.15	0.1

C.5. Sample processing pictures

(a) Sieving machine

(b) Sample 1-2

(c) samples after the oven drying

Figure C.3: Impression of process

D

Satellite data

D.1. Aqua Monitor data

In this part, one can find all the created maps for the water gains and losses from 1985-2025. Using the code from Deltares on Github, and adapting it to Google Earth Engine in function of the requirements from the team, one can find the following maps in Chapter 6.

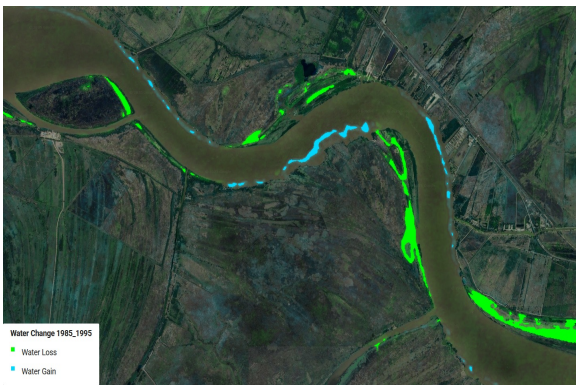

(a) 1985-1995

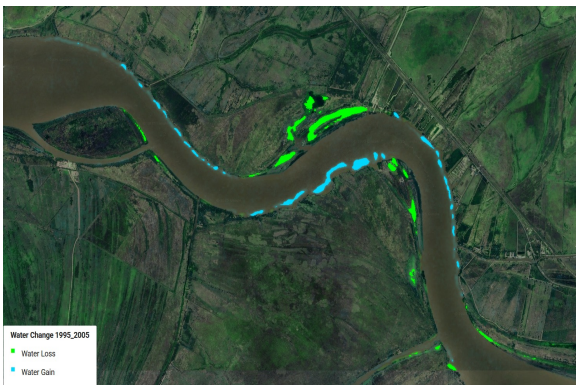

(b) 1995-2005

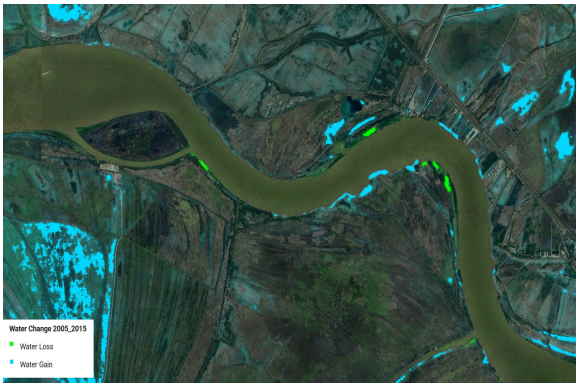

(c) 2005-2015

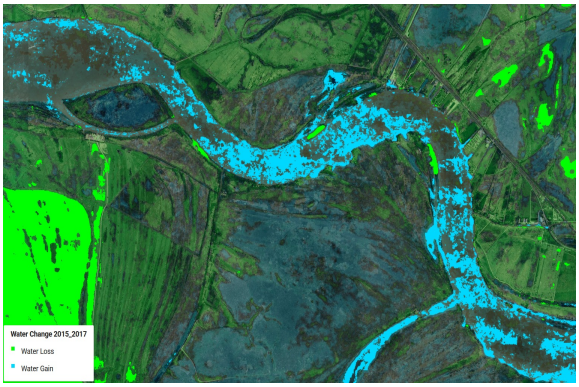

(d) 2015-2017

Figure D.1: All Changes in Water on the Area of Interest Part 1

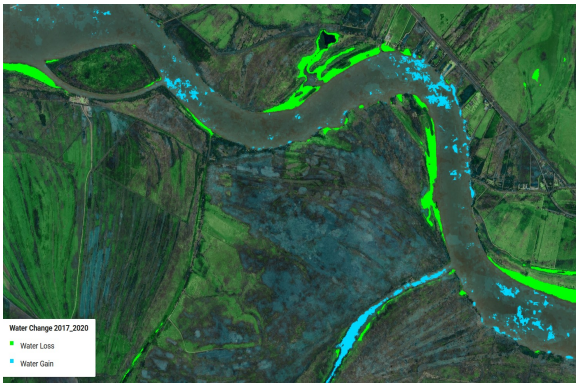

(a) 2017-2020

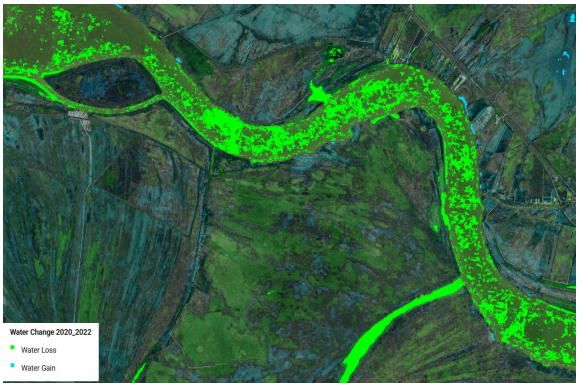

(b) 2020-2022

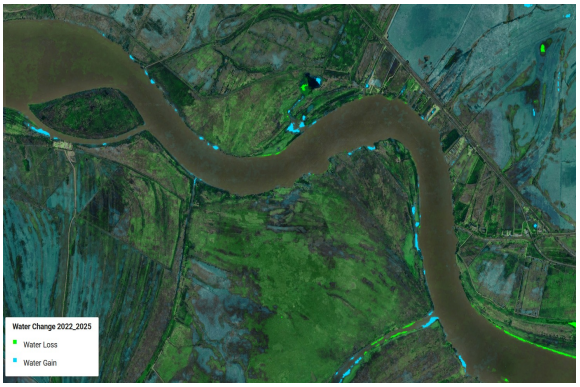

(c) 2022-2025

(d) 1985-2025

Figure D.2: All Changes in Water on the Area of Interest Part 2

D.2. Google Earth engine data

In this part, all the maps with the possible measurements in the last years are shown, for the years 2022, 2020, 2017, 2015, 2013, 2010, 2005, 2003, and 1985. First, the surface was recent surface was calculated based on the 2022 map on Google Earth. Then, the illustrations follow of this area of 2022 applied onto the other years data. All these images can be found below. After that, the same principle is applied for the second part of the camping which was not measured during the field trip, but seemed to be relevant based on the Google Earth study.

D.2.1. Camping surface of 2022

The values of the perimeter and surface of the Camping in 2022 can be found in the table below.

Table D.1: Measurements of Camping La Blanqueada in 2022

Location	Perimeter(m)	Area (m²)
La Blanqueada	1520.46 m	88494.3 m²

Next, follow the maps of how these measurements relate to the historical data of 2022-1985.

(a) 2022

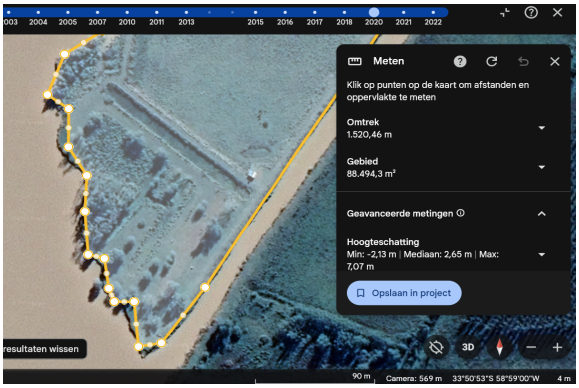

(b) 2020

(c) 2018

(d) 2017

Figure D.3: All Changes of the Surface in Camping Part 1

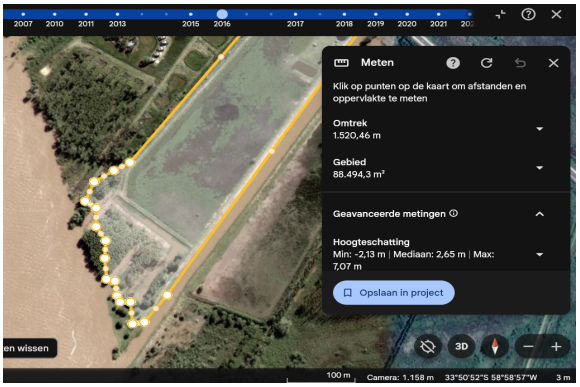

(a) 2015

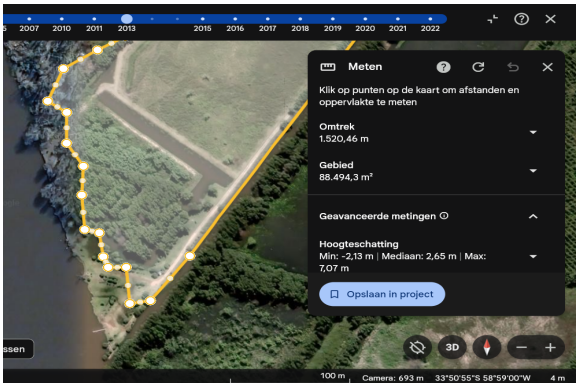

(b) 2013

(c) 2010

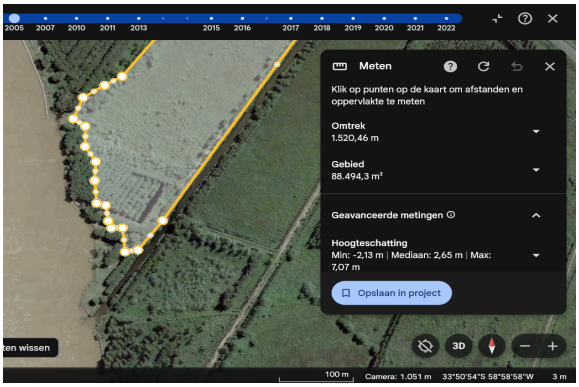

(d) 2005

Figure D.4: All Changes of the Surface in Camping Part 2

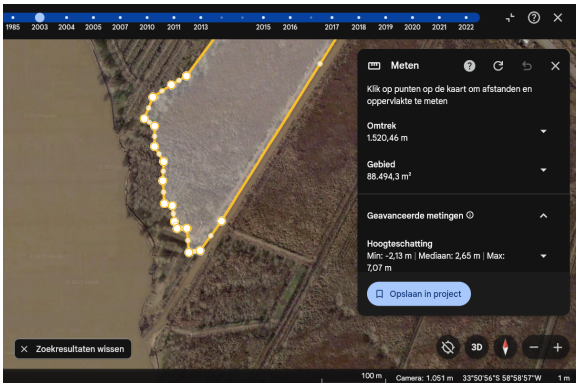

(a) 2003

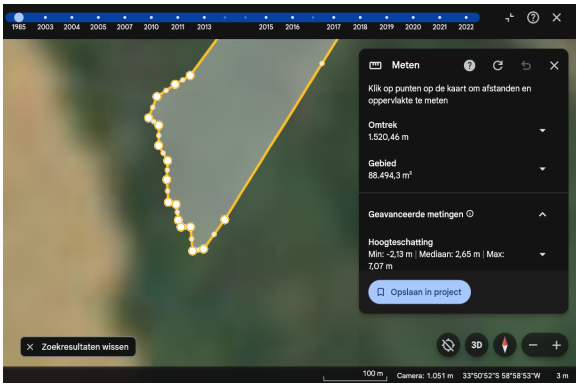

(b) 1985

Figure D.5: All Changes of the Surface in Camping Part 3

D.2.2. Surface losses camping 2022

Lastly, the same principle applied to the situation on the second part of the camping La Blanqueada. The values of the perimeter and surface lost compared to 2022 can be found in the table below.

Table D.2: Surface recap camping La Blanqueada in 2022

Location	Category	Colour		
East Part	Actual	Yellow	1520.46	88 494.3
East Part	Lost	Red	786.84	15 328.31
West Part	Actual	Blue	1203.31	71 231.39
West Part	Lost	Orange	466.7	8698.71
West Part	Dug out	Green	468.46	7622.01

Do keep in mind that the green part of the area is very likely to be digged out by the owner himself to build a channel for the boats. This probably contributes to an acceleration of the erosion around it, but it is still relevant to mention.

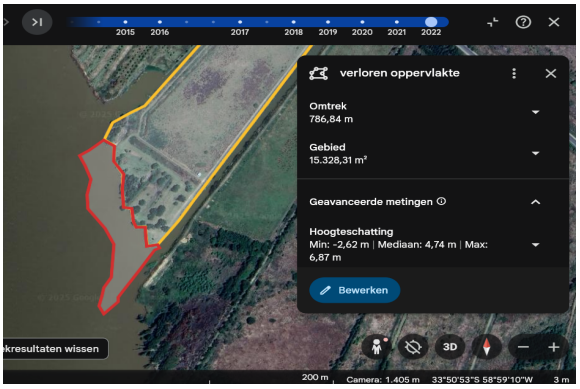

(a) surface lost in 2022

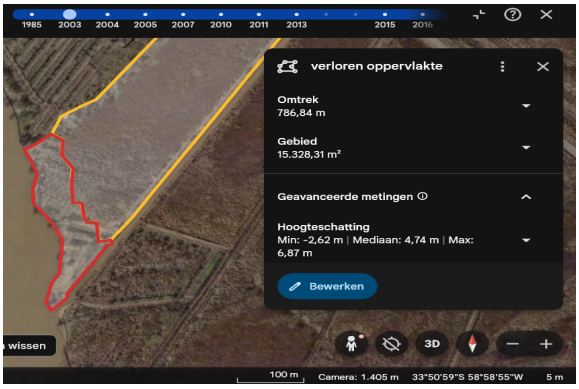

(b) surface lost in 2003

(c) second part camping 2022

(d) second part camping 2003

Figure D.6: All Surface Losses in Camping

From the values in Table G.2, one can calculate the rate of change in the last 20 years or so with the help of the following formula.

$$\text{Loss Ratio} = \frac{\text{Loss}}{\text{Total Surface}}$$

Consequently:

$$\text{Loss Ratio} = \frac{\text{Loss}}{\text{Surface in 2022 + Loss}}$$

Applying this to both sides of the Camping gives:

Loss Ratio (East) $= \frac{15328.31}{88494.3+15328.31} = \frac{15328.31}{103822.61} = 0.1476$

Loss Ratio (West) $= \frac{8698.71}{8698.71+7622.01+71231.39} = \frac{869871}{8755211} = 0.0994$

Together, these results are found in Table D.3 .

Table D.3: Loss Ratio for Camping La Blanqueada in 2022

Location	Loss Ratio (%)
East Part	14.76
West Part	9.94

Using geometry and more measurements on Google Earth, the loss in length of the land on the shore is ranging from 45 to 132 meters in the most extreme case down south east of the camping zone, which can be seen in the Figure below. They are shown by the purple lines.

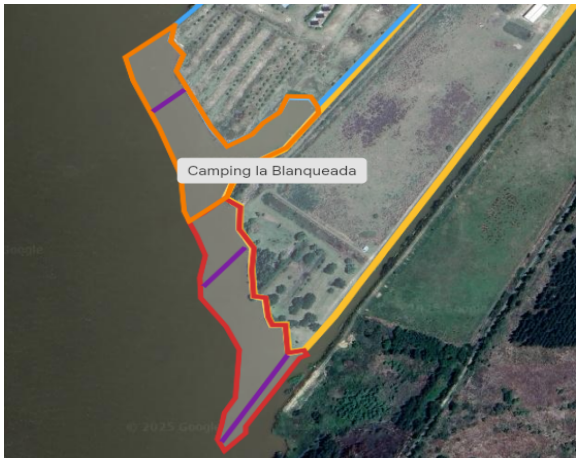

(a) Lengths of the lost land

E

ADCP results

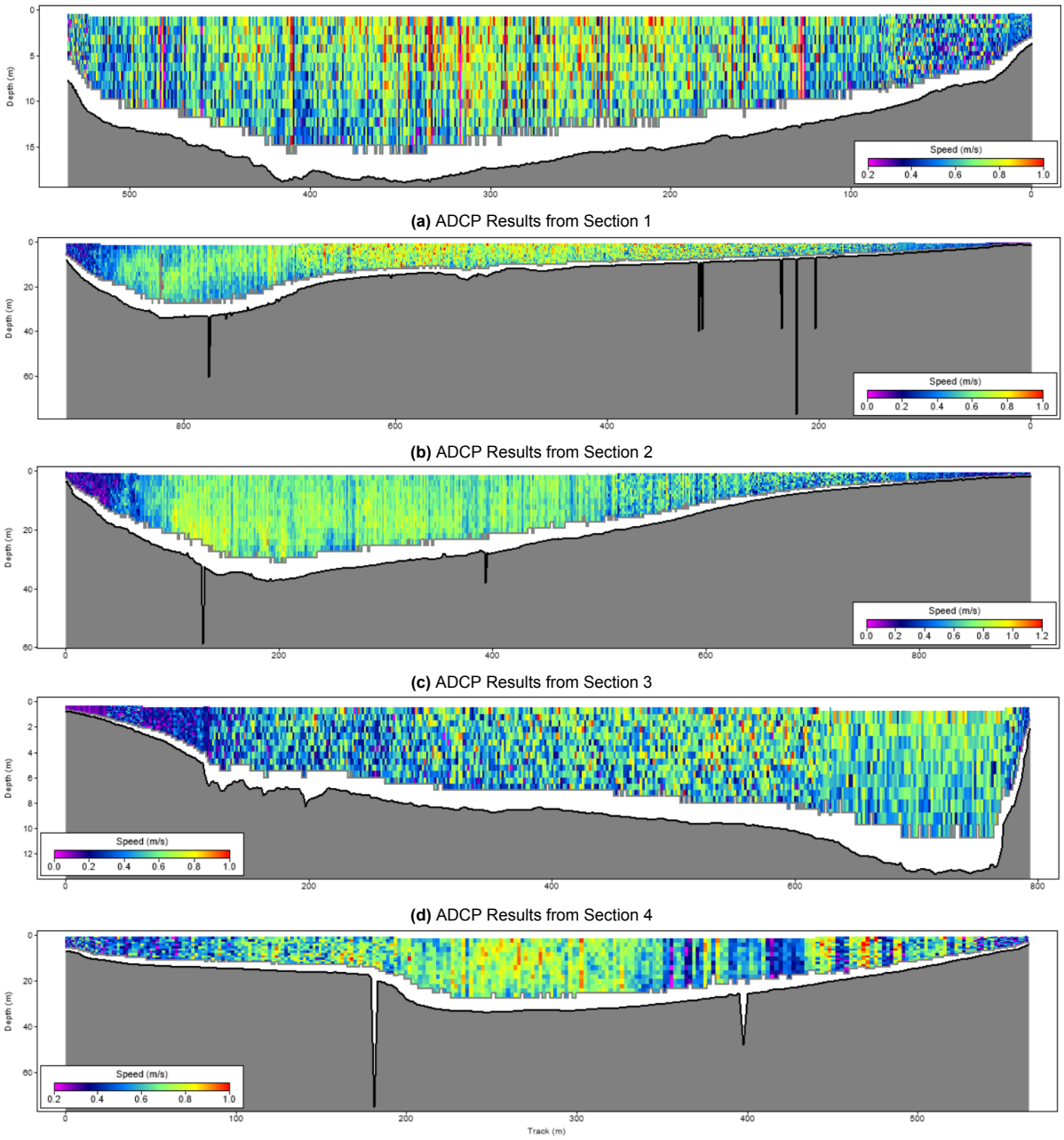

(a) ADCP Results from Section 1

(b) ADCP Results from Section 2

(c) ADCP Results from Section 3

(d) ADCP Results from Section 4

(e) ADCP Results from Section 5

Figure E.1: ADCP measurement results across Sections 1–5.

F

Design of steel sheet pile

F.1. Soil profile

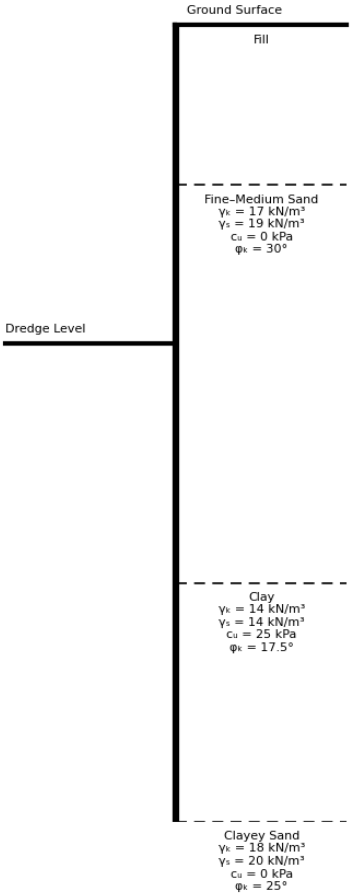

Figure F.1: Soil profile and properties

F.2. Vertical effective stress

Table F.1: Vertical effective stress on left and right sides

z [m]	$\sigma'_{z,l}$ [kN/m^2]	$\sigma'_{z,r}$ [kN/m^2]
0.00	0.00	0.00
1.47	0.00	17.64
2.00	0.00	18.80
4.00	0.00	37.18
7.00	27.57	64.75
10.00	40.14	77.32

F.3. Earth pressure and force

F.3.1. Earth pressure

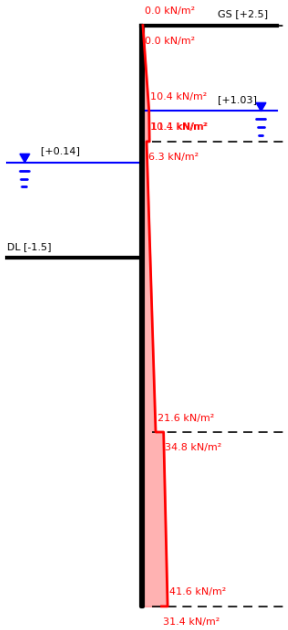

Figure F.2: Active earth pressures

Table F.2: Active earth pressure coefficients and pressures

z [m]	$K_{a,\text{above}}$	$K_{a,\text{below}}$	p_{above} [kN/m^2]	p_{below} [kN/m^2]
0.00	0.589	0.589	0.00	0.00
1.47	0.589	0.589	10.39	10.39
2.00	0.589	0.333	11.07	6.27
7.00	0.333	0.538	21.58	34.81
10.00	0.538	0.406	41.57	31.38

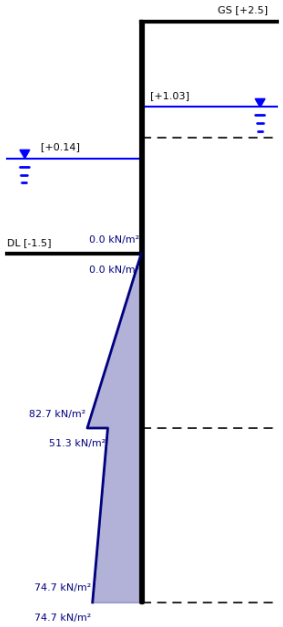

Figure F.3: Passive earth pressures

Table F.3: Passive earth pressure coefficients and pressures

z [m]	$K_{p,\text{above}}$	$K_{p,\text{below}}$	p_{above} [kN/m^2]	p_{below} [kN/m^2]
4.00	3.000	3.000	0.00	0.00
7.00	3.000	1.860	82.71	51.28
10.00	1.860	1.860	74.66	74.66

F.3.2. Forces

Table F.4: Resultant forces and centroids by segment

Side	Segment	Shape	F [kN/m]	z_c [m]
Active	1	Triangle	7.63	0.98
Active	2	Rectangle	5.50	1.73
Active	2	Triangle	0.18	1.82
Active	3	Rectangle	31.33	4.50
Active	3	Triangle	38.29	5.33
Active	4	Rectangle	104.44	8.50
Active	4	Triangle	10.14	9.00
Passive	1	Triangle	124.06	6.00
Passive	2	Rectangle	153.84	8.50
Passive	2	Triangle	35.07	9.00

F.4. Hydrostatic pressure and force

Table F.5: Pore pressure values along depth

z [m]	u_{right} [kN/m^2]	u_{left} [kN/m^2]	u_{net} [kN/m^2]
0.00	0.00	0.00	0.00
1.47	0.00	0.00	0.00
2.00	5.20	0.00	5.20
2.36	8.73	0.00	8.73
7.00	54.25	45.52	8.73
10.00	83.68	74.95	8.73

F.5. Bending moment

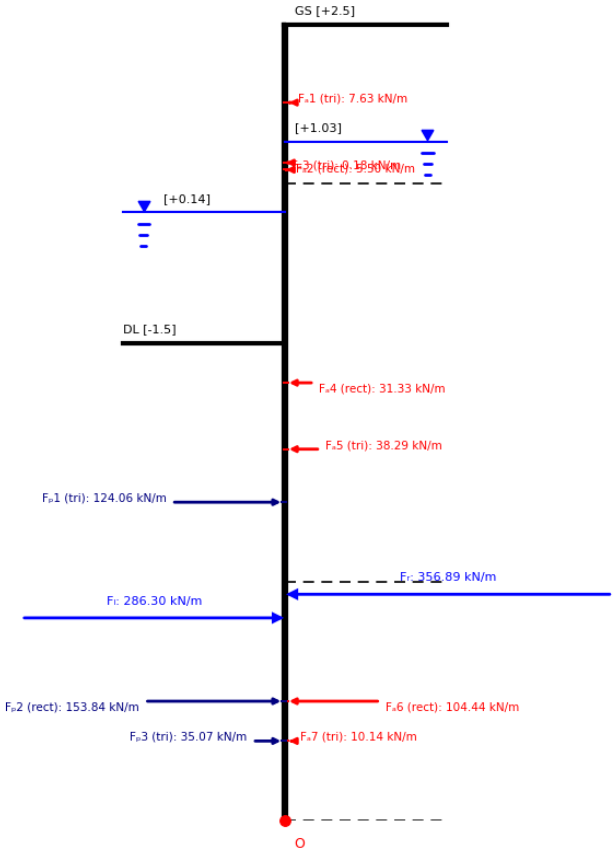

Figure F.4: Forces for t = 6.00 meters

Table F.6: Resultant forces, arms, and moments for t = 6.0 meters

Side	Shape	F [kN/m]	z_{base}[m]	M_{base} [kN·m/m]
Active	Triangle	7.63	9.02	68.86
Active	Rectangle	5.50	8.27	45.50
Active	Triangle	0.18	8.18	1.48
Active	Rectangle	31.33	5.50	172.34
Active	Triangle	38.29	4.67	178.69
Active	Rectangle	104.44	1.50	156.65
Active	Triangle	10.14	1.00	10.14
Hydro Passive	Triangle	286.30	2.55	-730.07
Hydro Active	Triangle	356.89	2.84	1014.8
Passive	Triangle	124.06	4.00	-496.26
Passive	Rectangle	153.84	1.50	-230.76
Passive	Triangle	35.07	1.00	-35.07
$\sum M_t$ (should ≈ 0 for equilibrium)				156.3

F.6. Ultimate Limit and Serviceability Limit State

F.6.1. DA1-1

Table F.7: Design values soil DA1-1

Layer	Soil type	Depth [m]	$\gamma_d\,[\mathrm{kN/m^3}]$	$\gamma_{sat}\,[\mathrm{kN/m^3}]$	$\varphi'\,[^\circ]$	$c'\,[\mathrm{kPa}]$	$c_u\,[\mathrm{kPa}]$
1	Fill	0.0 - 2.0	12	12	15.0	2.5	20
2	Fine/medium sand	2.0 - 7.0	17	19	30.0	0.0	—
3	Clay	7.0 - 10.0	14	14	17.5	0.0	25
4	Clayey sand	10.0 - 15.0	18	20	25.0	0.0	—
5	Clay	15.0 - 16.0	14	14	17.5	0.0	25
6	Clayey sand	16.0 - 17.5	18	20	25.0	0.0	—
7	Medium sand	17.5 - 32.0	18	20	32.5	0.0	—

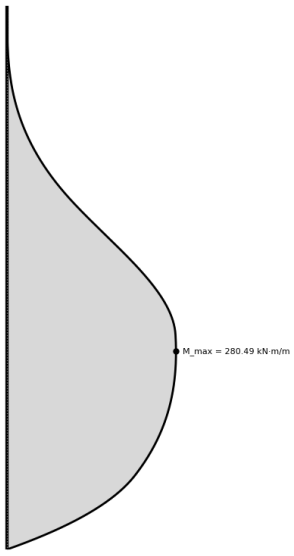

Figure F.5: Bending moment line DA1-1

Table F.8: Moment calculation summary DA1-1

Quantity	Value
Depth below ground [m]	7.374
Depth below dredge [m]	3.374
$M_{a,\text{soil}}(S)$ [kN·m/m]	339.481
$M_{wR}(S)$ [kN·m/m]	454.148
$M_a(S) = M_{a,\text{soil}} + M_{wR}$ [kN·m/m]	793.629
$M_{p,\text{soil}}(S)$ [kN·m/m]	234.980
$M_{wL}(S)$ [kN·m/m]	278.160
$M_p(S) = M_{p,\text{soil}} + M_{wL}$ [kN·m/m]	513.140
$M_{\text{max}} = M_a(S) - M_p(S)$ [kN·m/m]	280.489

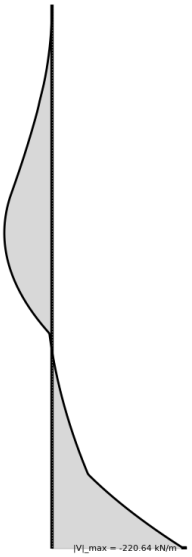

Figure F.6: Shear force line DA1-1

Table F.9: Shear and partial-resultants summary

Quantity	Value
Zero-shear depth z_S [m]	7.374
Depth below dredge at z_S [m]	3.374
$V(0)$ at ground [kN/m]	0.000
$V(Z)$ at dredge [kN/m]	67.749
$V(z_S)$ [kN/m]	-0.000
$V(z_{\text{toe}})$ [kN/m]	-220.641
$\lvert V\rvert_{\max}$ [kN/m]	-220.641
Depth of $\lvert V\rvert_{\max}$ [m]	11.575
$V_a(0 \to z_S)$ [kN/m]	129.746
$V_{wR}(\text{wt} \to z_S)$ [kN/m]	230.783
$V_p(Z \to z_S)$ [kN/m]	194.085
$V_{wL}(\text{wl} \to z_S)$ [kN/m]	166.444
Left-to-right sum @ z_S [kN/m]	-0.000

F.6.2. DA1-2

Table F.10: Design values soil DA1-2

Layer	Soil type	Depth [m]	γ_d [kN/m^3]	γ_{sat} [kN/m^3]	φ' [°]	c' [kPa]	c_u [kPa]
1	Fill	0.0 - 2.0	12	12	12.1	2.5	20
2	Fine/medium sand	2.0 - 7.0	17	19	24.8	0.0	—
3	Clay	7.0 - 10.0	14	14	14.2	0.0	17.9
4	Clayey sand	10.0 - 15.0	18	20	20.5	0.0	—
5	Clay	15.0 - 16.0	14	14	14.2	0.0	17.9
6	Clayey sand	16.0 - 17.5	18	20	20.5	0.0	—
7	Medium sand	17.5 - 32.0	18	20	27.0	0.0	—

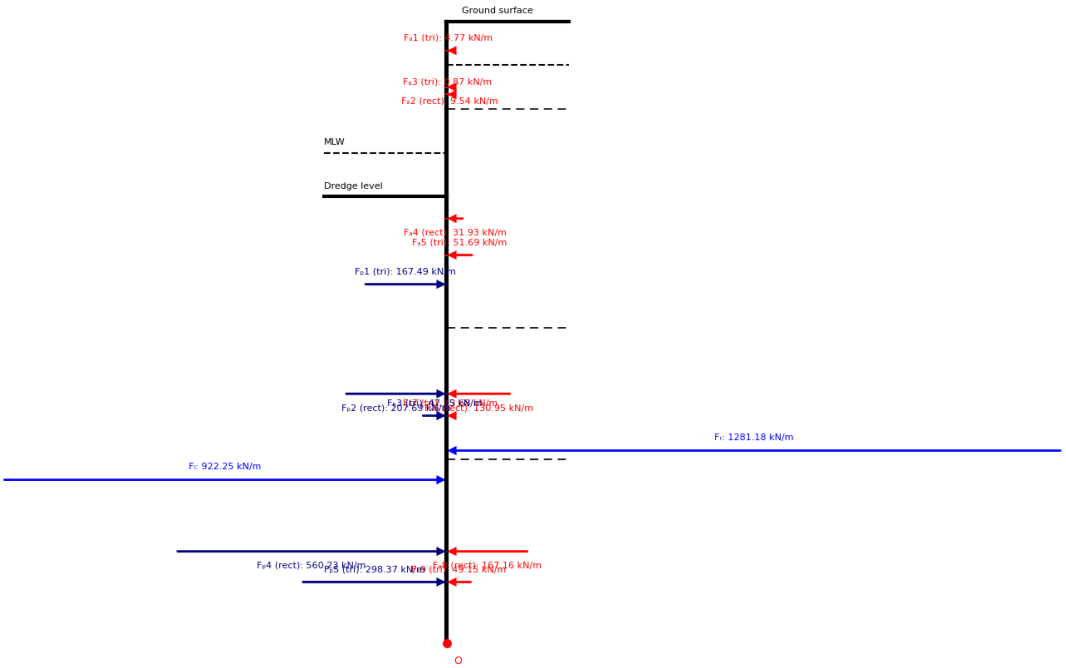

Figure F.7: ULS combination forces for t = 10.196 meters

Table F.11: Resultant forces, arms, and moments for t = 10.196 meters

Side	Shape	F [kN/m]	z_{base} [m]	M_{base} [kN·m/m]
Active	Triangle	4.77	13.53	64.52
Active	Rectangle	9.54	12.70	121.10
Active	Triangle	0.87	12.53	10.91
Active	Rectangle	31.93	9.70	309.57
Active	Triangle	51.59	8.86	458.14
Active	Rectangle	130.95	5.70	745.87
Active	Triangle	13.68	5.20	71.11
Active	Rectangle	167.16	2.10	350.69
Active	Triangle	49.15	1.40	68.74
Hydro Passive	Triangle	922.25	3.73	-3441.82
Hydro Active	Triangle	1281.18	4.40	5635.44
Passive	Triangle	167.49	8.20	-1372.72
Passive	Rectangle	207.69	5.70	-1182.97
Passive	Triangle	47.35	5.20	-246.00
Passive	Rectangle	560.23	2.10	-1175.33
Passive	Triangle	298.37	1.40	-417.31
$\sum M_t$ (should ≈ 0 for equilibrium)				-0.0763

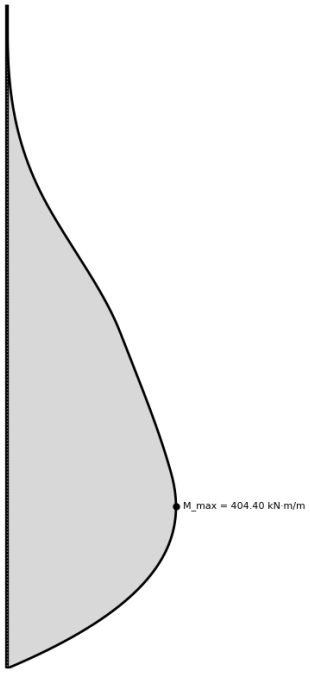

Figure F.8: Bending moment line DA1-2

Table F.12: Moment calculation summary DA1-2

Quantity	Value
Depth below ground [m]	10.721
Depth below dredge [m]	6.721
$M_{a,\text{soil}}(S)$ [kN·m/m]	922.641
$M_{wR}(S)$ [kN·m/m]	1294.480
$M_a(S) = M_{a,\text{soil}} + M_{wR}$ [kN·m/m]	2217.121
$M_{p,\text{soil}}(S)$ [kN·m/m]	857.051
$M_{wL}(S)$ [kN·m/m]	955.664
$M_p(S) = M_{p,\text{soil}} + M_{wL}$ [kN·m/m]	1812.715
$M_{\text{max}} = M_a(S) - M_p(S)$ [kN·m/m]	404.406

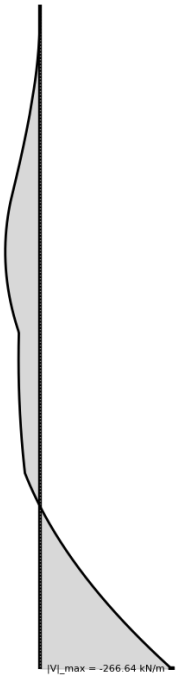

Figure F.9: Shear force line DA1-2

Table F.13: Shear and partial-resultants summary

Quantity	Value
Zero-shear depth z_S [m]	10.721
Depth below dredge at z_S [m]	6.721
$V(0)$ at ground [kN/m]	0.000
$V(Z)$ at dredge [kN/m]	55.882
$V(z_S)$ [kN/m]	0.000
$V(z_{\text{toe}})$ [kN/m]	-266.635
$\lvert V\rvert_{\max}$ [kN/m]	-266.635
Depth of $\lvert V\rvert_{\max}$ [m]	14.172
$V_a(0 \to z_S)$ [kN/m]	257.468
$V_{wR}(\text{wt} \to z_S)$ [kN/m]	419.782
$V_p(Z \to z_S)$ [kN/m]	334.353
$V_{wL}(\text{wl} \to z_S)$ [kN/m]	342.897
Left-to-right sum @ z_S [kN/m]	0.000